Scaling and Complexity in Simple Multicellular Animals

Mircea R. Davidescu

a dissertation
presented to the faculty
of princeton university
in candidacy for the degree
of Doctor of Philosophy

recommended for acceptance
by the Department of
Ecology and EVolutionary Biology

Adviser: Iain D. Couzin and Corina E. Tarnita

September 2017

Abstract

The earliest-diverged multicellular animals are decentralized organisms capable of growing to indeterminate sizes and highly variable morphologies. These organisms must coordinate activity among their constitutive cells at the scale of the organism in order to to leverage the benefits of multicellularity, and must do so using decentralized mechanisms that are robust to uncertainty in size and shape. This thesis investigates how coordination within the Placozoa - arguably the simplest animals - scales with organism size, quantifies the extent to which different developmental processes affect size regulation, and creates a framework for measuring morphological variability in what had been considered amorphous animals. In Chapter 1 I develop a method by which one can measure coordination and information propagation within an animal's body plan, and investigate how this propagation is affected by changes in size. I argue that such animals are poised at criticality, with evidence presented to suggest that this facilitates optimal information transmission, but that the physical constraints of multicellularity create a size-coordination trade-off in such decentralized organisms. The presence of size-induced trade-offs brings forth the question of how size is regulated, which in Placozoa occurs through growth and asexual fission. In Chapter 2 I investigate whether size is regulated in response to changing environmental nutrient conditions and find that animals adjust their sizes to match their environments. I further find that this change comes about primarily due to changing dynamics of growth rather than fission, and identify that growth is highly dependent on nutrient conditions, but find evidence that asexual fission could be an emergent phenomenon of poor coordination beyond certain sizes. Finally, in Chapter 3 I investigate the morphological variability in Placozoa and find evidence for allometric growth in such animals. In addition, Chapter 3 sets the groundwork for future comparative morphological studies between individuals and for behavioral stereotyping by developing a size and rotation invariant shape representation, which I use to identify the presence of idiosyncratic morphologies. I close the thesis with some remarks regarding future directions in exploring the effects of scaling on coordination, morphology, and behavior in this small yet evolutionarily significant Metazoa phylum.

Contents

Listing of figures

Acknowledgments

It is a rare privilege to work every day with and among the titanic figures of the Ecology and Evolutionary Biology department at Princeton University, and especially my committee members who played a decisive role in this thesis. First among these are my two co-advisors, Iain Couzin and Corina Tarnita. I have admired Iain's passion for science, and his ability to infect those around him with the same fanatical love for science. I have felt more and more energized about science with every meeting and discussion that we have shared, and understanding his way of thinking has helped me envision how we can expand the frontiers of human knowledge. Corina's pragmatism and desire for fundamental understanding has helped me ground this vision with a stoic realism about what is truly known and have discovered. She taught me the value of not being satisfied by superficial reasoning and jargon but to dig deeper to achieve a more fundamental understanding. Thomas Gregor, a *de facto* advisor on my committee, has been inspiration for my work through his superlative rigor. His work taught me to not be satisfied with "noisy biology" and "hidden variables" but to be fastidious and precise in all I intend to measure. Finally, Simon Levin has been a titanic figure in my life at Princeton and is in many ways the keystone of my committee. He is a font of wisdom, pragmatism, and objective reflection. The few hours in which I was fortunate enough to discuss my research with him have been life-changing.

Two other individuals have been my advisors in all but name: Pawel Romanczuk and Allyson Sgro. Pawel, both as post-doc and professor, has been an inspiration of what a scientist and mentor can be: curious, passionate, understanding, and has a sincere desire to mentor those around him. Words cannot describe the patience, enthusiasm, and kind-hearted guidance that Pawel has shown me, and this thesis would not exist without his help. Allyson's guidance on how to live a proactive proactive and self-reliant life as a researcher who takes ownership of one's projects is an invaluable lessons that I will cherish for the rest of my life. The "Whitesides method of writing papers" that she passed down to me is a critical reason why there is anything to read in this thesis right now. Best of luck to both of you on your new professorships!

I am thankful to all my friends both from Princeton and around the world. In the academic sphere, my friends in the Couzin, Tarnita, and Gregor Labs have been indispens-

able comrades on this journey. I am especially thankful to my labmates, especially Colin Twomey, Matt Grobis, Joe Bak-Coleman, Fernando Rossine, Eric Smith, Zoom Nguyen, and Hernan Garcia. Your companionship made every day in lab a treasure. Various friends in the EEB department have been outstanding in their support, and I am grateful for their intellectually stimulating conversations. A special regard must be given to my cohort who, no matter for how long I had dropped out of touch to battle my thesis demons, remained a steadfast harbor of friendship and support. I cherish their enduring friendship, and hope that it lasts a lifetime. Outside of the department I am grateful to my friends in PATS, especially Jen-Tang Lu, KC Lin, Amy Wu, Ting-Hsuan Chen, and Ai-Lei Sun, and my friends in Princeton Boxing Club. I am grateful for my good friends outside of the Princeton community as well, especially Trevor, Sean, and Nick, who have kept in touch with me since I began my studies here. Neal Skibinski, whom I consider my best friend, deserves special recognition for all of his support over the tumultuous past five years of my life.

I would be remiss not to include the Graduate Student Government and the many students who were part of Executive boards that I either joined or led, especially Sean Edington, Akshay Mehra, Rachael Barry, Julia Wittes, April Williams, Jonathan Balkind, Daniel Vitek, Andrew Edwards, Jose Ferreira, Mattias Fitzpatrick, Bradley O'Brien, Genna Gliner, and Akil Word-Daniels. Being a part of a dedicated team working on projects with immediate impact for my community, and being able to lead such a team, has brought me the greatest satisfaction in my time at Princeton. I am tremendously grateful that I was granted the opportunity to work with Dean Sanjeev Kulkarni, Associate Dean Lisa Schreyer, Assistant Dean Lily Secora, and Assistant Vice President Amy Campbell. The can be no better education in leadership for a graduate student than what I have been given.

I am grateful to my family. My mother Professor Mihaela Ulieru, who more than anyone I know demonstrates the strength of an indomitable spirit and great spirit, and who by her deeds proves herself time and again to be an unstoppable force of nature. She is the one person in my life who most deserves recognition for being my advisor and mentor. If I saw further, it was only by standing on her shoulders. I am also grateful to my older brother George, who imbued in me a thirst for knowledge and who by his personal example was a beacon of excellence in my life. My late grandfather George Ulieru, who taught me the importance of dignity and knowing oneself, and my grandmother Elena, who taught me the value of approaching any challenge in life with a light heart. I am also grateful to my father Rasvan Davidescu, whose correspondence and example taught me how to be happy and lead a fulfilling life while not being shaken by circumstance. My girlfriend and partner Sophia Li, among the wisest and most resolute people I have ever met, deserves special recognition. She has given my life much joy, wisdom, and energy in my time here. Thank you for your love and faith in me.

I am grateful to the Natural Sciences and Engineering Research Council of Canada

(NSERC) for their generous support through the Julie Payette Fellowship and the PGS D fellowships. I am also grateful for the financial support offered by the Ecology and Evolutionary Biology department. Very little could have been achieved without this support.

For all of my ancestors.

0

Introduction

0.1 Coordination and the evolution of multicelluarity

The evolution of multicellularity was a major evolutionary transition that fundamentally changed the form of life on Earth[118]. Understanding the forces and mechanisms that caused and sustained the evolution of multicellularity is one of the most important goals of evolutionary biology[101,123]. It is easy to understand the anthropocentric fascination with this

event: humans are multicellular organisms, as are the vast majority of organisms that we can see with the naked eye. However, multicellularity is also important because it is arguably the ultimate form of cooperation and coordination, whereby a cooperative group produces an emergent individuality at the level of the larger aggregate[123,38,33]. Multicellularity is also an interesting problem because it is a phenomenon that exists over a tremendous length scale, with multicellular organisms spanning over sixteen ordrs of magnitude in size[28]. The ability of cells to coordinate their activities to produce coherent organism-scale behaviors over such a wide size range is a feat without equal, and understanding the mechanisms by which such coordination is maintained can help us develop frameworks and rules for effective coordination in other biologiocal and social systems[133,124,136].

The evolution of multicellularity brought with it numerous benefits to constitutive cells that found themselves in this new context[206]. Some of the advantages are purely physical consequences, such as escaping predation[32,99] and becoming a predator of smaller organisms, division of labor[103,144,101], and improved environmental sensing and decision-making[113,197]. Harnessing these benefits requires effective coordination among the numerous constitutive cells of the organism. This coordination can be orchestrated with varying degrees of centralization. At the totally centralized extreme a single cell orchestrates the behavior of all others, while in the decentralized extreme all cells have equal say in the behavuior of the collective. Centralization of the control structures of an organism simplifies coordination, as it can reduce the number of decision-making cells, naturally reduces the dimensionality of the coordination problem, and can place decision-making cells in proximity of one another. Hierarchical control structures such as nervous systems and musculature simplify coordination, and while indeed a multicellular organ like the brain or spinal

cord are decentralized systems their own right[78], such organs still greatly simplify and reduce the coordination problem for the whole organism composed of numerous more cells.

Coordination in the earliest multicellular animals, however, was undoubtedly orchestrated in a decentralized fashion, and therefore understanding how multicellular life was sustained requires understanding the mechanisms of decentralized coordination. The earliest multicellular animals - Porifera, Placozoa, Ctenophora, and Cnidaria - all lack a central nervous system, some lacking neurons entirely[111], and many grow in a decentralized or modular fashion with highly variable body sizes and shapes[210]. Organisms with such simplified and unstructured body plans must have been able to coordinate in order to make multicellular life evolutionarily stable, and therefore we need to understand how effective coordination of decisions can be achieved in decentralized systems.

Three factors are central to the decision outcome of a collective system: the preferences of the individual agents, the network structure that defines interacting neighbors, and how susceptible each agent is to influence by its neighbors. Individual preferences are central to democratic collective decision-making, as even the idea of a democratic outcome is defined as one which reflects the biases of the majority (relative or absolute). This outcome is the typical result *ceteris paribus*, but there are many conditions under which a democratic decision is unstable, and the group's decision is no longer representative of the majority. A well-known case is when the strength of preferences between individuals constituting the majority and minority are unequal: a strongly-biased minority can overpower a weakly-biased majority. Several recent empirical and theoretical studies have revealed how adding unbiased ("uninformed") individuals to groups can prevent such a takeover by the extremist minority[49,73,109]. The network structure of interactions in a collective system can also

have a profound effect on the decision outcome. Studies on opinion dynamics across social and simulated networks have revealed that individuals may exert disproportionate influence on a group if their neighborhood is composed of easily influenced individuals[15,203]. Finally, the outcomes and dynamics of collective decision-making are highly dependent on how susceptible individuals are to their neighbors' influence. Should individuals be too sensitive, a collective might never make a decision as noise drives the system outside of any consensus decision state. On the other hand, should individuals be too insensitive, the collective might never equilibrate to a consensus state, and would be unable respond in a timely fashion to changing environmental stimuli.

The trade-off between stability and sensitivity in collective decision-making implies the question of whether there is an optimal tuning in sensitivity that allows a group to reach consensus while remaining responsive to new stimuli, which has inspired the notion that collective systems are optimally tuned at criticality. In criticality, the parameters that govern the behavior of individual components - whether cells within an animal or animals in a group - are tuned such that the collective system resides in a transition region between ordered and disordered behavior. The idea of criticality derives from the field of statistical mechanics of equilibrium systems, where it is used to describe the behavior of physical systems at a critical point in a phase transition. Well-known examples of phase transitions in physics include matter going from solid to liquid phase or ferromagnets transitioning to a magnetized state[207]. However, very similar phase transitions have also been identified in collective decisions, whereby a collection of individuals transitions from a disordered lack of consensus to an ordered consensus state. A well-known example arises in collective movement, where a phase transition has been characterized between disordered, random

movement and ordered, polarized marching[200,44,36].

Determining whether a system is at criticality is typically achieved by looking at the statistics and distributions of fluctuations that occur in such a system. Examples of fluctuations in complex systems include density fluctuations in a fluid at a critical point, clusters of aligned spins in a ferromagnet, the number of neurons involved in a signaling avalanche in the nervous system, or the number of animals changing direction in a moving group. At criticality, the size of these fluctuations occur at all possible length scales, whereby the observed phenomena sizes create a power-law distribution and the system produces fractal behavior[13]. Other phenomena that occur at a critical point include a slowing of dynamics, the presence of $1/f$-noise and Zipf's Law[152,13]. Remarkably, biological systems ranging from amino acids to neural networks to flocks of birds exhibit these signatures of criticality[130]. While this could suggest that such systems are indeed poised at criticality, caution is needed in using this inverse method to infer criticality as such phenomena may have have alternative explanations[159,121,81,115]. Nevertheless, criticality in complex systems remains a vibrant and attractive field of study.

The notion that biological organisms are poised at criticality, in the absence of any obvious external fine-tuning as can be controlled in physical systems, brings forth the question of how biological organisms acheived this particular state. One hypothesis for how this is achieved is that of self-organized criticality (SOC)[12]. In SOC, the set of parameter values that position a system at a critical state are a stable attractor in a system's dynamics[182], allowing a system to evolve to a state of criticality on its own, without needing any external parameter adjustment[14]. The archetypical example of self-organized criticality is a sand pile that grows in steepness as sand grains are added, and becomes shallower as the added grains

trigger avalanches, with the resultant avalanches exhibiting a scale-free distribution in sizes and the pile's steepness stabilizing at a critical slope angle[13]. The demonstration that criticality can be an emergent phenomenon from the dynamics of a system is particularly attractive for biological systems, where it was argued that criticality could not only be a self-organized phenomenon but that it could also be adaptive[95,107,96]. Not only was criticality argued to be adaptive, but some suggested that any system which could perform computation and was adaptive would drive itself to the "edge of chaos" in a purely self-organized fashion[3,174]. The adaptive significance of criticality on computation and information processing has been emphasized by a number of recent works in neuroscience and behavioral ecology that have argued that decision-making is optimal when the system is poised at criticality[78,19,23,102].

While the notion of SOC is particularly attractive for biological systems, a requirement of criticality is that a system can evolve its parameters quickly enough in response to changing conditions, and it is unknown if the earliest multicellular animals are endowed with such capabilities. In the classic case of the sandpile model, changing one of the system's parameters (e.g. making the sand wet) will change the pile's critical slope angle, but the sand pile will develop into its new critical morphology by the dynamics of adding more sand and the resultant flattening avalanches. In multicellular organisms, criticality can be maintained because specialized tissues like nerves and muscle can tune their excitability by an obvious feedback mechanism that allows for entrainment[135,19]. Little is known about whether tissues with similar properties exist in the earliest multicellular animals. Even if such organisms were to exist in a near-critical state due to adaptation on evolutionary timescales, it is unclear if this criticality can be responsively maintained due to changes in size or morphology that occur on faster, developmental timescales. Furthermore, even being at criticality or be-

ing an SOC system does not exclude the possibility that size could have a detrimental effect on coordination and collective decision-making.

0.2 Placozoa as a collective system for investigating coordination

Placozoa are an ideal system in which to investigate size-mediated trade-offs for coordination in the earliest multicellular animals. Placozoa are among the earliest-diverged and arguably simplest multicellular animals[153]. A more complete anatomical description is available from Smith et al.[169] and from Grell[68], but approximately Placozoa can be considered as two-dimensional cellular sheets that are three or four cell layers thick (*c.* 20 micrometers). It propels itself along surfaces with a ventral layer composed of tens of thousands of single-ciliated cells. The ventral layer is also embedded with gland cells that contain digestive enzymes which are released when the animal is atop of food, typically unicellular algae or bacteria. The dorsal layer is composed of similar, larger ciliated cells of unknown function. Importantly for coordination, the interior and ventral layer is also embedded with specialzed cells that contain neurotransmitter-like compounds, and also has an internal syncitium of specialized cells (fiber cells) that have processes resembling neurons or muscle but that have no known function.

Thought he animal has been known for over a century, it is only recently that the system has been revived for the study of animal behavior. Discovered in the late nineteenth century[158], Placozoa were initially dismissed as a larval stage of a hydra species and largely forgotten until the mid-20th century when the phylum was formally described[68]. Interest in the animal revived when new molecular evidence conclusively demonstrated that Placozoa are not derived cnidarians[61], and since then interest in Placozoa has focused on using

the organism in order to undertand the genetic and molecular requirements for simple multicellularity and to resolve the early animal tree of life[166,77,137,134,126]. A major contribution to this goal was achieved by the completion of the *Trichoplax adhaerens* genome in 2008[175]. In contrast to the genetics of Placozoa, its behavior and ecology have been largely overlooked. At the start of this dissertation in 2012, the most recent study on *Trichoplax* behavior was published in 1999[194] and the last description of Placozoa ecology was a review article from 2007[140]. There has been a small resurgent interest in the behavior of Placozoa as a pre-neural organism, with the goal of identifying how organism behaviors can be coordinated in the absence of neurons[150,168,171], but no effort has been made to integrate the present findings into the broader framework of collective behavior.

Placozoa must solve four important coordination problems that are imperative for the survival of any animal, and must do so in a decentralized fashion:

1. Placozoa must coordinate motility to find suitable habitats, nutrients, and reproductive partners. Being arguably the simplest and earliest-diverged multicellular animal with a motile dominant life stage, Placozoa coordinate this motility in the absence of bilateral symmetry, cephalizaton, or nervous system. These traits are thought to facilitate directionality and symmetry-breaking in locomotion[35,84], and therefore their absence in a motile organism is an anomaly that undoubtedly complicates the ability to establish consensus in locomotion.

2. Placozoa must coordinate behaviors involved in heterotrophy, which may include sensing nutrients, ingestion, and digestion. Feeding in Placozoa involves a well-characterized pulsing behavior that spans the entire organism's body[194,150], a behavior that is achieved in the absence of any known central control. Recent molecular ev-

idence has revealed that this behavior is coordinated by specialized cells embedded throughout the ventral epithelium of the animal that release neurotransmitter-like compounds ectopically when near food[171,168]. How this local ectopic signal cascades into an organism-wide response is largely unknown.

3. Placozoa must coordinate growth in order to regulate body size and produce morphologies that permit biological function. There is no evidence of central organization or a body plan involved in the growth of Placozoa. The animal has no known development although there are developmental signaling genes in the *T. adhaerens* genome[175]. Up until now, morphological characterization of *T. adhaerens* has progressed little beyond qualitative statements that the animal is disk-like or amoeboid, though the animal clearly has substantial inter-individual morphological variability (see Chapter 3). Nothing is known about any allometric development in Placozoa, with little theory to allow for hypotheses for what might be expected of a two-dimensional organism, and any allometry that is discovered may not have any adaptive significance and may, like SOC, simply be an emergent result.

4. Placozoa must proliferate and reproduce. Placozoa exhibit a wide variety of strategies for asexual proliferation, but almost nothing is known about how this process is regulated. The primary means of proliferation in laboratory conditions is binary fission, whereby a single Placozoa individual tears itself into two pieces, producing somatic ramets. Placozoa also has alternative forms of asexual propagation, including the producing of small spherical buds that disperse pelagically when local conditions deteriorate[186]. There is also evidence of a sexual life stage for Placozoa[58,175], though sexual reproduction has never been observed under laboratory conditions. Given

the sparse knowledge on sexual reproduction and budding swarmers, this thesis has focused on asexual reproduction through fission, which is the exclusive form of proliferation under hospitable conditions (see Chapter 2). It is unknown if this process is the result of developmental signaling that is driven by metabolic allometries, or if it is an emergent phenomenon that is produced by growth into sizes and geometries that are detrimental to coordination and therefore susceptible to fission by decision conflict[127,179].

Understanding Placozoa as a collective system requires understanding the commonalities and differences that this system has in relation to other collective systems. All collective systems can be understood in their most abstract sense as multiple similar component units expressing behaviors that are the product both of an intrinsic propensity and of the information received from a subset (possibly all) of the collective's other components[198,201,199]. This is easiest to appreciate by analyzing the commonalities of some of the well-known models of collective behavior, including the Ising model[7], the XY model[104], the Vicsek model[200], and the Kuramoto synchronization model[106,2]. Below I will describe these common properties, and how they relate to the context of *Trichoplax adhaerens*.

1. Collective systems are composed of numerous similar components. At a minimum the components within a collective system must be similar enough that they are susceptible to the same forces and environmental factors. In the case of the Ising model, one expects all components to be somewhat susceptible to magnetic fields and magnetic forces exerted by their neighbors. In the case of fish schools or flocks of birds, the behavior of all members is affected by the same visual, olfactory, and hydrodynamic cues and signals. For Placozoa, the constitutive cells of the animal are expected

to respond to chemical cues and signals, as wells as hydrodynamic and tensegrity forces exerted on the cells.

2. The components are coupled to one another. In all of these systems, components influence each other either through direct interaction or indirectly through stigmergy[54]. In *Dictyostelium* amoeba this coupling occurs through chemical signaling[67] while for swimming *Bacillus* bacteria the coupling occurs through hydrodynamic forces[45,173,53]. In the case of Placozoa, the necessity of physical contiguity undoubtedly makes tensegrity forces on cells the primary method by which their movements are coupled to one another, similar to other multicellular systems[190], though a secondary role may be played by hydrodynamic and chemical cues.

3. Collective systems are considered to be at energetic minima when there is consensus among components. As a consequence of the way in which collective behavior models are constructed, an emergent phenomenon in such models is the emergence of consensus in the absence of any external orchestration. In collective motion these consensus states are exemplified by highly ordered polarized or rotating movement[50,200], where deviations from these ordered states are caused by noise and fluctuations. In the case of synchronization systems, consensus occurs when all components have achieved the same phase, as in synchronizing fireflies[128] or ant colonies[26]. In the case of Placozoa, in keeping with other models of collective movement, the consensus state I use in chapter 1 is that of solid-body movement, the multicellular mass moves as a crystal composed of equally-spaced cells that minimize the tensegrity strain on the system. This assumption is consistent with observed inter-individual spacing in other collective systems that shows the signature of a characteristic spac-

ing consistent with Lennard-Jones type interactions[94,50,201]. A similar consensus state could be when the feeding pulsatile behavior is synchronized across the entire animal body plan, though this type of consensus is not investigated in this thesis.

At the same time, Placozoa can be characterized as a certain subclass of a collective system based on three fundamental properties:

1. Placozoa are effectively a lattice network collective system. Collectively acting systems can differ substantially in their network structure which in turn affects the behavioral dynamics of such systems[5,204]. Estimating the actual interaction network in biological collective systems is difficult[146] though different models can be evaluated based on how well they recapitulate observed collective phenomena[181]. In the case of Placozoa, there is little known about the true structure of the interaction network among cells, other than the adhaerens junctions joining adjacent cells in the epithelia[172] and a syncitium of "fiber cells" in the interior of the animal[20,185]. Given the dearth of knowledge about this network structure, I assume that such cells form a lattice-type network on a Voronoi grid, with cells (or cell clusters) communicating directly only with their nearest neighbors.

2. The interaction network in Placozoa is static on the timescale of decision-making. In addition to variability in the network structure, collective systems can also vary in how quickly the network structure changes. In the case of the Ising model the network has a fixed structure, while in the Vicsek model the network structure changes as component positions are updated and new components find themselves in each others' spheres of influence. Placozoa cells lack the tight junctions and basal lamina

found in later-diverged Metazoa[148] that stabilize the network structure of cellular tissues, but cells are nevertheless tightly compressed in a solid mass that must exert considerable steric hindrance. I therefore assume that the network structure of cells is essentially static on the time scale of decision-making in collective movement in chater 1, which is also in keeping with time scales for consensus decision-making in other animal groups[131]. Nevertheless, clearly this structure is altered substantially through the process of asexual fission and growth, and this effect is discussed to some extent in Chapters 2 and 3.

3. Placozoa are homogenous collective systems. Models of collective systems often assume that components are identical and interchangable. This assumption is invalidated in many real-world biological systems such as primate social groups that have clear hierarchies and physiological differences between constitutive individuals[180]. In the case of Placozoa, it is well-known that such animals are composed of several cell types[169], though for many of these cells their function is largely unknown. Due to the lack of tools that allow the separate visualization of each cell type *in vivo* and because at a certain spatial scale the composition of the animal becomes homogenous (see[169]), I treat *Trichoplax adhaerens* as a homogeneous bulk matter in Chapter 1. However, there is some evidence for differentiation between the bulk and boundary of this animal[157,160,169,117], which I consider in the allometry study conducted in Chapter 3.

1

Size increases produce coordination trade-offs in a simple multicellular animal

1.1 Abstract

A fundamental question in collective behavior is how the size of a decentralized system affects its coordination. This problem is apparent, for example, in the earliest-diverged mul-

ticellular animals, which must coordinate activity across decentralized body plans of indeterminate size. One interesting hypothesis for how such systems can remain coordinated across such a size range is that components within a collective might tune their responsiveness for optimal information propagation at different sizes, a phenomenon known as criticality. This phenomenon is often detected empirically by measuring how constituent components within a collective deviate from the group mean, and identifying scale-free correlations in such deviations. Such measurements, however, have never been performed simple multicellular animals. Here we present the first analysis of multicellular dynamics in one of the earliest-diverged and arguably simplest motile animal: the Placozoa. We measured the correlation structure of movement fluctuations among cells within individuals of different sizes, identifying scale-free correlations and use simulation models of elastic sheets to infer that such animals are near criticality. However, Placazoa and the corresponding critically-tuned model exhibit a substantial decrease in total correlation and collective order with system size. Thus, for decentralized multicellular animals, being poised at criticality creates a trade-off between size and coordination that may have important implication for the evolution of hierarchical structure.

1.2 Introduction

Coordination in collective systems is an area of active research in disciplines as diverse as biophysics, ecology and engineering[49,67,109,201]. One essential property of such systems is the capability of their components to execute a coordinated response to perturbations. This capability has been measured in a variety of systems through statistical inference[146,40,45,94] and agent-based simulations[200,50,76,73,81]. Coordination was also essential for the evolution

of multicellularity, as behavior at the scale of the organism is the integration of the behaviors of constitutive cells. However, the earliest multicellular organisms were decentralized (modular) entities, being composed of iterated units - polyps, zooids, ramets[71] or single cells[8] - arranged in structures of indeterminate size and morphology[84,91]. An important question in the evolution and ecology of such organisms is whether they can still coordinate organism-scale behaviors as the organism increases in size.

The earliest-diverged multicellular animals are of particular interest for investigating the effect of size on coordination in such decentralized organisms. Although they lack nervous systems, such organisms nevertheless exhibit organism-scale behaviors[150,55,111]. Though it has been argued that pre-neural behaviors lack specificity and directionality[35], a number of the earliest modular organisms show some degree of motility, which requires a directionality that in such organisms is not intrinsic to their body plans[84,194]. However, it is notable that only the smallest of such decentralized animals (e.g. the Placozoa[153]) are fully motile, while larger organisms (e.g. many Porifera species[187]) are sessile at their major life stage. Though this is considered as evidence that modular structure is detrimental to coordination at larger sizes[91], the effect of size on coordination in such systems has not been measured empirically.

Advances in biophysics, inspired by statistical mechanics, have enabled investigations on the effect of system size on coordination in biological systems. Though these methods have been applied to quantitatively understand collective behavior in a variety of biological systems[201,40,17,72,45], but similar study has yet been performed on decentralized multicellular animals, and it is unclear to what extent previous observations are generalizable to this new context. In general, these methods consider coordination as the product of forces - whether additive[200,112] or not[94] - exerted between components coupled with some intrinsic

noise[200,50,17]. The strength of these forces and noise are inferred from pair-wise correlations in fluctuations of a component's behavior about the collective state, such as deviations in a cell's movement from the movement of the whole animal. The strength of these correlations can be influenced by a wide variety of tunable parameters including the spacing[200,173], speed[22], biases[73], and noise strength[212]. As these parameters are tuned, a collective system typically undergoes a phase transition from disorder to a stable ordered state[201], but being in an ordered state that is too stable also reduces the system's sensitivity to perturbations, known as its susceptibility. In highly-ordered systems, an individual component's fluctuations are overwhelmed by the coherent forces of its neighbors, locking the system into one stable state[200,36].

One interesting hypothesis fueled by those previous studies, known as the criticality hypothesis[44,19,164], is that biological systems are tuned or poised to be at the phase transition between disorder and order[130,13]. Near this critical point the system exhibits fluctuations that span all length scales and a system's sensitivity to perturbations - its susceptibility - is maximized[207,11]. Biological systems might be poised at criticality by having their parameters - for instance, the synaptic responsiveness of neurons[78,102] - tuned to this critical point by evolution, assuming criticality has adaptive value[19,130]. Alternatively, biological systems may achieve self-organized criticality[12], adjusting its properties through self-reinforcing behaviors that drive the system to a critical point. This is a particularly attractive hypothesis for biological (finite) collectives, in which parameters needs to be continuously adjusted to match changes in system size[11,10]. Comparisons of models with empirical data[22] and direct measurement of response parameters[11] have lent support to the criticality hypothesis. The theory remains controversial however, as the statistical readouts that are often cited as evi-

dence of criticality, such as power law distributions or scale-free correlations, are also found in systems without critical tuning[81,159].

In spite of these advances in physical explanations for coordination in biological systems, very little progress has been achieved in understanding how size affects coordination in decentralized and modular animals. Studies on coordination problems in rudimentary colonial organisms, such as phototaxis in *Volvox carterii*, has revealed that performance diminishes strongly with increasing size[55]. While criticality may seem an attractive hypothesis for how decentralized organisms can coordinate across a wide range of sizes, such organisms lack specialized tissues with tunable properties such as neurons and muscle cells, both of which display critical phenomena[189,135] and which are found only in later-diverged organisms. It is therefore an open question whether early-diverged multicellular animals have the capability to coordinate at larger sizes. In this paper we investigate this question by studying the behavior of *Trichoplax adhaerens*, an animal in the early-diverged phylum Placozoa. *T. adhaerens* is anatomically the simplest animal[60,59,202,211,175], essentially a decentralized cellular carpet that propels itself across substrates by the collective action of tens of thousands of ciliated cells[169]. It is the only motile animal lacking cephalization, muscle, and neurons[154,150,153]. In the absence of any known hierarchical organization, *T. adhaerens* is assumed to coordinate cellular behaviors locally through mechanical and chemical communication[169,171]. We measured the effect of size on coordination by filming freely moving *T. adhaerens* individuals that varied in diameter by nearly an order of magnitude. We quantified the movement of ciliated cells in the ventral epithelium, and determined how correlated the velocity fluctuations between cells are at different spatial distances, comparing our observations to expected values for a system at criticality. We recapitulated our observations

with simulation models of motile multicellular sheets, revealing the importance of physical elastic interactions in reproducing our observed spatial patterns.

1.3 Results

We measured the coordination of cellular movements within *T. adhaerens* individuals using methods derived from statistical mechanics that have been applied to other mobile collectives[10,40]. These methods quantify the spatial extent of correlations among the velocity fluctuations of moving components, in this case cells. The thin, flat body plan of *T. adhaerens* allows us to quantify the general cell movement through non-invasive bright field microscopy using optical flow (Figure 1.1A). This produces a velocity field approximating the local movement of cells throughout the animal for every half-second increment (Figure 1.1B). By combining this microscopy setup with an automated stage, we were able to image each of our 84 sampled animals continuously for at least two hours, ensuring that our measurements accurately capture the statistics of cellular movements within *T. adhaerens*.

We extract the velocity fluctuations describing local movement relative to collective motion by removing the collective modes of movement from the full velocities. We perform this extraction for every instantaneous velocity field for every animal using a method developed by Cavagna *et al.*[40] and expanded upon by Attanasi *et al.*[10], which we elaborate upon in the Methods section. This method removes the translational, rotational and dilatational collective modes of movement observed in *T. adhaerens* (see Supporting Information). Figure 1.1C displays the velocity fluctuation fields corresponding to the velocity fields in Figure 1.1B. The fields exhibit large spatial domains of correlated and anti-correlated fluctuations both in direction and speed that are more than an order of magnitude larger in diameter

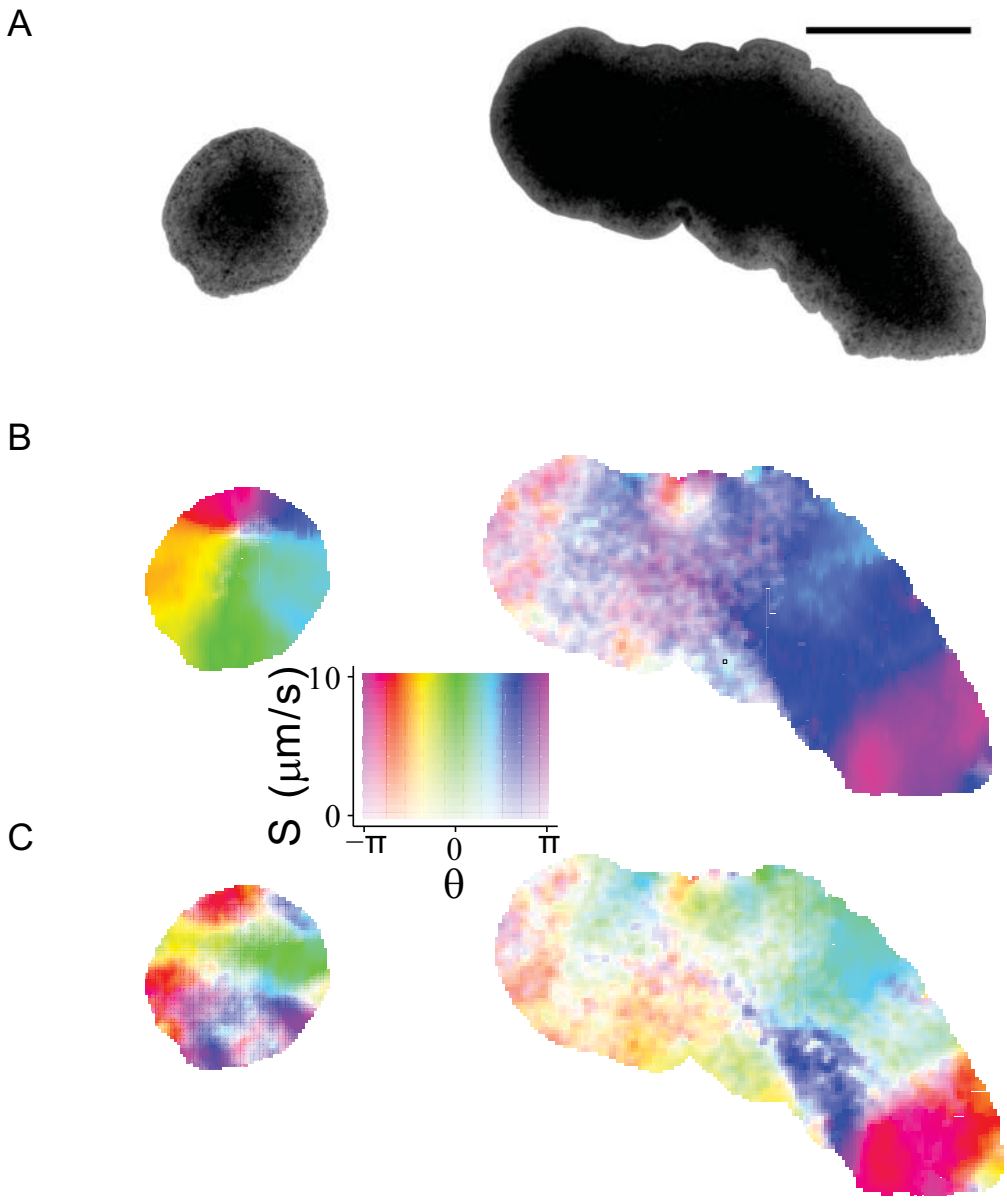

Figure 1.1: Velocity fluctuations have long-range correlations in *T. adhaerens*. (A) Images of two representative *T. adhaerens* individuals, shown to illustrate size variability. Scale bar is 0.5 mm. (B) The instantaneous local full velocities within those respective animals. The color map represents the velocity heading while opacity signifies speed. The animal on the left is rotating while turning whereas the animal on the right is gliding to the upper-right. (C) The instantaneous velocity fluctuations after subtraction of collective movement. Larger animals exhibit larger correlated domains. For dynamics see video SI_Fields.avi.

than the constituent cells. In the case of our two representative animals, we observe that the larger animal exhibits larger correlated domains. This suggests the presence of scale-free correlations, where the size of correlated domains scales with the system size, an often-cited indicator of self-organized criticality[130,40,45].

We measured the strength of pair-wise correlations among velocity fluctuations at different spatial distances in animals of different sizes using equation 1.1. This calculates the correlation between all pairs of local velocity fluctuations u_i and u_j, separated by a Euclidean distance r_ij. The summations and Kronecker delta function $\delta(r - r_ij)$ allow for measurement of the mean correlation for each separation distance $C(r)$. We normalize the correlations at all pair-wise distances by a constant c_o such that $C(0) = 1$. We define the relationship between the mean correlation between fluctuations and the Euclidean distance as the correlation profile. Similar equations are used to determine the directional and speed correlation profiles (see Methods). The range of the correlation profile is bound between 1 (perfect correlation) and -1 (perfect anti-correlation), with 0 signifying no correlation on average.

$$C(r) = \frac{1}{c_o} \frac{\sum_{ij} u_i u_j \delta(r - r_{ij})}{\sum_{ij} \delta(r - r_{ij})} \tag{1.1}$$

Figure 1.2A, C, and E show the mean correlation profiles for all animals in our dataset, where each profile is the mean of 100 randomly-selected instantaneous correlation profiles. By construction, every profile begins at $C(0) = 1$ and, due to the removal of any mean contribution, integrates to zero[40]. The profile must therefore possess domains of both positive and negative correlation. A correlation profile of random fluctuations would exhibit an arbitrary structure with multiple zero-crossings. Our system, however, exhibits a

strong spatial pattern, with the velocity (A), directional (C), and speed (E) pair-wise correlations possessing only one positively-correlated domain with correlation strength decreasing monotonically with increasing distance, with a singular singular zero crossing $C(\varphi) = 0$. There is no observable distance beyond which correlations are negligible, but rather the entire profile shows substantial positive and negative correlation.

The correlation profiles in Figure 1.2 indicate that the zero crossing distance φ, referred to as the correlation length in other studies [40,41] (though note that correlation does not asymptotically drop to zero beyond this point), increases with animal size. This proportional increase suggests the presence of scale-free correlations, with characteristic linear scaling observed for velocity (1.2B), direction (D), and speed (F) fluctuations. This pattern holds for animals varying in diameter by nearly an order of magnitude, comparable to previous studies [40,45,72,11]. Our observations also span the typical size distribution of *T. adhaerens* reared in laboratory conditions, which ranges from 200 to 1,000 micrometers in diameter [139]. Animal size in this case is a reflection of the cell count within an animal, with no evidence that cell size or density changes with animal size (Supporting Information and Smith *et al.* [169]). We are confident, therefore, that our observations describe how coordination scales with the number of component cells across the natural size variation.

Although the correlation length scales proportionately with animal size, we find that the total correlation within an animal decreases systematically with animal size, implying a decrease in collective order. When we transform the correlation profile of each animal in a scale-invariant form, $K(\frac{x}{\varphi}) = C(x)$, we observe that the data do not collapse on a single generic function, in contrast with other systems exhibiting scale-free correlations [45,40,41]. Instead, $K(\frac{x}{\varphi})$ decays faster in larger animals((Figure 1.3A). We quantify this effect by measur-

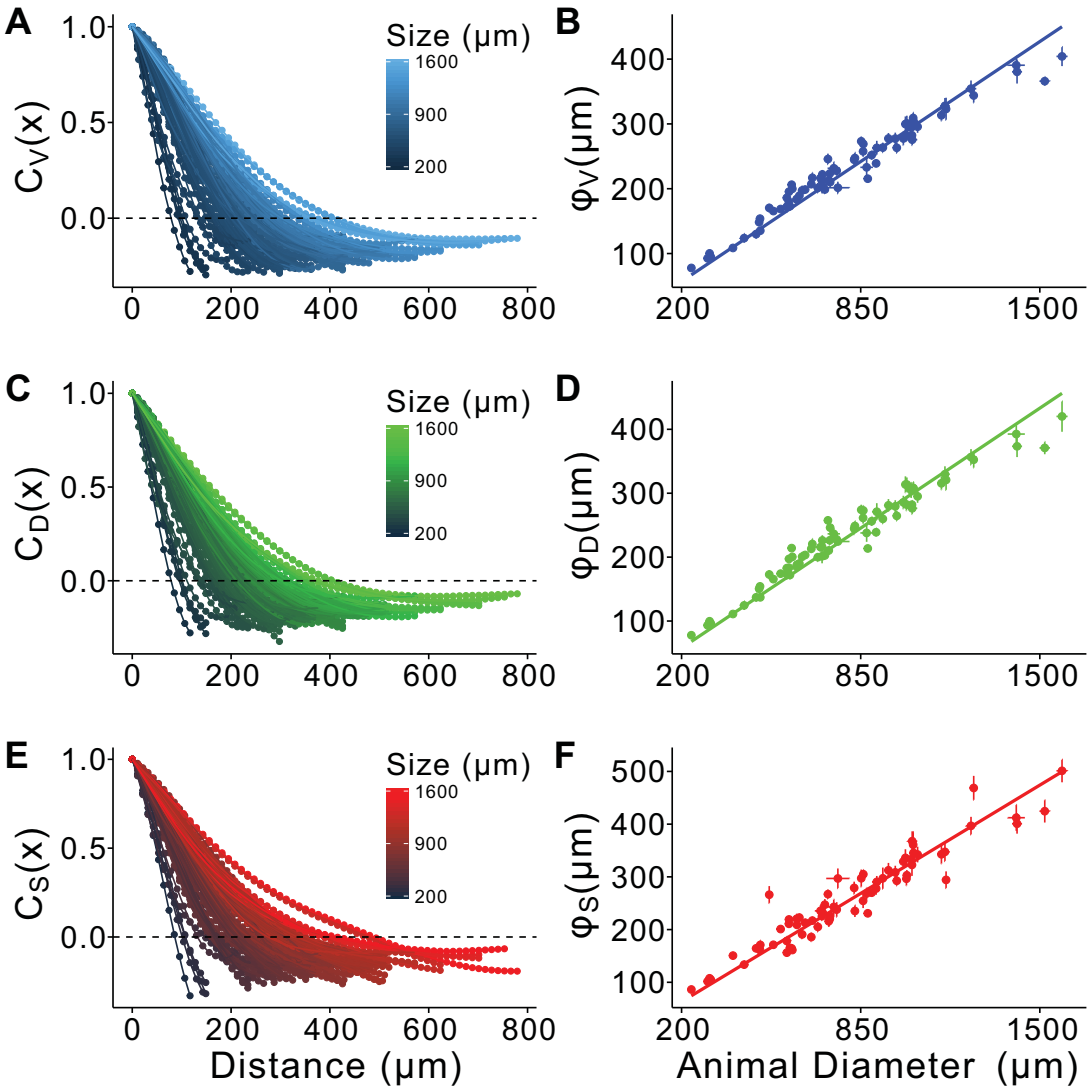

Figure 1.2: The spatial range of correlations increases linearly with animal size. The average velocity (A), direction (C), and speed (E) correlation profiles for all animals, with brightness proportional to animal diameter. All profiles decrease monotonically to $C(\varphi) = 0$, where φ is the size of the positively-correlated domain. φ increases linearly with animal size for all three measures: velocity correlation (B; $\beta = 0.29, p < 10^{-}16$), directional correlation (D; $\beta = 0.29, p < 10^{-}16$), and speed correlation (F; $\beta = 0.29, p < 10^{-}16$). Error bars are standard error determined by variability in the zero-intercept for 100 instantaneous correlation profiles.

ing the maximal cumulative correlation $Q(r)$, defined in equation 1.2, which is analogous to its finite-size susceptibility χ[10,11]. Here $\vartheta(r - r_{ij})$ is a Heaviside function that is 1 when $r_{ij} < r$ and 0 otherwise. We find that χ increases sub-linearly with the animal's diameter (Figure 1.3B), suggesting that fluctuations are more strongly damped in larger animals (sub-linear model: $\chi = \alpha D^{\beta} + \gamma$; $\alpha = 36.6$; $\beta = 0.296$; AIC $p < 10^{-4}$).

$$Q(r) = \sum_{i \neq j}^{N} u_i u_j \vartheta(r - r_{ij}) \tag{1.2}$$

The sub-linear scaling of susceptibility has two important consequences for the collective locomotion of *T. adhaerens*. At the scale of the organism, it becomes increasingly difficult for larger animals to establish a collective mode of locomotion, with mean collective order (see Methods) roughly 50 percent lower in the largest than in the smallest animals (Figure 1.3C). At the cellular scale, the fraction of kinetic energy in dissipated in fluctuations, $\omega = \frac{1}{N} \sum_{i=1}^{N} \frac{\|u_i\|}{\|v_i\|}$, doubles between the smallest and largest animals (Figure 1.3D), a direct result of the sub-linear scaling of susceptibility and the decreased propensity for collective order. Increasing size in *T. adhaerens* therefore has a detrimental effect on ordered collective locomotion in *T. adhaerens*.

It is unclear whether the effect of size on the correlation length, susceptibility, collective order, and locomotion efficiency in *T. adhaerens* is a generic consequence of the physics of such cellular sheets, or whether they only occur under in a restricted parameter space. The presence of scale-free correlations in particular is often argued to be an indicator of criticality[207,130], though such correlations can also be generated trivially in certain circumstances[159,81]. We used a self-propelled particle (SPP) model of collective movement, derived from a model developed by Szabó et al.[183] to describe the collective migration of cells, to

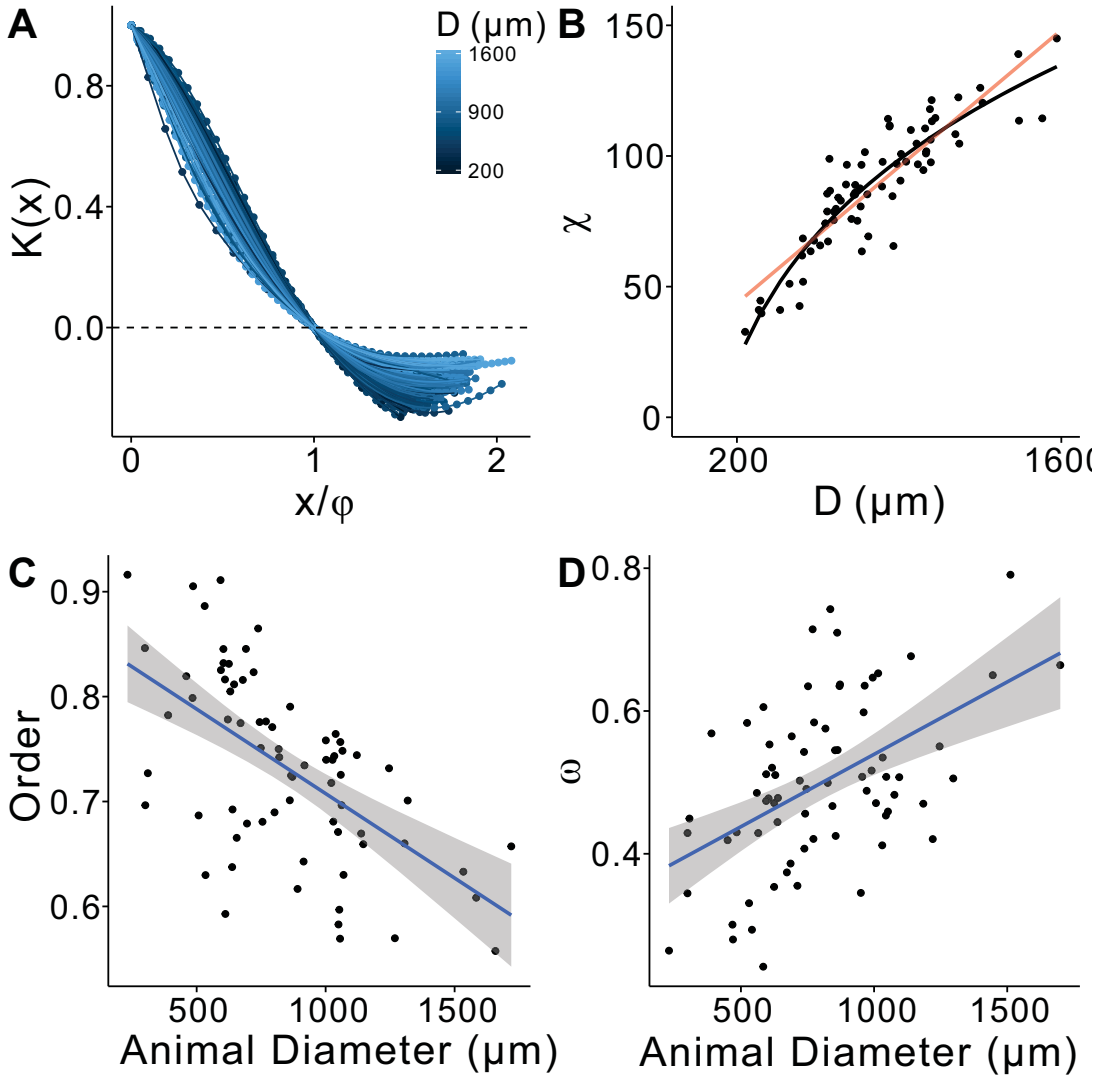

Figure 1.3: Collective locomotion in *T. adhaerens* becomes increasingly disordered at with increasing size. (A) The velocity correlation profiles of all animals rescaled by their respective zero-intercept with color indicating animal diameter. (B) Susceptibility χ increases sub-linearly with animal diameter, with the sub-linear fit (black line: $\chi = \alpha D^{\beta}$) compared to the linear model (red line, AIC-based probability of linear model: $p < 10^{-9}$).

provide corroborating evidence for whether *T. adhaerens* is or is not at criticality. Our simulated system is a two-dimensional sheet of SPP's coupled by spring-like interactions on a Voronoi network with some intrinsic noise η that has a constant intensity for all particles (see Methods). The size and location of our particles approximates the internal fiber cell network within *T. adhaerens*. Figure 1.4A shows an instantaneous snapshot of the velocity fluctuations of each cell in one simulated animal. We simulated systems that ranged in size by over an order of magnitude in linear dimension, and for values of η spanning the entire range for which our simulations were stable. We estimated the critical noise, η_C, by using the the Binder cumulant $U = 1 - \frac{\langle v^4 \rangle}{3\langle v^2 \rangle^2}$ [24], where v is the ensemble average velocity for each system. By plotting U as we systematically vary η for various system sizes L, and estimate η_C from the common intersection point of these curves[25]. In the case of our system, η_C occurs between 0.3 and 0.35 (Figure 1.4B).

We find that the scaling effects observed for *T. adhaerens* are only recapitulated by simulations near the critical point η_C. Firstly, both the scale-free correlation lengths (Figure 1.4C) and the sub-linear scaling of χ with system size (D) occur for a variety of values of η; these scaling phenomena are therefore generic to such systems. However, we find that system size has a substantial effect on the collective order (E) and the relative fluctuation energy (F) only when the system is poised near η_C, which is the range at which a second-order phase transition occurs between ordered and disordered states of collective movement. Our simulations thus provide evidence that the size-mediated effects on collective movement in *T. adhaerens* are a consequence of such systems being poised at criticality where increasing the system size - in the absence of any adjustment of a control parameter - naturally produces more disordered locomotion.

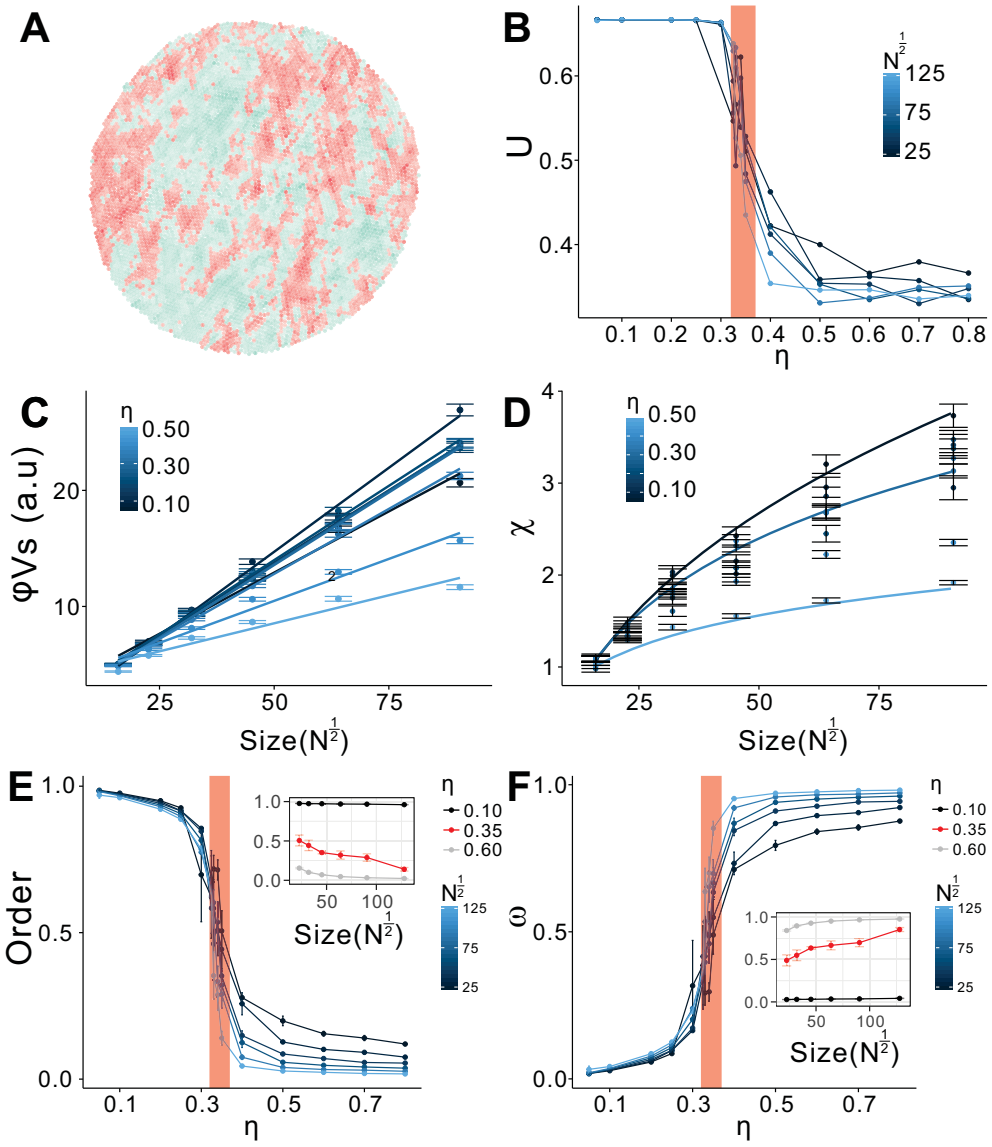

Figure 1.4: Elastic networks at criticality replicate the scaling phenomena in Placozoa. (A) Snapshot of velocity fluctuations in simulation for a simulated lattice (N = 8,192 particles). (B) The Binder cumulant for systems of varying in size and η. The intersect of the curves (red highlight) for system of different size occurs in the $0.3 < \eta_C < 0.35$. (C) The effect of size and η on the correlation length and (D) susceptibility. Sub-linear model fits shown for η at 0.1, 0.3, and 0.5. (E) Phase transition in collective order as η is increased (F) Phase transition in ω in simulations at varying noise levels (insets: effect of size on order and ω when η is 0.1, 0.6, and η_C).

1.4 Discussion

The internal dynamics of *T. adhaerens* statistically resemble those of systems near criticality, though one where the control parameter does not adjust to match changes in system size, which has several important consequences for collective locomotion. The sub-linear increase of susceptibility with animal size implies that such decentralized cellular sheets face a trade-off between size and responsiveness. This decreased responsiveness is likely the cause for the more disordered motion of larger animals, where a greater extent of the overal kinetic energy within the naimal is channeled into fluctuations. Qualitatively these size-mediated effects result in an increased propensity of larger *T. adhaerens* to deform, as local perturbations produce fluctuations do not propagate effectively across the animal. *T. adhaerens* thus faces a trade-off between increasing size and maintaining coherent locomotion. At the same time, our simulations reveal that scaling patterns such as scale-free correlations and the sub-linear increase in susceptibility arise generically in elastic sheets, indicating that caution is needed when relying solely on such measures to infer criticality. It is likely that such scaling is the consequence of kinetic energy being channeled into the lowest-energy vibrational collective mode, as demonstrated in previous studies of simulated mobile elastic sheets[81,63], which scales with system size for an elastic sheet. Our analysis expands upon those previous studies by elucidating how the system size affects the overall structure of the correlation profiles. Our observations stand in contrast to those on fluid-like collective systems like flocks of birds[40], schools of fish[191,72], and swarms of midges[10] and provide the first evidence that decentralized multicellular systems face trade-offs between size and coordination.

It may appear counter-intuitive that size has a stronger effect on susceptibility and order in contiguous animals than in animal groups. This is not surprising however when we consider that both are decentralized systems, with multicellular collective motion representing a more constrained version of collective movement with fewer parameters that can be tuned in response to changes in system size. For instance, strong volume-exclusion forces between cells prevent large local density fluctuations that were identified as an important tunable parameter in swarms of midges[11]. Cells in multicellular sheets, when compared to animal groups, are limited both in their sensory capabilities and the repertoire of effectors that can be used to respond to stimuli. Likewise, inter-cellular junctions in multicellular systems inhibit neighbor-switching, a phenomenon that could enhance information propagation in animal groups[23] (though see[131] for the relevant timescales). The sum total of these capabilities likely help poise animal groups near criticality[22], and their absence likely cause the size-mediated consequences for energetic efficiency (order) and responsiveness (susceptibility) in multicellular sheets.

Our study has several limitations, however, though these do not compromise the generalizable nature of our observations. One limitation is our simplified representation of *T. adhaerens* as a cellular sheet, abstracting its true but functionally-unknown anatomy. In particular, it is unclear if the internal fiber cells in *T. adhaerens*, whose function and network structure is unknown, is involved in coordination. Although previous hypotheses that these cells are neural or muscular precursors[68,20] were dismissed by more recent anatomical studies[169], there is still too little known about their network structure or process lengths to discount them having some role in coordination. In the absence of contradictory evidence, we have assumed that the number of such cells increases in proportion to

the animal's size with no substantial changes to their network topology or physical characteristics. *T. adhaerens* also possesses specialized cells that bind to neurotransmitter-like molecules[157,169] that were recently reported to arrest the beating of nearby cilia during feeding bouts[168,171]. However, nothing is known about their role in guiding locomotion outside of feeding, which is the context of our study.

We have found evidence that *T. adhaerens* are near-critical systems, but currently lack a theory of these organisms maintain such a state in the absence of clear biochemical feedback loops as in neurons. One interesting possibility is that the components in a system do not tune themselves to match the system size but rather that the system size adjusts itself for optimal coordination purely from the intrinsic responsiveness of the components[11,65]. Under this hypothesis, systems that grow beyond an effective coordination size will fragment to smaller size due to some decision conflict. This is a particularly attractive explanation for animals such as *T. adhaerens*, an organism that reproduces by asexual fission. Nothing is known about the cause for this reproductive process, though it is expected that such animals will fission at smaller sizes in nutrient-poor environments[161]. One possible mechanism linking these two phenomena is that starvation effectively agitates the locomotor activity of constitutive cells in *T. adhaerens*, effectively increasing η. This produces increased locomotor activity under starvation conditions[194], decrease the collective order, and allow for directional conflict within larger animals that results in force-mediated fission.

Our approach extends the knowledge of collective systems to provide insight into the effect of size variation on coordination in the earliest multicellular animals. We view this as part of a larger effort to reveal not only how system-wide coordination can be achieved spontaneously[48,47], but also to identify the limitations of such decentralized decision-

making. The detrimental effect of size on coordination in such decentralized animals reveals the limitations of such organization and provides a driving force for the evolution of hierarchical structures. If decentralized animals face a trade-off between increasing size and coordination, then the need to grow to bigger[28] while overcoming this trade-off would have motivated the evolution of hierarchically-structured specialized tissues such as muscle and nervous systems.

1.5 Materials and Methods

1.5.1 Data Acquisition

T. adhaerens were reared in 150 mm diameter petri dishes with 100 mL of artificial seawater at 35 parts per thousand concentration (35 ppt ASW, Instant Ocean Reef Crystals). Animals were fed a diet of *Rhodomonas salina* reared in algae growth media (35 ppt ASW + 1:1000 f/2 Guillard's growth media). Animals were sampled from exponentially growing cultures, with fresh cultures seeded every two weeks. Before imaging, animals were washed by successive transfer into three dishes of sterile ASW and kept isolated from food for 12 hours. Each animal was transferred to a recording tank containing 5 mL ASW and imaged under bright field microscopy at 40x magnification using a Photometrics CoolSnap or a Hammamatsu ORCA 4.0 monochrome camera. Distances were calibrated with a measurement slide. Images were acquired at 2 Hz for a duration of at least 2 and at most 8 hours, a time period that is insufficient for a significant change in starving animals.

1.5.2 Tracking and measuring velocity fields

We developed an in-house MATLAB software to segment the animals in each frame, ignoring frames where part of the animal was outside of the camera's field of view or where the stage was moving. We defined the animal size as the area enclosed within the animal's two-dimensional footprint, with the animal diameter defined as the diameter of a circle of equivalent area. To minimize measurement error in size caused by out-of-plane buckling of the animal, we only considered frames where the observed area was at least 80 percent of its maximum observed area. We found no trend of cell size with animal size (Supporting Information), in accordance with histological studies[169]. We computed the optical flow between frames using software described in[72], keeping only vectors within the animal's footprint for further analysis, providing the instantaneous velocity $v_i(t)$ for each 100 square micrometer region i at all times t.

1.5.3 Calculating velocity fluctuations.

Vectors within a distance of 10% of the animal diameter from the boundary removed from further analysis. We isolated the velocity fluctuations from the full velocity vectors by subtracting the translational, rotational, and dilatational collective modes of movement from each vector. Each cell cluster i has a position y_i in relation to the center of mass of the animal as defined in 1.3.

$$\mathrm{y}_i(t) = \mathrm{x}_i(t) - \frac{1}{N}\sum_{k=1}^{N} \mathrm{x}_k(t) \tag{1.3}$$

We can use each cell cluster's relative position, its velocity, and the mean velocity $\langle \mathrm{v} \rangle =$

$\frac{1}{N}\sum_{k=1}^{N} v_k$, to determine the expected future position of each cell cluster relative to the expected future center of mass:

$$\mathrm{y}_i(t+dt) = \mathrm{y}_i(t) + \mathrm{v}_i dt - \langle \mathrm{v} \rangle \, dt \tag{1.4}$$

We then determine the velocity fluctuation using equation 1.5 for each cell cluster at any given time, $u_i(t)$, as the difference between the future relative position and the affine transformation of the present position with an optimal rotation matrix R and a dilatation factor Λ. We define optimality as the values of R and Λ that minimize the total positional deviation defined in equation 1.6.

$$\mathrm{u}_i(t) = \mathrm{y}_i(t+dt) - \Lambda \mathrm{R} \mathrm{y}_i(t) \tag{1.5}$$

$$\varepsilon = \sum_{k=1}^{N} \left\| \mathrm{y}_k(t+dt) - \Lambda \mathrm{R} \mathrm{y}_k(t) \right\| \tag{1.6}$$

In the case of solid-body translation, rotation or expansion, $y_k(t+dt)$ is an affine transform of $y_k(t)$ with $\varepsilon = 0$. The fluctuations of a vector differ from 0 only if the future positions of the cell clusters cannot be explained by an affine transform of the present positions. To further safeguard against trivial sources of correlation through off-center rotation or sharp turning, we only considered velocity fields recorded at times when the where the centroid trajectory curvature $\Gamma(t) = \frac{V(t)}{L(t)} < 0.7$. $\Gamma(t)$ is dependent on the ratio of the vector displacement $V(t) = \left\| x(t_f) - x(t_s) \right\|$, with the path chord length $L(t) = \sum_{t_i=t_s}^{t_{f-1}} \| x(t_{i+1}) - x(t_i) \|$. We considered that a separation of 15 seconds between t_f and t_s was sufficient to capture the path curvature.

1.5.4 Correlation profiles

In addition to the velocity correlation function defined in 1.1, we also determine the directional correlation $C_D(r)$ and the speed correlation $C_S(r)$ defined as

$$C_D(r) = \frac{\sum_{ij} \mathrm{w}_i \mathrm{w}_j \delta(r - r_{ij})}{\sum_{ij} \delta(r - r_{ij})} \tag{1.7}$$

$$C_S(r) = \frac{1}{c_o} \frac{\sum_{ij} \eta_i \eta_j \delta(r - r_{ij})}{\sum_{ij} \delta(r - r_{ij})} \tag{1.8}$$

Here δ and c_o have the same meaning as in equation 1.1. $\mathrm{w}_i = \frac{\mathrm{v}_i}{\|\mathrm{v}_i\|}$ is the unit vector of the velocity fluctuation of cell cluster i and η_i is its speed fluctuation with respect to the global mean speed, $\eta_i = \|\mathrm{v}_i\| - \frac{1}{N} \sum_{k=1}^{N} \|\mathrm{v}_k\|$.

We measure the slope of the correlation profile at the zero-corssing using the five-point stencil method, fitting a second-order polynomial to the points closest to the crossing and then evaluate the slope as the first derivative of the fitted function at the crossing. We measured the susceptibility (integral) of the correlation profile by applying a cubic spline fit of the average correlation profile, interpolating 100 evenly-spaced data points across the domain, and then integrating using Simpson's rule.

1.5.5 Collective Order

We define three modes of collective movement: polarization P, rotation R, and dilatation Λ using equations 1.9-1.11. Here N is the number of regions in an animal and $\hat{r}_{ic}$ is the unit vector from the animal center of mass to the region, while $\hat{v}_i$ is the unit vector of its velocity. These three measures can be combined into a Euclidean distance $O = \sqrt{P^2 + R^2 + \Lambda^2}$,

which ranges from 1 (movement as a solid crystal) to 0 (completely uncorrelated movement across the animal).

$$P(t) = \frac{1}{N}\left|\sum_{i=1}^{N} \hat{v}_i\right| \tag{1.9}$$

$$R(t) = \frac{1}{N}\left|\sum_{i=1}^{N} \hat{r}_{ic} \times \hat{v}_i\right| \tag{1.10}$$

$$\Lambda(t) = \frac{1}{N}\sum_{i=1}^{N} \|\hat{r}_{ic} \cdot \hat{v}_i\| \tag{1.11}$$

1.5.6 Self-propelled Particle Model

We model indivdual *T. adhaerens* as ensembles of N coupled self-propelled particles in two spatial dimensions, using a modification of the model introduced by Szabo et al.[183]. The displacement of each cell i is given by an overdamped equation of motion

$$\frac{d\mathrm{r}_i}{dt} = v_0 \hat{\mathrm{v}}_i(t) + \mu \sum_{j \in N_i} \mathrm{F}_{ji}(\mathrm{r}_j, \mathrm{r}_i) \tag{1.12}$$

with r_i being the position vector, v_0 the self-propulsion speed, $\hat{\mathrm{v}}_i$ the unit vector determining the self-propulsion direction, μ the mobility of the focal particle, and F_{ji} the spring-like attraction-repulsion forces resulting from the coupling to the neighboring cells. The unit vector of the self-propulsion $\hat{\mathrm{v}}_i = (\cos\varphi_i, \sin\varphi_i)^T$ is determined by the polar angle φ_i,

which evolves according to:

$$\frac{d\varphi_i}{dt} = \frac{1}{\tau}\sin(\vartheta_i - \varphi_i) + \eta_i(t) \tag{1.13}$$

with ϑ_i being the polar angle of the total attraction-repulsion force $\mathrm{F}_i = \sum_j \mathrm{F}_{ji}$: $\vartheta_i = \arctan(F_{i,y}/F_{i,x})$. Thus, ϕ_i relaxes towards the force direction with a characteristic time τ. Finally, $\eta_i(t)$ is Gaussian white noise with vanishing correlations. Each particle interacts only with its direct Voronoi neighborhood, and we assume a fixed interaction topology (no neighbor switching). Further model and simulation details are given in the Supporting Information.

2

Size Regulation as an Emergent Phenomenon in *T. adhaerens*

2.1 Abstract

The regulation of growth and size is paramount to any biological organism's fitness, with size affecting numerous aspects of an organism's ecology. While some organisms grow to

genetically or ontogenetically determined sizes, many of the earliest multicellular animals have a colonial or decentralized structure that permits growth to indeterminate sizes and allows for the continuous adjustment of size in response to changing environmental conditions. This responsiveness occurs through growth, degrowth, and vegetative reproduction through fission. We study the dynamics of population size and size structure of *T. adhaerens* proliferating in environments with differing nutrient conditions, and analyze the dynamics of growth and asexual fission to understand the processes that result in the observed size structure. We show that growth is regulated in response to nutrient conditions, but that the propensity to fission at a given size is independent of the nutrient richness of the environment. These results suggest that asexual fission in Placozoa is an emergent phenomenon, driven by decision conflict at sizes larger than a certain threshold, and the observed size variability across environments is caused by changes in growth rate rather than the propensity to fission.

2.2 Introduction

Size is the fundamental determinant of numerous ecological and life history traits for any organism[28,42]. For animals, size affects numerous factors including predator-prey associations, energetics[162], intra- and inter-specific competitiveness, and in some cases even the sex of an individual (for a comprehensive review, see Ebenman, 1988[57]). The regulation of size is therefore paramount to an organism's survival and fitness. While most organisms grow to sizes that are pre-determined either genetically or ontogenetically, known as determinate growth, there is a class of organisms capable of indeterminate growth whereby they can rapidly adjust their size and growth in response to changing environmental con-

ditions[163,161]. Such indeterminate growth is often facilitated by animals being capable of substantial growth, degrowth, and asexual reproduction.

The problem of size control is particularly complex when size determines not only an individual's survival and metabolic efficiency, but also its fecundity, especially when these two aspects affect one another directly. If these factors do not interact, it is typical for an organism to grow to a metabolic optimal size and then invest any energetic surplus into reproduction to the exclusion of further growth[141]. This idealized strategy typically does not occur in animals of indeterminate growth when the optimal size for reproduction differs from the metabolic growth optimum, which can occur for a variety of reasons (e.g. mate competition, gonad size limitations, *etc.*, see Sebens (1987)[161] and Charnov (2001)[43] for more examples). One particularly interesting problem is when asexual propagation involves a substantial loss of somatic tissue, such that growth and reproduction are directly antagonistic processes. In spite of the storied existence of many of the aforementioned ecological models for indeterminate growth, there has not yet been an empirical study on the interaction of vegetative fission and growth.

The marine colonial organisms, among the earliest examples of multicellularity, are a good model organism for studying the interaction of these growth and asexual propagation. These earliest forms of multicellularity grow to indeterminate sizes and, due to their great regenerative capabilities, can produce asexual propagules by a wide array of mechanisms including fragmentation and fission[84,83,165]. Additionally, such organisms can rapidly adjust their growth (and degrowth) rates to match environmental conditions[161]. Fission and fusion are typically the dominant processes that determine the size structure of populations of such species, erasing any correlation between age and size[87]. This process also typically

serves as the major source of local population growth (defined by number of new individuals)[92,93], such that one clone can quickly dominate a local environment by producing multiple clonal ramets through asexual fission[79]. Therefore, understanding how fission is regulated is essential to understanding fitness and competitive dynamics in benthic marine ecosystems.

In spite of the importance of fission for a population's size structure, little is understood about how this process is regulated is regulated in these early examples of multicelluarity. Both fragment survival[79] and fragment growth rate[165] are strongly dependent on the initial fragment size, so the ability to regulate the size of fission products - by the size of the parent animal and the fraction of that size given to the daughter - has adaptive value. The dominant ecological theory on sessile organisms holds that fission in such benthic organisms is the reult of extrinsic forces such as storms or tissue degradation[84], though the size the produced fragments may be biased in an emergent fashion by the geomtry of growth[179,93]. In motile organisms, fission may generated by intrinsic forces caused by antagonistic pulling of different parts of an animal[120,147,127], though little is known about what sorts of environmental conditions instigate this process.

Metabolism is considered the major factor affecting size[161,162,163], but to date no empirical study has been performed on whether fission dynamics are adjusted when such constraints are relaxed or exacerbated. While we may be tempted to extrapolate from metabolic theory of animals with unitary body plans to animals with decentralized construction, this is often inaccurate[210]. Taking the example of metabolism, which is known to scale in an allometric fashion in animals with unitary body plans, following a well-known $\frac{3}{4}$ power law[205]. One could imagine that this rule applies to modularly-constructed or colo-

nial animals that grow in three dimensions, caused by factors such as nutrient diffusion and self-shading in resource capture[100]. Nevertheless, in the case of filamentous or two-dimensional colonial growth, there is some evidence that metabolism scales linearly with colony size[82,163,149]. Organisms with such geomtries, including the Placozoa, are the most likely to exhibit metabolic isometry[85], and it is likely that motility further relaxes allometric constraints on resource acquisition.

We used experimental cultures of the Placozoa species *Trichoplax adhaerens* to determine the dynamics of size regulation through growth and fission in response to varying nutrient conditions. Placozoa are motile multicellular animals that are effectively two-dimensional cellular sheets with amoeboid shape. They are the morphologically simplest and among the earliest-diverged multicellular animals[175,153,140]. Placozoa are benthic organisms that graze on deposited microalgae on hard substrates, ingesting nutrients through their ventral epithelium. Due to their geometry, the ventral feeding surface of Placozoa scales linearly with the animal's overall size. Placozoa reproduce asexually by fission, a phenomenon that has been known for over a century[158] but whose regulation is still unknown. Sparse data on the animal's proliferation[140,74] suggests that animals reach a stable mean individual size in experimental cultures, but the substantial variability around this mean[139] could indicate that such stability is simply a statistical property of increasing population size, rather than evidence of regulation. Here we report the first systematic study of size regulation in such organisms in response to changing nutrient conditions. We record the population dynamics and size structure of clonal ramets under different nutrient conditions, and identify the causal changes in growth rates and propensity to fission. We further develop a simulation model to investigate the optimality of the parameters that govern size regulation in *T. ad-*

haerens, and discuss the development of a high-throughput experimental setup that can allow us to estimate such parameters in Placozoa.

2.3 Results

The first indicator that Placozoa adjust their growth or fission in response to varying nutrient conditions is if there is any change in population size or size structure when animals are grown in different conditions. We cultured *T. adhaerens* from clonal ramet populations that were identical in initial size, growing them in artificial seawater (ASW) seeded with *Rhodomonas salina* microalgae at a concentration of either 0.20 or 0.40 optical density (OD). Animals proliferate under such conditions for one week (Figure 2.1A) before cultures begin to degenerate, indicated by a decline in the population size. Though we find that environments richer in nutrients tend to support larger populations of *T. adhaerens*, this difference is not statistically significant, even when the difference in population size between these two conditions is maximal (at 84 hours; Welch Two Sample t-test: $t = -1.53$, $df = 5.18$, $p = 0.19$). In contrast to the total number of individuals, we find that the mean size of individual ramets is highly dependent on the nutrient condition in which these organisms are reared. Though we used founding populations for both conditions that were identical to each other with regard to the mean ramet size (Figure 2.1B; Welch Two Sample t-test:$t = -0.58$, $df = 26.3$, $p = 0.56$), after around three days (84 hours) of growth in different conditions the mean ramet size between the two conditions was highly significantly different (Welch Two Sample t-test:$t = -5.59$, $df = 91.7$, $p < 5 \times 10^{-7}$). Not only did the size structure of these meta-populations diverge over time, but they also diverged from their initial size structure (Welch Two Sample t-test: OD 0.20: t = 3.30, df =

41.6, p = 0.002; OD 0.40: t = -1.93, df = 46.6, p-value = 0.06). These results suggest that *T. adhaerens* adjust their proliferation strategy in response to changing nutrient conditions, which could occur either by changing their growth rate, their rate of asexual fission, or both of these processes.

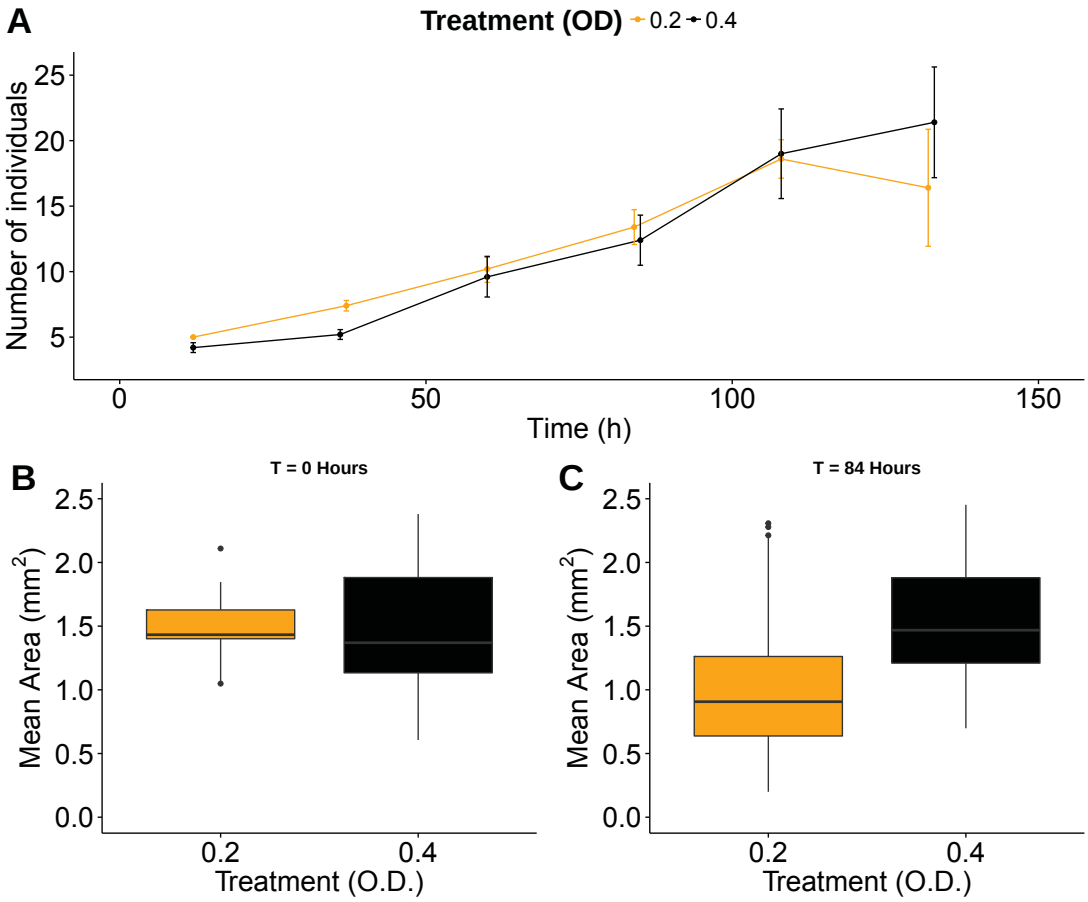

Figure 2.1: Placozoa proliferation under varying nutrient conditions. (A) Cultures of *Trichoplax adhaerens* grown in ASW of either 0.20 or 0.40 OD of *R. salina*. Measurements are averaged over five simultaneous replicates for each condition, each culture started with a population of 5 randomly selected ramets. Error bars represent standard error. Error increases at the end as some cultures suffered population collapse before others. (B) Mean ramet size of the founding populations under each condition. Error bars represent standard error on the mean value. (C) Mean ramet size for each condition measured at the time of maximum population size. Error bars are the same as in (B). The final size distributions are significant different across conditions, and are significantly different from the initial size distributions in their mean value.

Identifying which of these two factors - growth and fission - contribute to the observed size structure requires the ability to track the proliferation fate of individuals of varying size. We do so by imaging one of the culturing dishes used in the previous experiment over 24 hour time periods at a sufficiently high time resolution to track and maintain the identity of each animal throughout the entire recording. The largely two-dimensional body plan of *T. adhaerens* enables the quantification of animal size through tracing of the animal boundary. Feeding Placozoa have high dynamic variability in footprint size[139,194], which we can overcome by measuring the average footprint size of the animal over a 10 minute interval, or one complete feeding bout. By measuring the initial animal size, determining whether the animal fissions, and recording the final animal size after 24 hours when fission did not occur, we can discern how these mechanisms are regulated to produce the observed population structures.

We measure the growth response to nutrient conditions by considering, for any animal which did not fission, what was its size at an initial time point of recording and its size after 24 hours of growth in such conditions (Figure 2.2A). We identify the factors that contribute to the final animal size by linear regression. Because we do not know the response curve of growth to nutrient condition at all possible animal sizes, we treat the growth conditions as factors in our analysis and observe simply if growth is different between the two conditions. As expected, the initial animal size has a highly significant effect on the final size after 24 hours of growth ($t = 7.27; p < 5 \times 10^{-5}$). Though nutrient concentration is not a significant factor ($t = -1.84; p = 0.09$), the interaction of organism size with nutrient concentration is significant ($t = 3.00; p = 0.01$). The predictive strength of this regression, which contains only the two most essential factors, is striking, with a very high correlation

coefficient and a very high significance of the fit in general (adjusted $R^2 = 0.98$; $p < 10^{-10}$).

Another measure of ecological importance, in addition to the final sizes attained by each ramet, is each ramet's production of new clonal biomass or the net growth. We quantify this value - the difference between the final and initial size - for each animal and find that nutrient concentration has a very pronounced effect on the total growth output for a given initial size (Figure 2.2B). In the case of 0.20 OD, a doubling or even tripling in size does not substantially change the total growth output. In contrast, growth output under 0.40 OD conditions scales nearly one-to-one with initial size of the animal. This significant difference between the two treatments in their size-dependent growth is undoubtedly a significant factor in producing larger animal sizes under richer nutirent conditions.

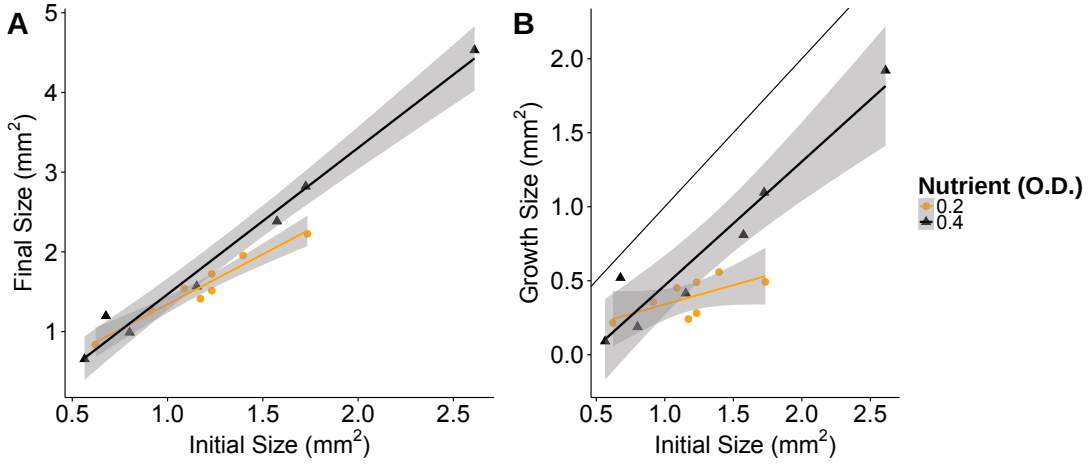

Figure 2.2: Growth of *T. adhaerens* of varying sizes under varied nutrient conditions. (A) The final size compared to the initial size for non-fissioning animals shown size after 24 hours of growth in either 0.20 or 0.40 OD nutrient conditions. Lines represent linear regressions of best fit for each condition. Shaded area is the 95% confidence interval on the linear fit. (B) Total biomass added to each individual shown in relation to an individual's starting size. Line and shaded area rerpesent the best linear fit to the data and the confidence interval on the fit. Black line: $y = x$. The slope of the growth line for 0.40 OD is significantly different from the growth line for 0.20 OD but not from the $y = x$ line.

In additiion to growth, asexual fission plays a critical role in size regulation in *T. adhaerens*. Though this organism has multiple modes of sexual and asexual reproduction[186,175],

these occur primarily under deteriorating environmental conditions. Here we focus on exponentially growing cultures where the primary method of propagation is asexual binary fission[139]. Through fission - an example of which is shown in Figure 2.3A - a *T. adhaerens* individual produces two daughter animals roughly equal in size (though note that the relative size of daughter animals has never been investigated quantitatively). We investigate the effect of the size of an animal on its propensity to fission within 24 hours of the initial size measurement. We find that size is a highly significant factor in an animal's propensity to fission within this time period (Figure 2.3B). The majority of animals above 1 mm^2 in size fission within this time, compared to no animal below 1 mm^2. This size-mediated effect on fission is highly significant (Mann-Whitney-Wilcoxon test: $W = 35, p < 5 \times 10^{-05}$). One unexpected result is that the propensity to fission at a given size is not affected by the nutrient richness of the environment. This is evident in the logistic regression model of fission (2.3C), in which we detect that size has a highly significant effect ($z = -2.74, p = 0.006$) while nutrient conditions have no effect ($z = 0.15, p = 0.88$). This provides some support that a lack of coordination above a certain size, and not metabolic constraints, are resonsible for inducing fission.

2.4 Development of High-throughput systems

Acquiring longitudinal data on growth and fission is time-intensive both in its acquisition, and in the need to manually identify and track animals over prolonged times in order to compare final and initial sizes. The problem of tracking is exacerbated when multiple individuals are placed in a single dish, as is done above, since collisions can result in swapped identities that must be manually corrected. To overcome this challenge and enable the ac-

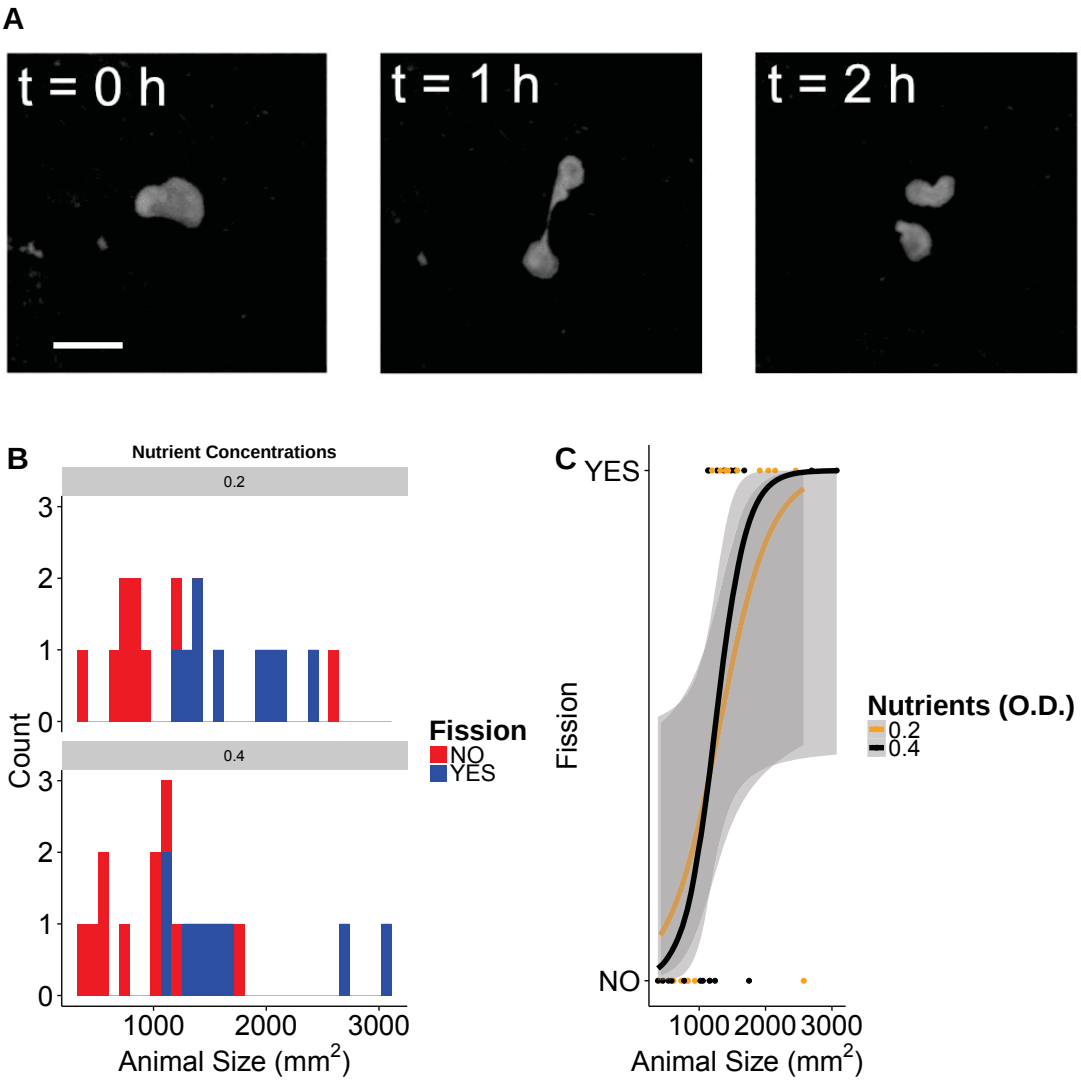

Figure 2.3: The propensity to fission is dependent on animal size but not on the local nutrient conditions. (A) An example *T. adhaerens* undergoing vegetative fission, producing two components of roughly equal size. Scale bar: 0.50 mm. (B) The distribution of initial animal sizes in both the 0.20 (top) and 0.40 OD (bottom) nutrient conditions. Animals are classified by whether they undergo fission within a 24 hour time period. Animals are characterized by a threshold size at 1 mmm^2 at which fission is never observed. (C) Logistic regression of the probability to fission given the initial animal size and nutrient conditions. Points represent the initial sizes of individual animals, categorized by whether the animal underwent fission (top) or not (bottom). Lines are logistic regression functions of the probability of fission at a given size. Shaded areas represent 95% confidence intervals on the logistic regressions.

quisition of data in a high-throughput fashion, I developed a robotic time-lapse photography apparatus that enables the monitoring of growth and fission of multiple ramet clones grown in isolation (Figure 2.4A). This setup enables the recording and tracking of 96 simultaneously growing animals at sufficient time resolution to overcome the dynamic time variability in the animal's footprint tha toccurs while feeding (Figure 2.4D; see also[139,194]). By varying both the initial size and the initial nutrient conditions in a combinatorial fashion (Figure 2.4C), and doing so with animals reared in isolation, this mechanism both removes confounding variables of nutrient consumption by cohabiting animals and greatly simplifies the tracking problem, enabling the quantification of animal size through an automated image processing pipeline. This setup furthermore allows for non-continuous illumination of a sample, allowing for brighter illumination to be used when imaging that enables the visualization of animal feeding tracks across the substrate (2.4C).

2.5 Theoretical model for size regulation in Placozoa

2.5.1 Analytical Model Description

In addition to using empirical data to understand the growth and replication dynamics of *T. adhaerens*, we developed an analytical model to investigate the optimality of the observed fission function given the observed size-dependent growth function. In other words, to Placozoa fission to maximize total biomass growth for a given environmental nutrient condition? An example model is presented in Figure 2.5 and described below. It is hoped that this model can be used to provide a more complete analytic solution of the optimum fission behavior for a given growth function.

We consider a deterministic growth model for an animal of size ξ which grows in accor-

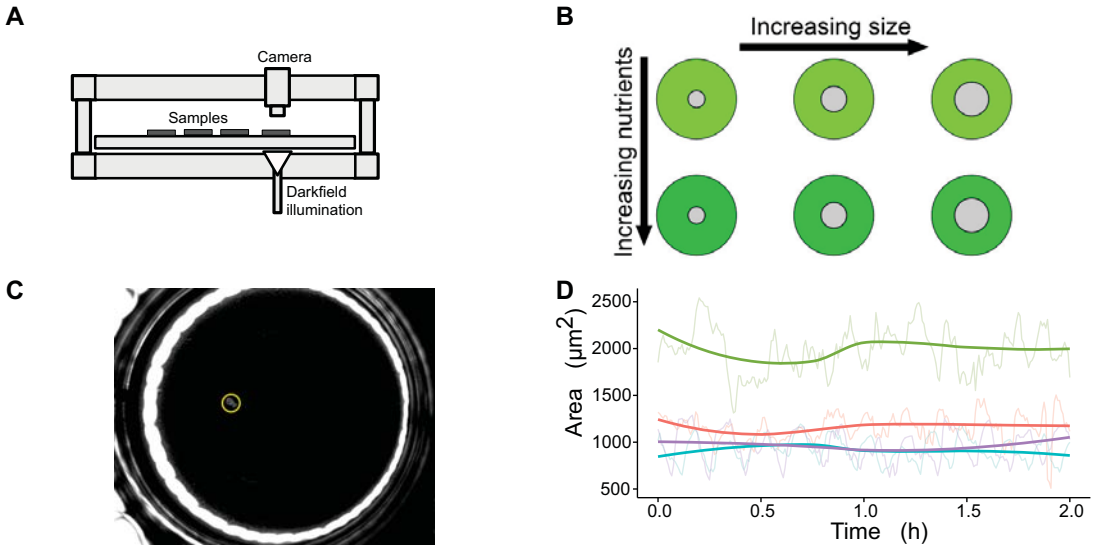

Figure 2.4: High throughput imaging of *T. adhaerens* growth and proliferation. (A) Robotic system for recording size information (courtesy of [151]). (B) Experimental design of varying the starting animal size and initial nutrient conditions. (C) Image of an animal growing in 0.200 OD. Yellow circle highlights the animal. One can observe darker feeding tracks that the animal has made in the sedimented microalgae. (D) Representative growth curves for several individuals, shown in different colors. Faded line represents the direct measurement of the footprint area, with the darker line being a LOESS regression.

dance to the differential equation $\frac{d\xi}{d\tau} = G(\xi, \nu)$ until a certain threshold size ξ_f, at which point the animal fissions into m components of equal size $\frac{\xi}{m}$. Of course, the dynamics of this model are heavily dependent upon the growth function $G(\xi, \nu)$ that governs the differential equation $\frac{d\xi}{d\tau}$, where G is assumed to dependent on the current size ξ and on the environment's nutrient richness ν. The total biomass produced after a certain time period T is dependent on the size at fission ξ_f, the daughter animal size $\xi_o = \frac{\xi_f}{m}$ and the time required for an animal to grow from ξ_o to ξ_f, known as the replication time τ_f. The optimal growth and fission function for a clonal organism is considered the one that maximizes the total clonal biomass, ξ_T, produced over some total time T, where $T \gg \tau_f$. The dynamics of this model are similar to an unbound exponential growth shown in equation 2.1. A graphical

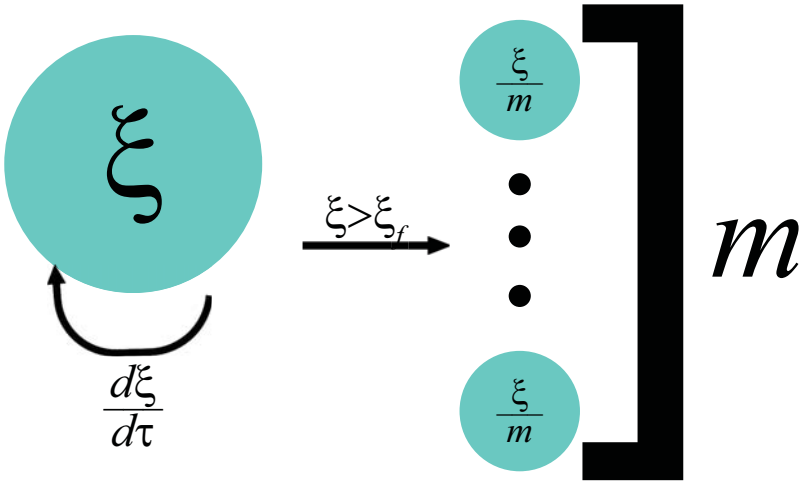

Figure 2.5: A simple model of growth and proliferation of *T. adhaerens*. An initial animal of size ξ grows at a rate $\frac{d\xi}{d\tau}$. The animal fissions deterministically when it exceeds the size ξ_f into m components of equal size, that then continue to grow following teh same growth function.

schematic of our model is shown in figure 2.5.

$$\xi_T = m^{\frac{T}{\tau_f}}\xi_f \tag{2.1}$$

We note that for a given deterministic growth equation $G(\xi, v)$, the time to fission is entirely dependent on the size at fission, which is simply a multiple of the initial ramet size $\tau_f(m\xi_o)$. Substituting this into equation 2.1 produces a function that is no longer dependent on time but only on the initial fragment size.

$$\xi_T = m^{\frac{T}{\tau_f(\xi_o)}+1}\xi_o \tag{2.2}$$

The optimal or maximal $\xi_T(\xi_o)$ occurs where $\frac{d\xi_T(\xi_o)}{d\xi_o} = 0$ and $\frac{d^2\xi_T(\xi_o)}{d\xi_o^2} < 0$. Solving these derivative equations requires an explicit form of $\tau_f(\xi_o)$. We consider the simplest possible

realistic growth function, which is a concave-down quadratic equation.

$$\frac{d\xi}{d\tau} = -(\xi - 1)^2 + g \tag{2.3}$$

Here, ξ is the current size of the ramet and 1 is the nondimensional optimal size at which growth is maximal. The nondimensional optimal growth rate is given by g, and the two real roots represent and maximum and minimum viable size. To solve for size as a deterministic function of time, we substitute $\xi' = \xi - 1$, with $d\xi' = d\xi$ to produce 2.4, with the corresponding integral 2.5. This has a known hyperbolic function as a solution $\int \frac{1}{a^2 - x^2} = \frac{1}{a} \tanh^{-1}(\frac{x}{a}) + C$, which for our specific case is equal to equation 2.6.

$$\frac{d\xi'}{d\tau} = -\xi'^2 + g \tag{2.4}$$

$$\int \frac{d\xi'}{-\xi'^2 + g} = \int d\tau \tag{2.5}$$

$$\frac{1}{\sqrt{g}} \tanh^{-1}(\frac{\xi'}{\sqrt{g}}) + C = \tau + K \tag{2.6}$$

By letting $\beta = K - C$ and reversing our substitution $\xi' = \xi - 1$ we can now solve ξ as a function of τ.

$$\xi = \sqrt{g} \tanh(\sqrt{g}(\tau + \beta)) + 1 \tag{2.7}$$

We must solve for the initial condition of 2.7, where $\xi(t = 0) = \xi_o$ and then solve for β in terms of ξ_o.

$$\xi_o = \sqrt{g} \tanh(\sqrt{g}\beta) + 1 \tag{2.8}$$

$$\beta = \frac{1}{\sqrt{g}} \tanh^{-1}\left(\frac{\xi_o - 1}{\sqrt{g}}\right) \tag{2.9}$$

Substituting the initial condition back into equation 2.7:

$$\xi(\tau) = \sqrt{g}\tanh\left(\sqrt{g}\tau + \tanh^{-1}\left(\frac{\xi_o - 1}{\sqrt{g}}\right)\right) + 1 \tag{2.10}$$

We now solve for the replication time τ_f, which is the amount of time it takes an organism from an initial condition side ξ_o to reach a size $\xi_f = m\xi_o$ at which point the organism would fission and the replication cycle would repeat. Solving for the replication time as a function of the replication size produces

$$\xi_f = m\xi_o = \sqrt{g}\tanh\left(\sqrt{g}\tau_f + \tanh^{-1}\left(\frac{\xi_o - 1}{\sqrt{g}}\right)\right) + 1 \tag{2.11}$$

$$\tau_f(\xi_o) = \frac{1}{\sqrt{g}}\left(\tanh^{-1}\left(\frac{m\xi_o - 1}{\sqrt{g}}\right) - \tanh^{-1}\left(\frac{\xi_o - 1}{\sqrt{g}}\right)\right) \tag{2.12}$$

At this point, ideally one would substitute this into equation 2.2 and produce the first and second derivatives of this function using the chain and product rules for integration. Unfortunately this integral does not have a trivial analytical solution, requiring a numerical solution instead.

2.5.2 Simulation Model Description

We used a deterministic agent-based simulation identify the optimal fission strategy for organisms capable of vegetative proliferation. Our simulations consider Placozoa agents

that grow according to a simple quadratic growth function (Figure 2.6A), with an optimal size $\xi^* = 0.5$ where growth is maximal. Each Placozoa agent grows until its size equals or surpasses the size ξ_f, at which point the animal fissions into $m \in \mathbb{Z}^+$ fragments of size $\frac{\xi_f}{m}$. Each simulation began with a single individual with a starting size $S_o = \frac{S_f}{m}$ and is run for a constant but arbitrary growth time that is much greater than the replication time $T \gg \tau_f$. The results presented below are not sensitive to our choice of T.

Our results provide two key insights: firstly that binary fission is a superior reproductive strategy to fragmentation, and secondly that the optimal fission size does not correspond to the metabolic optimum (where growth is maximal). Taking into consideration simply the total biomass produced, which is a good measure of fitness for a clonally propagating organism[75], binary fission ($m = 2$) is the dominant strategy in all cases up until *c.* $\xi_f > 0.95$ If we consider the maximum biomass ξ_T* that can be produced for a given m, we find that this quantity decreases monotonically with decreasing m (Figure 2.6C). As m increases, the optimal fission size ξ_f* also increases from roughly 0.7 for $m = 2$ to 0.9 for $m = 9$. This occurs because the optimum growth strategy is for ramets to maximize the amount of time they spend growing at a size close to the optimal growth size $\xi = 0.5$. As m increases, the parent animal needs to increase to ensure that $\frac{\xi_f}{m}$ is still in the neighborhood of the metabolic optimum. However, this forces each agent to outgrow the optimal size further and therefore spend a greater proportion of time in a slow-growth regime.

While these results help us understand why Placozoa have evolved to perform near-equal binary fission as their main method of asexual propagation, a more empirically-derived model would be more informative for studying the reproductive behavior of our system. In particular, using an empirically-derived growth curve instead of our simplified function

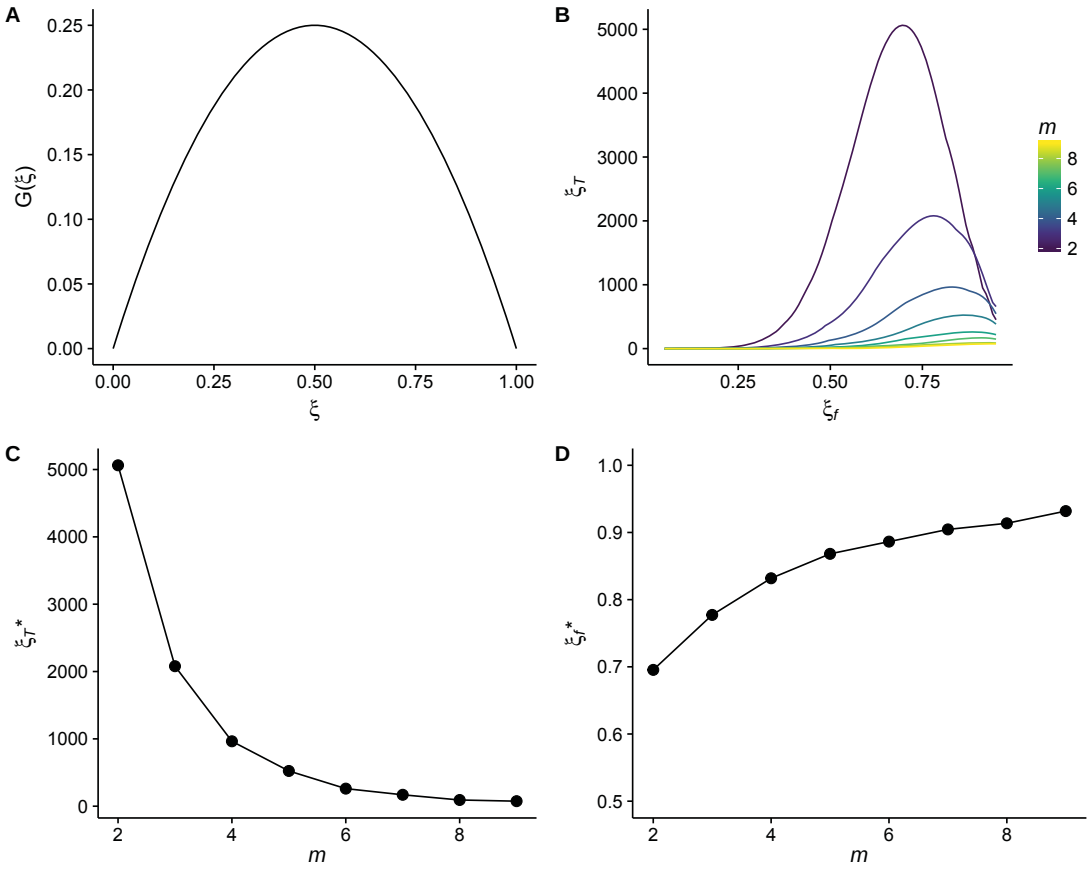

Figure 2.6: Numerical analysis of fission-mediated meta-populations. (A) The quadratic growth function used in our simulations, with an optimal size at $\xi = 0.5$. (B) Total amount of biomass produced over a fixed time limit as a function of the size at fission and the number of fission fragments. (C) The maximum total biomass achievable in a fixed time limit given a certain number of fragments produced by each fission replication. (D) The optimal fission size.

in Figure 2.6A would allow the use of such a model to determine the optimal fission size, ξ_f*, for $m = 2$, and compare this optimal size with our data-driven logistic model of fission discussed in chapter ??. Once this type of measurement is achieved for a given environment, one could then replicate this experiment in multiple nutrient conditions and determine if the changing fission dynamics match what would be expected from the given empirically-observed growth function for each condition.

2.6 Discussion

We have investigated the dynamics of individual and population growth in one of the simplest multicellular animals, *T. adhaerens*, in order to determine to what extent such organisms adjust their sizes in response to changing environmental conditions, and identify the processes that mediate this response. We have identified that *T. adhaerens* perform such an adjustment, primarily by adjusting their growth rate in richer environments rather than by delaying asexual fission. One curious result is that the total population size of organisms does not change substantially under such varying conditions. As such, attempting to understand the population dynamics of this animal by focusing exclusively on ramet count and ignoring size (as was done in Schleicherova *et al.*[155]) is likely to misrepresent the ecologically relevant unit of total biomass production.

That propensity to fission is dependent on size but not on nutrient concentrations leaves open the question of what is driving this process. In particular, it would be interesting to investigate this phenomenon from the perspective of internation coordination and decision conflict among cells within an animal. No evidence exists to date of a central organizing center of activity in Placozoa, and the one study that has analyzed its feeding behavior at

high spatial and temporal resolution has found that this behavior is locally triggered by the presence of food causing an ectopic release of neurotransmitters[171]. This local release causes the Placozoa to not only cease moving but also to adhere tightly to the substratum in order prevent the loss of digested nutrients trapped beneath the ventral epithelium[172]. One possible cause for fission, then, could be asynchronous feeding by different parts of the animal, resulting in a motile portion of the animal tearing away from its non-motile remainder. Indeed, we find that fission is extremely rare in the absence of food (data not shown). Use of automated tracking coupled with high spatial and temporal resolution recordings, as described in Chapter 1, would be the key to testing this hypothesis. Such a study might be able to place the phenomenon of asexual fission in this animal in the broader studies on group fission based on decision conflict in animal groups[109,49].

With regard to growth, the nutrient-dependent modulation of this process prompts further investigation of this effect through metabolic theory[162]. A more comprehensive dataset of animals whose change in size is measured over a 24-hour period would be useful for determining the metabolic optimum size for a given nutrient condition. One could then compare then use such a metabolic model, combined with size-dependent propensity to fission, to determine if the proliferation strategy of Placozoa is optimal (in the sense of producing the maximum possible total biomass) at all nutrient conditions. The possibility that such an optimum size regulation could be an emergent product without tuning the propensity to fission would itself be a very interesting result.

Our study is limited in its scale, notably in the dearth of data on individually-tracked ramets that was used to determine growth and fission fates for animals of different sizes, and therefore follow-up studies should be performed to replicate our current results. This

limitation is largely due to pragmatism and logistics: using our current setup, acquiring 24 hours of data for one individual is a very laborious and time-consuming endeavor. This type of analysis is similar to survival analysis in other organisms[132], which requires longitudinal observational datasets. We are further limited by our need to image each individual at relatively high time resolution in order to robustly measure size in the face of the large dynamic variation in the animal's footprint while feeding. Given the predictive strength of our statistical growth model, it is likely that more observations will continue to follow the very robust trend that we have identified (Figure 2.2). With regard to fission, the nutrient-invariance of the process is interesting, but the relatively wide confidence intervals resulting from the dearth of data prompts the need for further replication. The development of a robotic unit that could allow for the massive screening of clones isolated in controlled environments would aid significantly in this endeavor.

Aside from pragmatic considerations, this study is also limited at a conceptual level on several accounts. Firtly, we considered only the population dynamics that take place under asexual fission, ignoring the full repertoire of reproductive strategies available to *T. adhaerens*. Though fission is the dominant form of reproduction in nutrient-rich environments, *T. adhaerens* also performs asexual reproduction through rapid degeneration into numerous small dispersing buds[186], and attempts sexual reproduction when environmental conditions deteriorate[166,58]. The production of dispersing buds may be particularly important for escaping inhospitable conditions and colonizing new patches. Several lines of evidence argue, however, that the major driver of population dynamics should be the asexual fission we have described. Firstly, in marine benthic species, asexual propagation through fission and fragmentation is the major driver in recruiting new individuals to patches[92],

and often one asexually-propagating old genet will dominate a habitat to the exclusion of incoming propagules[210]. Secondly, among asexual propagules, it is typical that mortality increases precipitously with decreasing fragment size, with most surviving ramets being derived from particularly large fragments as produced by fission[79]. In Placozoa in particular, there is a strong relationship between size and anti-predator defense[89]. Therefore, we expect the size structure of a population of *T. adhaerens* within one patch to be determined primarily by production of large fragments through asexual fission, as occurs in other benthic species[79,87].

Here we have produced a quantitative understanding of how growth and fission regulate the population size structure of *Trichoplax adhaerens*, one of the earliest-diverged and simplest multicellular animals. Our discovery that such organisms can rapidly accelerate their growth in response to increasing nutrient concentrations suggests that these organisms may provide an important ecological role in marine coastal ecosystems, buffering these systems against hazardous algal blooms[119,196,86]. At the same time, our analysis of the propensity to fission at a given size, and its invariance to nutrient conditions, suggests that this process may be an emergent result of decision conflict within larger animals as opposed to a metabolically-regulated developmental process. This study may also help us establish theoretical models for the proliferation of such animals, enabling the comparison of the observed proliferation dynamics of Placozoa to a theoretically predicted optimum strategy.

2.7 Methods

2.7.1 Animal husbandry

T. adhaerens were reared in 150 mm diameter plastic petri dishes filled with 100 mL of artificial seawater (ASW) at 35 parts per thousand concentration (ppt, Instant Ocean Reef Crystals). The seawater was seeded with *Pyrenomonas salina* microalgae to a concentration of 0.200 optical density (OD), measured using a spectrophotometer at 600 nm. *Pyrenomonas salina* were reared separately in 1 L ventilated cell flasks filled with algae growth media (35 ppt ASW + 1:1000 f/2 Guillard's growth media). Algae cultures were diluted every two weeks, while Placozoa cultures were started every week with haphazardly-selected animals from previously established cultures, using ten animals as the founder population for each new culture.

2.7.2 Population growth measurements

We used the same dishes as were used for culturing animals, filling each dish with 50 mL of artificial seawater at a concentration of either 0.20 or 0.40 OD of microalgae. Five animals were washed and transferred into each experimental dish. Starting at the 12th hour post-seeding, dishes were imaged every 24 hours under red light darkfield microscopy using a DSLR camera (Panasonic Lumnix DMC-GH3) five times in ten minutes. Animals were counted in each dish, and the size of each animal was measured in the frame when the animal's size was maximal. The censusing effort for each plate was standardized at 2.5 minutes per dish, with counts performed in ImageJ. One dish was imaged under the same red light darkfield conditions every minute for twenty-four hours at t = 0, 48, and 96 hours to gener-

ate data on individual ramet fates. When not being recorded, the dishes were kept under a constant but weak light conditions in a temperature-controlled room (22 degrees C).

2.7.3 Individual growth and fission fate measurements

We used the 24-hour recordings of the animal at t = 48 and 96 hours to perform our growth and fission measurements. Animals were identified at the start of the recording as in the population growth measurements, their size being measured in the first five frames/minutes of the recording in ImageJ using the magic wand tool or manual tracing. Each animal was then followed throughout the 24 hour recording. If the animal underwent fission before the recording was completed, it was noted as such and was not used for the final size measurements. Animals that did not fission had their final sizes recorded in the last five frames/minutes of the recording with the same method as used for the initial size.

2.7.4 Sample preparation for high-throughput system

Vibrations induced by the motorized system will cause any algae that has not adhered to the substrate to slowly drift to the center of the well, producing an uneven distribution of nutrients in the environment over time. To overcome this technical limitation, we produce produce substrates with uniform algae sedimentation through centrifugation. Firstly, we match the nutrient concentrations in our 6-well plates to the conditions present in the larger culturing dishes described in chapter ??. 50 mL of 0.20 OD (10 OD units) in a 15 cm diameter dish produces a per-area concentration of 0.05 OD per square centimeter. To achieve a corresponding nutrient cover in our wells (of 3.5 cm diameter) requires the addition of 0.54 OD units per well. Half of this biomass content is added to 6 mL of ASW

to each well, after which the wells are centrifuged at 700 rpm for 10 minutes. The second half the biomass content is added adn the wells are centrifuged again with their orientation reversed, to minimize any gradient effect created by the centrifugation process. After this is performed, animals that were starved for 24 hours are added to each well, and recorded immediately. Growth data are measured from 24 to 48 hours post-transfer, to ensure that animals have acclimatized to the new nutrient conditions and removes effects of hysteresis and inconsistency in culturing conditions.

3

Morphological Allometry in Two-Dimensional Organisms

3.1 Abstract

Morphology is fundamental to ecological function, whose quantification and comparative analysis has been enabled by techniques developed over the past thirty years. In spite

of these advances, little progress has been made in the morphological analysis of animals with highly variable, decentralized forms, including the earliest invertebrate animals. Here we present a quantitative analysis of form and allometry in one such animal, the Placozoa, using both shape factors and the elliptical Fourier transform. These methods allow us to represent the shape of such organisms in a rotation and size invariant fashion. Through these methods we find evidence of allometric growth in this two-dimensional organism, and provide several explanations for why this allometry should occur. Our EFT-based method also allows us to identify significant idiosyncratic shape variation in such animals, and reveals that larger animals are harder to differentiate morphologically due to their high intra-individual shape variability. We identify several prospective uses for this method, including in inter-specific morphological comparisons and using this postural information in a dynamic framework to create behavioral maps.

3.2 Introduction

From the beaks of Darwin's finches to the shape of bacterial cell walls, morphology is fundamental to ecology. Morphological variation is one method by which organisms exploit new resources and partition their niche from competitors. While morphological variation has been of interest for centuries, it was only in the mid-twentieth century that a quantitative framework for comparing morphology - morphometrics[188] - was developed, and only in the past thirty years that quantitative tools for such morphological investigations were systematically developed[29,30]. The ability to not only describe but also quantify shape differentiation was greatly enabled by the incorporation of multivariate statistics in morphometrics, giving rise to the field of geometric morphometrics[4].

While these advances have enabled the quantification of shape variability among organisms with conserved anatomic structure and fixed landmarks[1,29], relatively little progress has been made in the systematic classification and quantification of emergent collective structures[84]. Standard morphometric methods have relied on alignment of different shapes using conserved identifiable landmarks - joints, appendages, organs - using techniques such as Procrustes' alignment, which enables morphological comparisons in a size and rotation-invariant fashion[30], eliminating variation induced by sample orientation and magnification. The development of Procrustes' alignment, thin-plate spline methods, and multivariate statistics has solved the problem of landmark-based morphometry, with tools that are now canonical in biology[31]. However, there are a large number of organisms and cells that have no set body plan - such as amoeba, colonial organisms, fungi and bacterial colonies - and have highly variable shapes lacking any conserved landmarks. Such systems have largely defied quantitative morphological description using standard tools[114,209].

Two techniques are available for the study of morphology in the absence of conserved landmarks. The first of these is the use of shape factors, or dimensionless quantities that are invariant to affine transformations[34]. Such shape factors are typically dimensionless ratios of an object's perimeter, area, diameter, and its convex hull. While shape factors can be applied generically to any closed two-dimensional shape, from powder grains[142] to cells[193], they have two fundamental limitations. Firstly, they are ambiguous quantities, in that two very different shapes could be well-matched using such measures. As an example, consider the circularity measure $C = \frac{4\pi A}{P^2}$, where A is the area and P is the perimeter of a shape. $C = 1$ for a perfect circle and between 1 and 0 for any other shape. It is entirely possible for an ellipse, a rectangle, and snaking shape to have very similar values of C in spite of their

very obvious morphological differences. Secondly, while one can attempt to deal with this ambiguity by representing a shape using a combination of shape factors, most shape measures (e.g. circularity and eccentricity) are strongly correlated. It is therefore very unlikely one can find a practical set of shape measures that can be used to unambiguously reconstruct the original shape that they represent.

A more rigorous method of morphological comparison involves decomposing the outlines int a series of harmonic trigonometric functions, known as the elliptical Fourier transformation (EFT)[105]. The EFT is a powerful method of shape analysis because, like the aforementioned shape factors, it does not require the identification of any landmarks, and even enables shape alignment and standardization by simply using the Fourier coefficients of the first Fourier harmonic (the best-fitting ellipse)[27,46]. A second advantage is that the EFT is a lossless and reversible transformation, allowing a vector of Fourier harmonics to unambigously represent a shape in EFT space to any arbitrary level of precision. EFT's also allow for arithmetic operations on shapes, such as calculating mean shapes and exaggerating shape characteristics. Finally, EFT's allow for the compression of shape information with often negligible information loss, as sequential boundary coordinates from a traced outline typically have high auto-correlation. One can measure the information loss by this compression through calculating the Fourier power spectra and determining what proportion of power is stored in each harmonic. These advantages have made EFT's a tool of choice for the analysis of shapes without landmarks including amoebas[192], mollusk shells[143], bivalves[51], hominid crania[18], and dipteran wings[145].

These techniques could also be of considerable utility in quantitative morphological studies on decentralized and colonial marine animals. Previous morphological studies have

categorized such organisms into broad "morphological strategies"[90], such as whether an organism grows as a thin filament, as a two-dimensional sheet, or as three-dimensional mound or branched structure. Such classification has been useful in finding patterns of inter-species competitive dynamics[90,37], but suffers from two very significant limitations. Firstly, it has no explanatory power for competition among species using morphological strategies in the same category, which is precisely where one would expect to be in the fiercest competition. Secondly, it is unable to quantify the ontological and idiosyncratic variation among organisms such organisms, which is necessary for determining the presence of important ecological phenomena such as allometric growth. As such, this technique has no explanatory power on the substantial and real size-mediated effects on survivorship[79] and growth[97].

We propose the use of multi-variate shape factors and the EFT to quantify and characterize morphological variability in such organisms, using the Placozoa as our model system. Placozoa are arguably the simplest and earliest-diverged multicellular animals, fundamentally characterized as two-dimensional mobile cellular sheets[153] with a largely undifferentiated anatomy that enables considerable variation in size and shape even within the same individual[139]. This combination of simplicity and flexibility has resulted in a relatively ambiguous "amoeboid" shape classification for these animals[125], but this classification potentially obscures systematic shape variability among such animals. This perceived morphological ambiguity has obscured actual biological variability within this taxa, as Placozoa have long been characterized as a phylum composed of the singular species, *Trichoplax adhaerens*, but more recent genetic evidence has found that this phylum contains an array of cryptic species[202,166]. The small sizes (< 1 mm in diameter) suggests such organisms should

be near ubiquitous[16], and worldwide sampling has revealed considerable overlap in the geographical distributions of different Placozoa strains[60,59 6]. Morphological variation could thus be an important method by which this biodiversity is sustained in the absence of any discernible biogreography.

Like many decentralized animals, Placozoa are capable of considerable size variation, though it is unclear if they also exhibit a corresponding allometric shape variation as found in other systems[88,156,28]. The two-dimensional morphology of Placozoa typically produces metabolic isometry with body size[82,149]. In the case where allometric shape variation is found in two-dimensional organisms, such as in encrusting corals, this is typically imposed by skeletal constraints on growth, whereby only the boundary of the disk-like organism is capable of further growth[97]. Placozoa, as soft-bodied two-dimensional invertebrates, lack this constraint, but there is some evidence that the boundary is differentiated from the bulk and could contain a preponderance of stem cells[116,160]. It is therefore unclear *a priori* if Placozoa grow in an allometric fashion.

In this chapter we investigate the morphological variability among clonal *T. adhaerens* individuals varying in size by over an order of magnitude. We first demonstrate the validity of applying shape factors and EFT's to Placozoa, and then use these methods to determine if such organisms exhibit allometric shape variation. We then demonstrate how the shape characteristics of *T. adhaerens* are well-represented using the EFT to produce a rotation and size invariant representation of shape. We use this shape representation to determine if *T. adhaerens* have idiosyncratic forms, and evaluate how shape discernability is affected by the absolute sizes and the relative size difference of animals being compared in a pair-wise fashion.

3.3 Results

3.3.1 Shape normalization

Shape, as defined by Kendall, is the information in an animal's morphology that is invariant under translation, rotation, and isotropic rescaling[98,167]. Any morphological comparisons based purely on shape requires the production of normalized shapes that remove such affine transformations. Using the well-established morphometric techniques implemented in the Momocs R package[27], we develop a shape transformation procedure that allows us to standardize Placozoa shapes in the absence of any landmarks. Shapes are aligned by the principal axes, given by the variance-covariance matrix of the Cartesian coordinates of outline points, and positioned such that their center of mass is at (0, 0). We rotate the normalized shape in 180 degree increments to ensure that the shape's area to the left of the y-axis is greater than the area to the right. This shape is then scaled such that the entire shape is inscribed in a square with sides of length 2. Once aligned, we digitize our boundary to standardize the number of boundary points as follows: we define the start position of the boundary as the point closest to the positive y-axis (to the "North" of the centroid) and then interpolate evenly-spaced points (in boundary chord length units) along the boundary in a clockwise fashion.

A good shape representation is insensitive to affine transformations. We quantify our representation's sensitivity by considering a sample image of a *T. adhaerens* individual (Figure 3.1A) and digitally altering the image by rotation and re-scaling. These types of transformations will usually produce subtle changes in pixel intensity values, due to the need for cubic interpolation of new values from the original image's pixels, and these digitization

artifacts will have subtle effects on the image binarization and segmentation of the animal. Because our shape analysis is dependent on the boundary information, it is particularly susceptible to such artifacts. To measure the error introduced by these artifacts, we binarize each adjusted image using the same threshold selected for the unaltered image (by Otsu's method[138]), recording the boundary contour for each animal (Figure 3.1B). we then produce standardized shapes using the protocol described above, attempting to remove the effects of the affine transformations (Figure 3.1C). This results in some positional error between any two outlines $\mathcal{A}$ and B, defined as $\delta_{AB} = \frac{1}{n}\sum_{i=1}^{n} \|\mathrm{x}_{\mathcal{A}i} - \mathrm{x}_{Bi}\|$ where i is a certain point along the boundary. Figure 3.1D illustrates the values of δ_{AB} (black) between the original and altered shape, as well as the maximum point-wise positional error (red). It is reassuring that 90 degree rotations, do not produce any digitization artifacts, have no positional error, suggesting that our numerical method of alignment does not contribute any error. The remaining tests show error introduced by digitization, with the mean error being roughly one percent of the normalized maximal radius. This provies a threshold of measurement error at which we can consider two shapes identical. When we transform these shapes using an EFT and measure the Euclidean distance between shapes in the EFT vector space (methods described below; Figure 3.1E) we find that the distance between two shapes in EFT space and inin Cartesian space correspond well with one another, suggesting that a Euclidean distance measure in Fourier space is a valid measure of shape similarity (Figure 3.1F, $\Delta = \beta\delta, \beta = 1.1, R^2 = 0.97, p < 10^{-12}$).

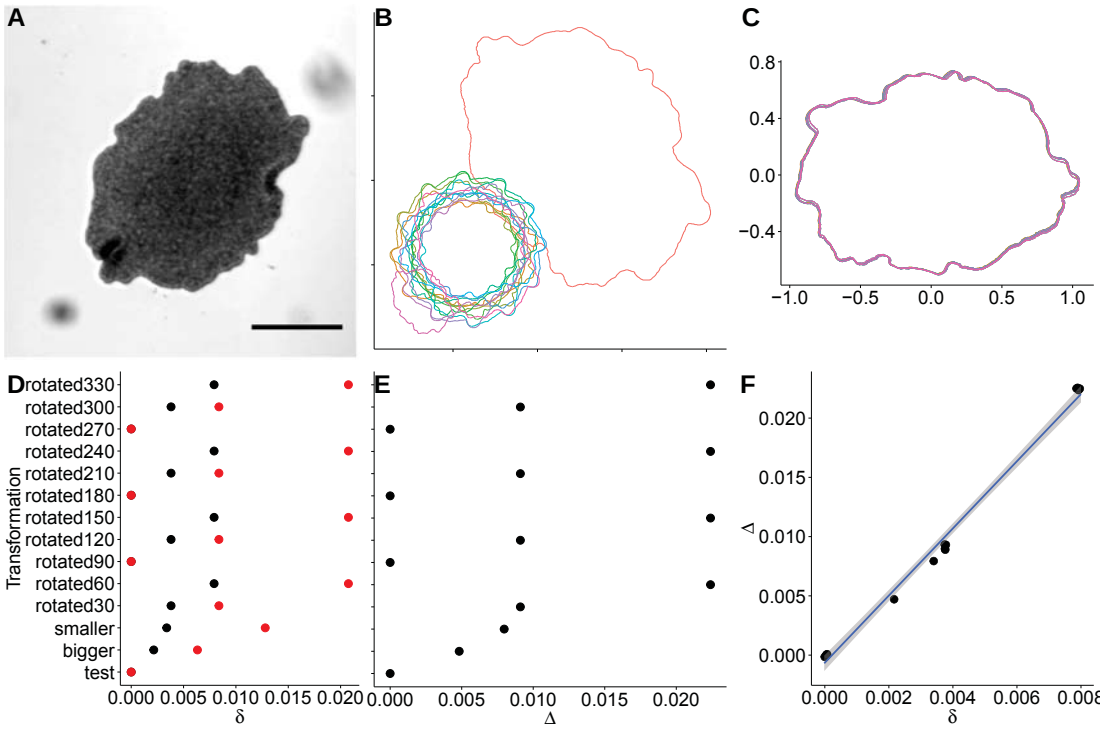

Figure 3.1: Measurement sensitivity to affine transformations. (A) Original image of an example *T. adhaerens*. Scale bar is 0.50 micrometers in length. (B) Digitized boundaries of animals extracted from transformed images. (C) Normalized shape boundaries plotted on top of each other in Bookstein coordinates, whereby the major axis of teh animal has a radius of 1. (D) The reconstruction error, measured in RMS average point-wise distance for each Cartesian point that defines the boundary, comparing normalized boundaries extracted from transformed images to the normalized boundary extracted from the original image. The transformations enlarged or shrunk the image by a factor of 2, or rotated it in 30 degree increments. The zero value of the 90-degree rotations suggests all error is induced by digitization. (E) Reconstruction error as Euclidean distance between the boundary extracted from the original image and the boundary extracted from the transformed image. The reconstruction error is the distance between the multi-dimensional points in Fourier space that specify the Fourier parameters that define each boundary. (F) Comparison of the error measurements in Cartesian and Fourier space, showing that error in Fourier space corresponds well with error in Cartesian space. The line represents the linear fit of the relating the two error measurements, with the shaded area representing teh 95% confidence interval of this fit.

3.3.2 Evidence of allometric growth using shape factors

We characterized the shape of each *T. adhaerens* individual at any instant in time using six non-dimensional shape factors (see Methods). We find that these shape factors vary systematically with animal size (Figure 3.2A), and also covary extensively with one another. This suggests that we can reduce the dimensionality of our shape description through a principal components analysis (PCA). We find that only two principal components are significant in explaining the shape variability of Placozoa according multiple selection criteria (Kaiser's selection criterion, Scree test, 90% variance threshold; Figure 3.2B). When we consider the loadings of our original shape measures on these PC's, we find that the first component is loaded with ratiometric factors of an animal's minimal and maximal diameters (eccentricity, aspect ratio, circularity, and compactness), while the second principal component is loaded heavily by shape factors that involve comparisons between a shape and its circumscribing convex hull (waviness, solidity). The first PC is thus a measure of elongation while the second is a measure of shape complexity.

Two patterns are apparent when we consider the component values for each animal. Firstly, we find that larger animals exhibit greater variability in these two components than smaller animals (Figure 3.2D). If we consider a convex hull defined by the five smallest (blue) and largest (yellow) animals, we find that very small animals occupy a smaller segment of this shape space than large animals. Both of these components are also significantly correlated with animal size (Figure 3.2E), indicative of allomtric growth (PC1: $t = -6.76, p < 10^{-8}, R^2 = 0.38$, PC2: $t = -9.85, p < 10^{-14}, R^2 = 0.56$). These two observations suggest that larger animals have more varied shapes than small animals, and that the shape difference between two animals will correlate with their size difference.

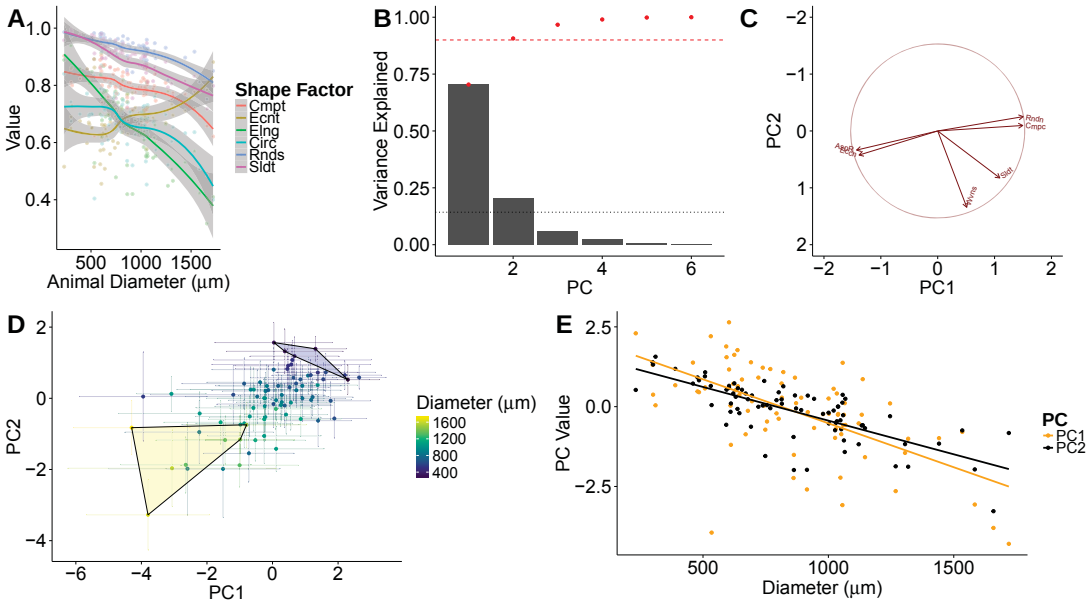

Figure 3.2: Shape variability in *T. adhaerens* is low-dimensional and suggests allometric growth. (A) Variation of six different shape factors (Compactness, Eccentricity, Elongation, Circularity, Roundness, and Solidity with animal size. (B) Variance explained by principal components of the shape factors. Solid bars represent the proportion of variance explained by each component. Red dots represent the cumulative variance explained by the first N components. Dotted black line is the cutoff threshold as defined by Kaiser's Rule. The red dashed line is the threshold for explaining 90% of the variance. Only the first two components are considered significant by both criteria. (C) Biplot of the contribution of each shape factor to first two principal components. The first component is a mixture of values that define how elingated the animal is in one dimension, while the second value defines boundary complexity. (D) Mean values of first two principal components for each animal. The error bars on each point represents the variance of each animal in both PC dimensions. The blue and yellow polygons define the area bounded by the mean principal component values of the largest (yellow) and smallest (blue) animals. (E) Mean values of both principal components regressed on animal size. The solid lines represent the best-fit line for a linear regression of each component on size.

3.3.3 Elliptical Fourier transform and standardization

We use the elliptical Fourier transform (EFT) to create a more refined shape representation that will allow us to evaluate how distinct two animals are from each other in their shape characteristics. The EFT provides a more precise method of characterizing the morphology of two-dimensional closed contours, making it ideal for organisms that grow primarily in two dimensions such as *T. adhaerens*. In brief, the EFT converts the Cartesian points that define a shape's boundary into harmonic frequencies of elliptical trigonometric functions (Equation 3.1), where each harmonic function can be defined by four Fourier coefficients (Equation 3.3). This method is not only a lossless transformation, whereby any combination of Fourier coefficients maps unambigously to a distinct shape, but by virtue of having each coefficient defined by global boundary characteristics, the comparisons between shapes can also be size and rotation invariant[105,46].

The EFT is defined by the following equations. Any two-dimensional closed contour can be represnted by an abscissa of length/perimeter T, where each position t (varying from 0 to T) on that boundary defines the Cartesian coordinates $x(t)$ and $y(t)$). These Cartesian coordinates are decomposed into N elliptical functions that are multiples of a fundamental frequency $\omega = \frac{2\pi}{T}$, where N can be arbitrarily large for an arbitrary level of precision. The resultant $4N$ Fourier coefficients can then be analyzed using traditional multivariate statistics to compare shapes.

$$x(t) = \frac{a_0}{2} + \sum_{n=1}^{N} [a_n \cos(n\omega t) + b_n \sin(n\omega t)] \tag{3.1}$$

$$y(t) = \frac{c_0}{2} + \sum_{n=1}^{N} [c_n \cos(n\omega t) + d_n \sin(n\omega t)] \tag{3.2}$$

$$a_n = x(t)\frac{2}{T}\int_0^T x(t)\cos(n\omega t)dt \tag{3.3}$$

$$b_n = x(t)\frac{2}{T}\int_0^T x(t)\sin(n\omega t)dt \tag{3.4}$$

$$c_n = x(t)\frac{2}{T}\int_0^T y(t)\cos(n\omega t)dt \tag{3.5}$$

$$d_n = x(t)\frac{2}{T}\int_0^T x(t)\sin(n\omega t)dt \tag{3.6}$$

One strength of this transformation is that one can significantly compress the number of coefficients without introducing significant positional error in the shape representation. We use the method proposed by Baylac and Friess[18] of transforming the outline into a Fourier form first by using an exessively large number of harmonics, and then performing PCA on those coefficients and reducing the dimensionality until we reach the precision threshold identified in the previous section. Each shape is transformed into $N = 128$ Fourier harmonics on the normalized boundaries, representing each shape as a 512-dimensional vector of the coefficients. We then perform a PCA on this vector using the variance-covariance matrix (without standardization, see Crampton (1995)[51] for motivation). We select a training set of 1,000 randomly-selected shapes from each animal (78,000 shapes in total) determine the appropriate PCA rotation matrix and centering values. We use those two properties of our PCA to convert any arbitrary *T. adhaerens* EFT vector into this PCA space.

Once we have transformed our shapes into principal component, we can identify the

appropriate number of components by compressing this shape representation (removing less-relevant principal components) and measuring the positional error introduced by this compression. We find that using this criterion tends to be both more conservative and more justifiable than basing the compression decision is often a decision based on either the eigenvalue magnitudes of each PC or by using a threshold for the proportion of variance explained. Neither of these latter two methods are particularly informative. For instance, if we consider the cumulative proportion of variance explained, we find that this quantity increases gradually with harmonic number and therefore there is no well-defined threshold value (Figure 3.3A). In contrast, we can use the positional error (Euclidean distance) between respective boundary points belonging to the original normalized shape and the shape that is reconstructed from the data retained in the compressed PC space, and compare this value to the expected error that would be induced on the same shape after underoing an affine transform (Figure 3.1). Figure 3.3B provides an example plot of a shape that has been reconstructed using an increasing number of PC's. While a low number of PC's does a poor job of reproducing the original shape, including only 35 PC's (7% of the original dimensionality) already allows for a rough reconstruction of concavities, while 80 and above captures nearly the entire shape. We quantify the error of this compression on 50 randomly-selected shapes from our dataset, applying varying levels of compression, and measuring the pointwise positional error. We find that retaining around 80 PC's recapitulates the shape with comparable fidelity to errors that would be introduced by an affine transformation (Figure 3.3C). For tractability, we use this reduced PC shape space for the remaining analyses.

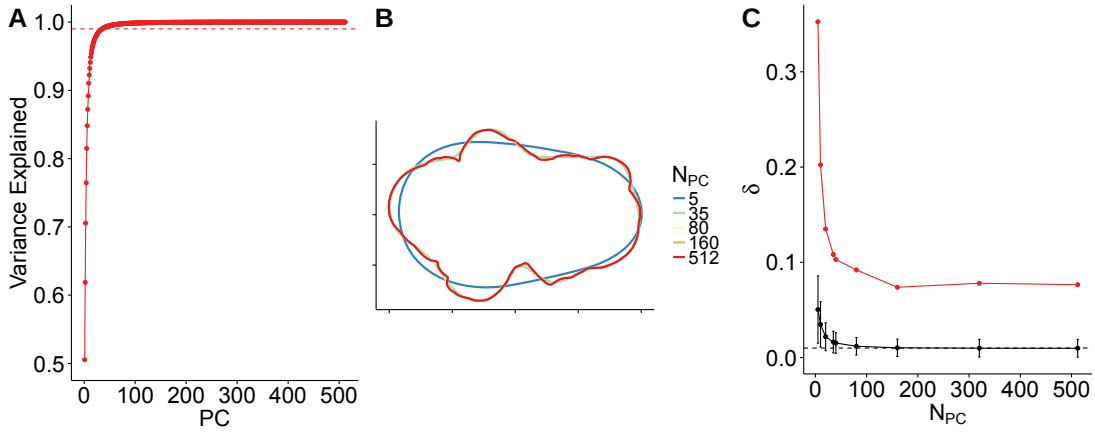

Figure 3.3: Error induced by shape compression after applying a PCA to the EFT shape transforms. (A) The cumulative variance explained by the first N principal components, attained by performing a PCA rotation on the EFT coefficients for each shape. Dashed line represents the 95 % cutoff threshold. (B) Outline reconstructions made by taking increasing subsets of principal components for the PC vector of an arbitrarily-selected shape, performing the inverse PCA rotation, and then performing the inverse Fourier transform. (C) Outline reconstruction error, measured by comparing the mean squared error of points in the normalized form of the original digitized boundary to points in the boundary that was reconstructed using a subset of PC's. The error was estimated in point-wise fashion between each point in order around the chord length. The black points and line represents the mean positional error between points in the reconstruction and the original normalized points. The error bars represent standard error across all 1,000 points for each boundary. The red line represents the maximum positional error among all boundary points. The dashed black line is the error induced by digitization. Beyond 80 PC's the mean positional error is below the expected digitization error.

3.3.4 Morphological discrimination of animals

We sought to understand to what extent size similarity corresponds to shape similarity by performing a linear discriminant analysis (LDA) between pairs of animals, attempting to discriminate between them based on only on their shape information. For a given pair of animals, we sample 2,000 shapes from each animal and use that as a training set for our linear discriminant function. We then evaluate the separability by predicting the animal of origin for each shape given it's LD score, and evaluate the accuracy of this LD-based assignment (percentage of true positives *vs.* negatives). The separability test is performed on an independent test set of 2,000 shapes that were not used in training. Figure 3.4A provides two example results of this analysis, performed respectively on two animals of similar size (left) and very different sizes (right). These results suggest that the ability to discriminate between animals based on morphology is dependent on their relative size difference.

We determined that several factors affect discrimination performance in pair-wise comparisons between all animals (Figure 3.4B). Firstly, it is interesting that discrimination performance is significantly better than random (0.5) for all animal shapes. This suggests that even the smallest animals have distinctive shapes. Secondly, as expected, a greater size difference, defined as $f_A = \frac{2|A_1 - A_2|}{A_1 + A_2}$ corresponds to a better discrimination performance. This observation buttresses the initial pattern of allometric growth observed in Figure 3.2. Lastly, and perhaps counter-intuitively, when animals are relatively similar in size, discrimination performance is worse for larger animals than for smaller animals. This reveals that the flexibility in morphology at larger sizes is sufficient to compensate for idiosyncratic growth, though this nevertheless does not compensate for the allometric changes in form. Both of these effects can be quantified using a logistic regression: the size ratio between the two an-

imals is highly significant and improves discrimination ($\beta = 2.64, z = 6.22, p5 < 10^{-10}$), while the size of the largest animal has a significant negative impact on discrimination performance ($\beta = -0.13, z = -2.02, p = 0.044$). The effect of increasing dynamism in shape at larger sizes can be quantified by measuring the pair-wise distances between all shapes from the same animal, measured using the mean Euclidean pair-wise distance Δ between shapes. We find that Δ is weakly correlated correlated with animal size in a highly significant fashion (linear regression: $t = 4.196, p < 10^{-4}$, adj. $R^2 = 0.18$), suggesting that small animals are more restricted in their dynamic morphologies, which contributes to their morphological distinctiveness.

3.4 Discussion

In this chapter we developed a new method for comparing the morphology of simple multicellular animals in the absence of any anatomical landmarks. We demonstrated that, even at a coarse-grained level, Placozoa show allometric growth. We then developed a more refined and unambiguous definition of shape through developing a method of shape standardization and the use of EFT and PCA. We then demonstrated how this shape representation can be used to evaluate how discernible or distinct animals are in their morphologies. In addition to determining the presence of allometric growth in such organisms, we have also revealed that small animals are more easily discerned from one another than large animals. This is largely due to more restricted shape dynamics of smaller animals. Together, these findings set the groundwork for future studies on taxonomic comparisons in morphology between different strains of Placozoa and for the capability to investigate whether the shape dynamics of Placozoa have stereotyped patterns or behavior.

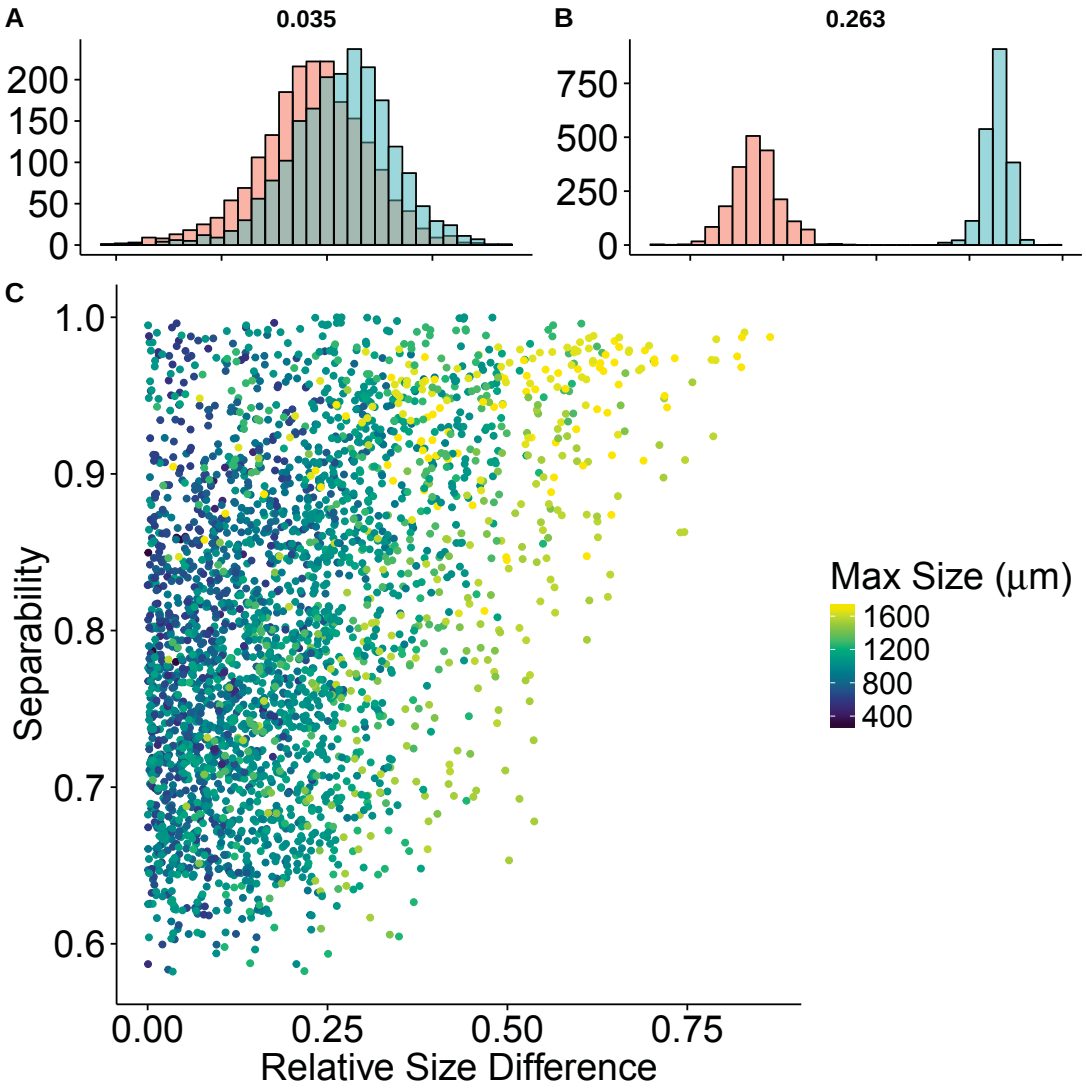

Figure 3.4: Animals are easier to distinguish morphologically when the difference in their sizes is greater or when the animals are on average smaller. (A) The distribution of linear discriminant values for 100 shapes gathered from two animals. Left: animals that ahve a small difference in mean size, where $f_A = 0.035$. Right: animals that have a relatively large size difference, where $f_A = 0.263$. Larger size differences result in a smaller overlap in LD values. (B) Pair-wise discrimination performance between animals organized by their relative size difference. The color represents teh mean size of the largest animal in the pair-wise comparison.

The issue of allometry is interesting in a two-dimensional organism, precisely because such organisms circumvent the traditional volumetric and metabolic arguments that are used to motivate the occurrence of this phenomenon. It is evident that Placozoa become more complex in their shapes as they become larger. It is likely that this more complicated shape has significant detrimental consequences to the coordination of *T. adhaerens*, and investigating the relationship between shape and ordered collective movement is likely to be a fruitful direction for future studies. Nevertheless, such allometry could also provide certain advantages for sensing or growth. Recent histological studies revealed that the boundary of *T. adhaerens* is functionally distinct from the bulk of the animal, with a high concentration of cells that are capable of binding the neurotransmitter RFamide[157] and other neurotransmitter-containing cells[169,170]. It is possible that these cells are responsible for chemotaxis and sensisng, and that elongating the boundary allows a larger animal to disproportionately improve its sensory capabilities. The animal boundary is also the region distinct for expressing ancestral growth factors such as *Trox*-2[52], suggesting that this region of the animal may contain pluripotent stem cells and be especially important for growth, thereby allowing animals with more complicated shapes to grow more quickly. Such hypotheses could be tested by observing chemotaxis performance and growth in different animals both using the natural shape variability of *T. adhaerens* and by surgically producing animals with extreme morphologies.

In this chapter we have investigated shape variability primarily by comparing different individuals, attempting to discern whether individuals have distinct morphologies, but these methods could just as easily be applied to study the dynamics of shape within individuals in an attempt to find temporal patterns and behaviors. Recent advances in compu-

tational biology have enabled the use of dimension-reduction techniques to quantify and map the structure of behavior in an unspervised fashion for a variety of species ranging from nematodes[176,178,177], flies[21], and mice[208]. These techniques have not been easily transferred to organisms like *T. adhaerens* because they are dependent on identifying axes of symmetry to be used for alignment of animal body postures observed at different points in time. It is arguably in organisms such as *T. adhaerens*, whose anatomy is so far-removed from our own, that such unsupervised pattern recognition techniques would provide the insight above observer intuition. Though some advances have been made in understanding the behavior of amoeboid organisms by studying the morphology of single-celled amoeba with regard to their direction of motion[56,110,66], these methods rely on the presence of persistent directional motion for alignment, which not only is often not present but it is also difficult to tune the sensitivity of this method of alignment to ignore the noise in a trajectory while remaining sensitive to actual locomotion behavior[192]. The shape normalization method we have used and propose does not share these sensitivities.

In spite of the strength of the elliptic Fourier transform (EFT), it has not become a widely-adopted tool in morphometrics because there are several closely-related variants of such a technique and there is no consensus as to which method is most robust[70]. Of chief concern regarding the EFT is that it identifies the majority of the shape information - the information that determines the position of a boundary point - as being encoded in the lowest-frequency harmonics such as the best fitting-ellipse. While at face-value this is true for any shape, this tendency to emphasize the lowest-order harmonics could obfuscate important morphological differences that occur only at higher-order harmonics when performing statistical analyses. One method by which this can be mitigated is to remove the first-order

(major ellipse) from the analysis entirely, but often the next-lowest components (second, third, etc.) become the decisive factors of the analysis instead[51]. Another alternative is to standardize the components before using a PCA, but this could exaggeerate variation in the highest-frequency components, which might not only be arguably insignificant to the general morphology, but also are the most susceptible to digitization noise and smoothing[64,70]. A second issue with the EFT is that it is a quantification of shape information that occurs at a global scale, with each harmonic acting on the entire boundary of an organism. This poses a problem when the features that are relevant for comparison occur only locally, such as defined limbs or other local structures. In the case of Placozoa, the absence of any identifiable anatomical components and any indication that the first-order harmonic is irrelevant prompted us to use the simplest approach of considering all of the EFT shape information in my analysis, but care needs to be taken when applying this method to other systems.

It is an exciting time for behavioral sciences as unsupervised methods of quantifying behavior are being more widely adopted, creating the potential for more refined and unbiased classification of behavior[195]. These techniques however, rely on the ability to identify distinct postures. This work demonstrates a method by which one can produce a shape representation (posture) for animals with decentralized morphologies. That we have found persistent inter-individual differences in shape, and that we have found shape variation with size, suggests that this approach is a valid method by which such shape can be quantified. Future studies can then use the elementary components of shape or posture identified with this method, and determine the dynamic relationships between forms, identifying the components of behavior[178]. From this vantage point, it may become possible to map and understand the behavioral repertoire available to the ancestors of all animals, and measure

the complexity of behaviors in one of the world's simplest animals.

3.5 Methods

3.5.1 Animal cultures

T. adhaerens were reared in 150 mm diameter plastic petri dishes filled with 100 mL of artificial seawater (ASW) at 35 parts per thousand concentration (ppt, Instant Ocean Reef Crystals). The seawater was seeded with *Pyrenomonas salina* microalgae to a known concentration, measured as optical density at 600 nm using a spectrophotometer. *Pyrenomonas salina* were reared sep arately in 1000 mL cell culture flasks with vented caps, filled with algae growth media (35 ppt ASW + 1:1000 f/2 Guillard's growth media). Fresh cultures were started every two weeks with haphazardly-selected animals from previously established cultures, using ten animals as the founder population for each new culture.

3.5.2 Shape registration and frame selection

Animals were transferred to individual dishes with sterile ASW and allowed to rest for 30 minutes before filming. We developed an automated stage and microscopy that allowed us to record videos of each animal's behavior at 2 Hz frame rate for at least two hours. We binarized the image and segmented the animal on each frame, measuring the shape factors of the selected regions. Frames in which the animal was only partially in the field of view or where the automated stage was moving were discarded from further analysis. curled-up state, where the footprint area was less than seventy-five percent of the maximal area observed, were discarded from further analysis. The specifics of the numerical methods used in the morphological comparisons are described in the results section.

3.5.3 Shape factors

The shape of an object can be quantified by a variety of non-dimensional morphological measures, also known as shape factors. Such non-dimensional measures are made either by comparing the properties of a shape amongst themselves, or by comparing the shape's properties to equivalent properties for the shape's convex hull. We used the shape factors of aspect ratio, eccentricity, circularity C, solidity S, waviness W, and compactness K to define each shape using a 7-dimensional vector in this non-dimensional space. The measures we used are defined in the equations below. In these equations, A is the area of the animal's footprint and P is the perimeter, A_C and P_C are the area and perimeter of the shape's convex hull, D_e is the diameter of a circle of equivalent area, and D_M is the caliper (Ferets') diameter.

$$C = \frac{4\pi A}{P} \tag{3.7}$$

$$S = \frac{A}{A_c} \tag{3.8}$$

$$W = \frac{P_c}{P} \tag{3.9}$$

$$K = \frac{D_e}{D_M} \tag{3.10}$$

All other morphological methods and statistical tests are explained in the main text of the results.

4

Conclusion

A fundamental goal of evolutionary biologists is understanding the forces that drive and sustain the major evolutionary transitions that have gradually increased the complexity of life on Earth[184]. Advances in the study of collective behavior have shown how complexity can arise in a self-organized fashion[129,13,39]. One can understand the driving forces behind this increase in complexity from two perspectives: either identifying the advantages of com-

plexity, or the limitations of simplicity. I apply this framework to the specific case of early multicellular organisms, investigating coordination in such decentralized organisms and determining the limits imposed on coordination by this decentralized architecture.

In chapter 1 I used methods adapted from statistical mechanics to quantify how size affects coordinated locomotion in *Trichoplax adhaerens*. I use a fluctuation-correlation framework to measure how movement information is transmitted across the decentralized multicellular network, and how the corrleation structure created through this information transmission is affected by changes in size. Through our measures I identify that not only do *Trichoplax adhaerens* show signatures of being at criticality - that is, optimally tuned for information transmission - but also that even at this special parameter regime, the physical limitations imposed by simple multicellularity produce size-mediated trade-offs in coordination. This provides a general method by which we can estimate information propagation through such a decentralized system that we can apply to important behavioral phenomena such as emergent changes in travel direction[9] or how the animal-wide feeding response propagates throughout the animal[171]. These topics would provide promising avenues for future studies.

Identifying how size imposes limitations on coordination in such systems naturally leads to the question of whether and how size is regulated. In Chapter 2 I demonstrated that we can predict, with very high precision, the growth of an animal if we know it's initial size and the nutrient conditions over a given time window. One very interesting result is that asexual fission is rare below a certain size regardless of nutrient conditions. Two important future directions are opened up by this research, one behavioral and the other ecological. The size-fission relationship I have discovered implies that there is some physical constraint

- a diffusion coefficient on information propagation - that is sufficiently large to prevent fission at small sizes but makes larger animals susceptible to fission. One hypothesis, fueled by the observation that fission is rare when animals are not feeding (data not shown) is that the feeding behavior could have a delayed propagation across large animals, and might even occur asynchronously across very large animals, resulting in force-mediated fission. Analyzing recordings of high spatial and temporal resolution of this feeding behavior in larger animals would certainly reveal if there is a dependence on animal-wide behavioral synchronization with animal size. Regarding the ecological consequences of size regulation, more comprehensive studies with finer time resolution could relate the size at fission to metabolic theory for such decentralized, modular animals[161,162,165] and identifying whether the combination of growth and fission poises *Trichoplax adhaerens* at a metabolically optimum size for a given nutrient condition.

Our current investigations have primarily focused on size, but network topology - which in the case of a lattice is effectively shape - is also also very significant for network dynamics and information propagation[5]. In Chapter 3 I developed a framework by which one can compare shape between animals in a size and rotation-invariant fashion, and showed that Placozoa exhibit allometric shape variation. One of the most obvious allometries is the tendency for increasingly elongated form and more complex boundaries at larger sizes. Ecologically, an open question is why this allometry exists when there are several arguments for why such animals should grow isometrically (see Introduction of Chapter 2). One interesting hypothesis is that, by their benthic exploration, such animals encounter new resources in proportion to their perimeter and at most with only one half of the perimeter at any time. By growing in elongated shapes, *T. adhaerens* can form a wide, phalanx-like feeding

front that encounters nutrients at a faster rate than a circular animal. Of course, this benefit can only accrue if there are not significant coordination trade-offs between shape elongation (effectively increasing the mean pair-wise distance between cells) and coordination. In Chapter 1 I did not find any effect of shape (circularity) on the correlation structure within an animal, but this could simply be masked by the fact that shape correlates so strongly with size (as seen in Chapter 3). A more rigorous test of this effect could be done by taking advantage of the great regenerative capabilities of Placozoa, surgically producing animals of different sizes and morphologies, and then measuring both effects independently.

The earliest multicellular animals, in spite of their evolutionary importance, have often defied our understanding by their ability to grow to highly variable sizes and morphologies[210]. Such animals must possess behavioral and morphological strategies that enable them to resolve their important ecological challenges in the face of such uncertainty of scale. In this thesis I expanded upon and developed methods that allow us to understand how various properties are affected by scaling in such organisms, including coordination (Chapter 1), size regulation (Chapter 2), and morphology (Chapter 3). By understanding the advantages and trade-offs imposed by scaling in arguably the simplest multicellular animal, we can also elucidate the evolutionary forces that led to increasing complexity in the later-diverged Metazoa.

A

Supporting Information for Chapter 1

A.1 Measurement sensitivity to noise

Our optical flow algorithm is based on the Horn-Schunk method[80], which while offering very good performance in estimating flow for smooth, continuous motion, will introduce spurious correlations over image discontinuities. To ensure that the range and form of our correlation profiles are not caused by sensitivity to noise, we measured the sensitivity of our

optical flow measurement to noise with two controls: a positive control on a scrambled image, and by measuring the flow field produced by an immobile, dead animal, where any movement should be caused by measurement noise of the camera sensor.

We produced white noise video by taking recorded images in our datasets and scrambling the pixels, and then producing a video a from a sequence of such images. Our optical flow algorithm produces long-range correlation artifacts on such a video (Figure A.1A), as expected based on the limitations of the algorithm. However, these long-range fluctuations are ephemeral, being completely uncorrelated between subsequent frames (A.1B). By comparing the fluctuations recorded from real data on animal movement (A.1C, top) with the fluctuations produced by a scrambled animal image (A.1C, bottom), we find that fluctuations observed for real data are stable over long time periods, while those produced by noise are completely uncorrelated across time. This very different timescale of the noise-derived fluctuations and the velocity fluctuations from our animal data makes it impossible that our own measurements are artificially-induced by such noise.

A second control we performed was to take a recording of an animal that perished in the middle of our recording and had begun to degenerate, and measure the velocity field within this dead organism. In this case, any correlations that arise should be driven entirely by noise in the camera sensor and illumination system. We performed the same segmentation and fluctuation calculation as in our methods, producing a velocity fluctuation field within the dead animal (Figure A.2A). We find that the range of spatial correlations in the velocity fluctuations is significantly smaller than those we record in living animals. When we compare the correlation length of the velocity fluctuations within the dead animal to those recorded in living organisms (A.2B). Not only is the correlation length for our dead speci-

men much smaller than what would be expected for an organism of such a given size, but it is also almost half the size as those recorded in even our smallest individuals. We therefore are confident that our measurements are outside the range of those inducible by noise.

A.2 Measurement error induced by optical flow estimation parameters

The effect of spatial distance on the strength of velocity correlation between cells at different spatial distances is likely to be influenced by the granularity with which we can measure local the local velocity of a cell. Using optical flow, the measurement of this velocity is the result of integrating the movement of a pixel intensity pattern within a certain radius of the position of the estimated vector. The granularity with which our optical flow field estimates the movement in a sequence of frames is influenced by two parameters: averaging window size λ and the polynomial expansion n; more details on these parameters are available at[62]. Increasing these values results in optical flow fields that are more robust to image noise and allow for detecting faster motion, but results in a smoother motion field. Our reported results are generated with parameter settings $\lambda = 45$ and $n = 7$; the rest of the parameters are the defaults specified at[108].

We tested the effect of varying λ and n when generating correlation profiles using the fluctuations on an arbitrarily-selected flow field for our largest (Figure ??A) and smallest (??B) animals. As expected, increasing λ does increase the strength of correlations at larger spatial distances, with only very subtly, and at a more pronounced effect in smaller animals. This is because, when taken to extremely large values of λ that approach the size of the animal, the motion at any point within the animal is estimated by the movement of a substantial fraction or all of the animal. Though our results vary with the parameters used,

we find that such variation is insufficient to explain the strength of the scaling phenomena we observe on susceptibility χ. Though χ increases by up to 28 percent in our smallest animals and up to 20 percent in our largest animals as we vary λ from 15 to 240 (??C), these increases occur in near-proportion to each other when one uses reasonable values of λ that are below 100 pixels. In this case, the ratio of these two susceptibility values, $\frac{\chi_L}{\chi_S}$, changes by less than 10 percent (??D), which is insufficient to explain the much smaller value of β for the fitted sublinear scaling of this observable in our organisms.

In order to establish ground truth regarding our measurement error of these correlations using the optical flow parameters and our isolation of fluctuations by subtraction of collective modes, we produced synthetic videos of textures deforming with a known correlation length. We simulated particles whose movement is determined by a random velocity v_i. We then use a two-dimensional Gaussian kernel smoothing function with varying kernel sizes k to correlate the velocities of particles across different spatial distances. Calculating the correlations among the particles based on their positions and velocities allows us to establish a ground truth to the movement's correlation structure. We test the output of our optical flow algorithm against this ground truth by making an image sequence of the particles visualized as large dots that have their positions in each frame updated according to their respective velocities. This produces a deforming random texture with a known correlation structure. We ran our optical flow algorithm on these videos and by varying λ produce flow fields with different levels of granularity and smoothness. Figure ??A, provides a snapshot of the original image, with figure ??B showing the velocity fluctuation of each particle and ??C showing the estimated velocity field of these moving particles using optical flow.

We can compare the correlation profiles calculated from velocity fields generated by mea-

suring optical flow in videos made of plots of our moving particles, $C(r)_f$, and compare these correlation profiles $C(r)_p$ to the ground truth correlation profile based on the actual particle positions and velocities . The results of this analysis are shown in figure ??. As is expected, the correlated domain size increases with the size of Gaussian kernel smoother k (thick black line). When we compare this ground truth correlation profile to the $C(r)_f$ profiles produced with varying values of λ, we find that $C(r)_{f(k,\lambda)}$ closely follows $C(r)_{p(k)}$ provided that λ is not excessively greater than k. $C(r)_{f(k,\lambda)}$ only grossly overestimates $C(r)_{p(k)}$ when λ is approximately an order of magnitude greater than k.

We quantify this effect of λ on the error in the correlation profile estimation for any given $C(r)_{p(k)}$ by comparing the ratio of the the cumulative correlation (integral) of the correlation profiles computed from particles and from the flow field estimation. We find that error is induced in the flow estimate only when particles are correlated over a relatively short range by using a small k (Figure ??A), and this occurs only when the the averaging window λ far exceeds the actual value of k (??B). Unfortunately the inability to track cells within an actual animal precludes a direct estimation of k. However, k has a systematic effect on the observed correlation length φ for a system. We can therefore consider how the error in estimating χ is affected by the ratio of λ utilized in flow estimation with the observed φ. We find that λ only induces error in our measurement when it grossly exceeds the observed φ (Figure ??C). When we consider the range of $\frac{\lambda}{\varphi}$ for our animals, we find that at most the smallest animals may have a slightly overestimated internal correlations, with the largest animals being unaffected by our chosen value of k. Therefore, the sub-linear scaling of χ with animal size is at best underreported in our current results, whereby a more accurate direct measure of cell movement could only produce an even more exaggerated

sub-linearity.

A.3 Ensemble averaging

A key problem of applying concepts from statistical mechanics to active matter is understanding how to perform ensemble averaging necessary to define statistical quantities. Many of the previous studies that have looked at such systems have considered only spatial averages rather than ensemble averages over time[40,9,81,41], presumably because such systems are non-stationary. However, one can assess the validity of this approach by comparing both spatial and ensemble averages over time. For instance, one can compare the average correlation length φ for each correlation profile $C(r)$ at every point in time t, $\langle \varphi(C(r), t) \rangle$ with the correlation length of the average correlation profile, $\varphi(\langle C(r) \rangle)$. The error estimate of the latter quantity we bootstrap this ensemble calculation samples of fifty percent of all of our data over 100 iterations. A procedure is performed for χ.

In figure A.7 we see the comparison of averaging these two quantities spatially and as an ensemble over time for both φ (A) and χ (B). We find that these two values correspond well with each other regardless of the method used. In the case of χ, the spatial average systematically overestimates the temporal ensemble average, but it does so systematically at all sizes and ultimately does not affect the sub-linear scaling that we observe of susceptibility with size.

A.4 Non-significant factors on correlation structure

Larger Placozoa have increasingly irregular shapes, deviating substantially from the perfect disk morphology of smaller specimens. This deviation can be quantified as an organism's

circularity, $C = \frac{4\pi A}{P^2}$ (Figure A.8A). We determined whether such shape deformation has an effect on the correlation structure within an animal by investigating a dimensionless quantity, namely the ratio of φ to the animal diameter L, which is between one-quarter to one-third of the animal diameter in our system. Though there may initially appear to be a slight correlation between the circularity of an animal and this ration (Figure A.8B), we find that this relationship is statistically not significant when we account for the effect of L itself on $\frac{\varphi}{L}$ (linear regression: $\frac{\varphi}{L} = \beta_1 L + \beta_2 C + \gamma; p(\beta_2) = 0.71$).

Aside from size, another parameter that could affect the internal correlation structure of an animal is its speed, or more generally, the magnitudes of the collective modes of movement. For instance, if our animal behaves analogously to the XY-model, then we would expect fluctuations to be largest in magnitude when the mean field or collective modes are negligible. In contrast to these systems, we observe no such effect. When we consider the extent of the correlation length φ, we find that this quantity has no correlation with the magnitudes of either the full velocity, the velocity fluctuation, or the collective velocity (defined as $w = v - u$ (Figure ??).

A.5 Collective Order

The ordered forms of collective movement within *T. adhaerens* individuals varies substantially and systematically with animal size. In our study we consider a collective mode of movement to be any transformation in the spatial position of a collective's components that can be explain by an affine transform, or a combination of rotation, translation, and dilatation. These transformations are defined in the Methods section of the main text. We present Figure A.10A to illustrate the dynamics of these order parameters for a represen-

tative small animal, with Figure A.10B showing the distribution for these three measures throughout the entire recording. As is typically for such a small animal, the dynamic range of dilatational order is quite small when compared to the rotational and polarization order, emphasizing the solid-body like motion of such animals. When we compare our largest and smallest animals (Figure A.10C), we find that the behavior of the smallest individual is well-represented by a thin manifold defining a mixture of behaviors ranging from high polarization to high rotation. Our largest individual exhibits much more disordered locomotion, with a greater proportion of time spent in lower rotation and polarization states. We can consider a general value of collective order, defined as $O = \sqrt{P^2 + R^2 + \Lambda^2}$, we find that O decreases significantly with increasing animal size. Values of O from five animals - sampled uniformly across the range of animal sizes - illustrates this decrease in order with increasing size (Figure A.10D).

A.6 Cell size is invariant to animal size

Our arguments about the effect of size on correlation structure require that cell count increase in proportion with animal area. No data on the ultrastructure of *T. adhaerens* indicate any change in cell size with animal size[169,69,68]. We nevertheless tested against this assumption by measuring the density of epithelial cells in animals of varying size. We took measured the diameter of cells within images of an animal's lower epithelium taken at 200x magnification under bright field conditions using an inverted microscope. Cells are roughly visible as dark spots that dot the animal tissue, though it is difficult to identify exact cell boundaries without staining techniques. We used ImageJ to perform histogram equalization for each image and then use the built-in local minimum detection algorithm in ImageJ

to count the number of minima within a selected sub-region of the animal. We do this in several regions from several arbitrarily-selected frames that we recorded for each animal. The tolerance for detecting local minima was 5 intensity values in an image of 8-bit color depth. As can be seen in ??, though there is substantial variability in cell density for a single animal, reflecting an animal's propensity to stretch or contract, there is no systematic effect on size on cell density. Therefore, we assume cell count increases linearly with animal area in our experiments.

A.7 Numerical Model

The overall microscopic dynamics of moving animals at the level of individual cells, will in general represent a complex interplay of inter- and intracellular mechanical forces, as well as possible chemical signaling between neighboring cells. However, despite recent advances in uncovering the detailed structure of the animal many specific aspects of the microscopic dynamics remain unknown. Thus, in order to be able to systematically study the large scale animal dynamics, we use simplified model description, based on three main assumptions:

- interactions between parts of the animal are local, restricted only to the first shell of neighboring units (Voronoi neighborhood),
- the mechanical interactions can be mapped to an effective "mechanical" spring-like forces
- each unit is self-propelled with a preferred direction of motion, which on a finite time scale relaxes towards the average direction of the resulting mechanical force. Furthermore the heading direction of self-propulsion is subject to fluctuations.

We model individual Placozoa as an ensemble of coupled self-propelled particles (SPP) in two spatial dimensions. Each particle corresponds to 'disc' of 10μm diameter. This is the experimentally resolved scale and allows us to parametrize our simulations using experimental data. The dynamics of such an ensemble of N of particles is described by a set of stochastic differential equation. The motion of each particle i ($i = 1, \ldots, N$) in 2d is described by the overdamped equations of motion given by Equation XXX in the main text.

The total force acting on an agent is a sum of two components: repulsion and attraction:

$$\vec{F}_i = \vec{F}_{i,rep} + \vec{F}_{i,att} = \sum_{j \in N_i} \mu_{att} \vec{r}_{ji} \vartheta(r_{ji} - r_o) - \mu_{rep} \vec{r}_{ji} \vartheta(r_o - r_{ji}) \tag{A.1}$$

with $\vec{r}_{ji} = \vec{r}_j - \vec{r}_i$. The strength of the different interactions is set by a constant μ_X. $\vartheta(x)$ indicates the Heaviside function and r_o the equilibrium distance. For $\mu_{att} = \mu_{rep} = \mu$, the attraction repulsion term corresponds to a simple linear restoring force towards r_o with the spring constant μ. The general case, $\mu_{att} \neq \mu_{rep}$, corresponds to an asymmetric spring with different spring constants for attraction and repulsion. Here, we assume $\mu_{att} < \mu_{rep}$ which implies lower compressibility for $r < r_o$

The interaction neighbors of a focal particle i, correspond to its Voronoi neighbours. Here we can distinguish fundamentally between two model variants:

1. dynamic: the interaction network is recalculated at each step, so that particles may change positions within the network.

2. static: the Voronoi network is fixed after an initial relaxation period, so that particle maintain their neighbors

A.8 Response of correlation profiles to varying intrinsic noise in simulations

We identify two scaling phenomena We systematically varied the intrinsic angular noise in our simulations to determine if our results are sensitive to this parameter, repeating our correlation measures under these different noise regimes. The correlation profiles all show the same characteristic increasing concave decay with increasing system size (Figure A.10) When we plot the respective susceptibility of these profiles, we observe a sub-linear trend of susceptibility with system size at all noise levels, with the exception of when noise is extremely low (Figure A.13).

A.9 Matching noise levels to empirical data

We determined which noise strength from our simulation most closely approximated the statistical relationship between our full velocity fields and the fluctuation velocity fields for our animals. We estimated the mean value of the fluctuation contribution ζ to the velocity vector as the ratio of the two moduli of the velocity vector v_i and the fluctuation vector u_i, where i is the identity of the cell cluster.

$$\zeta = \sum_{i=1}^{N} \frac{\|\mathrm{u}_i\|}{\|\mathrm{v}_i\|} \tag{A.2}$$

Figure ?? reveals that ζ increases as the strength of noise increases, with a relative sigmoidal response. We believe the reason for this sigmoidal response is two-fold: firstly, cells are more likely to deviate from the collective order if their angular noise is hight, and secondly, excessive angular noise inhibits the creation of collective movement. Both of these

factors combined will produce the nonlinear response observed. We measure $\zeta = 0.51$ for *T. adhaerens* based on a sample of 500 recorded frames taken from all animals. The corresponding noise level to produce this ζ is approximately 0.31, which is just on the cusp of this sigmoidal response where noise has a substantial detrimental effect on the collective modes of locomotion.

A.10 Alternative methods of rescaling

Rescaling r by the correlation length φ is one possible method of analyzing the size invariance of correlation structure, and is the method used in other studies of a similar nature[40,45,41]. Nevertheless, the poor collapse of the correlation profiles in our system when using this method prompted us to consider other methods by which we could produce rescaled correlation profiles. One such method is χ^2 minimization, where the domain of each profile is rescaled a scalar parameter α, selected in order to minimize the sum of the squared difference between the two profiles, divided by the uncertainty[122]. The results of such a minimization are shown in Figure ??. The correlation profiles again do not collapse on top of each other in an invariant fashion. By observing the concavity and convexity of each profile, it is trivial to conclude that no better rescaling is possible.

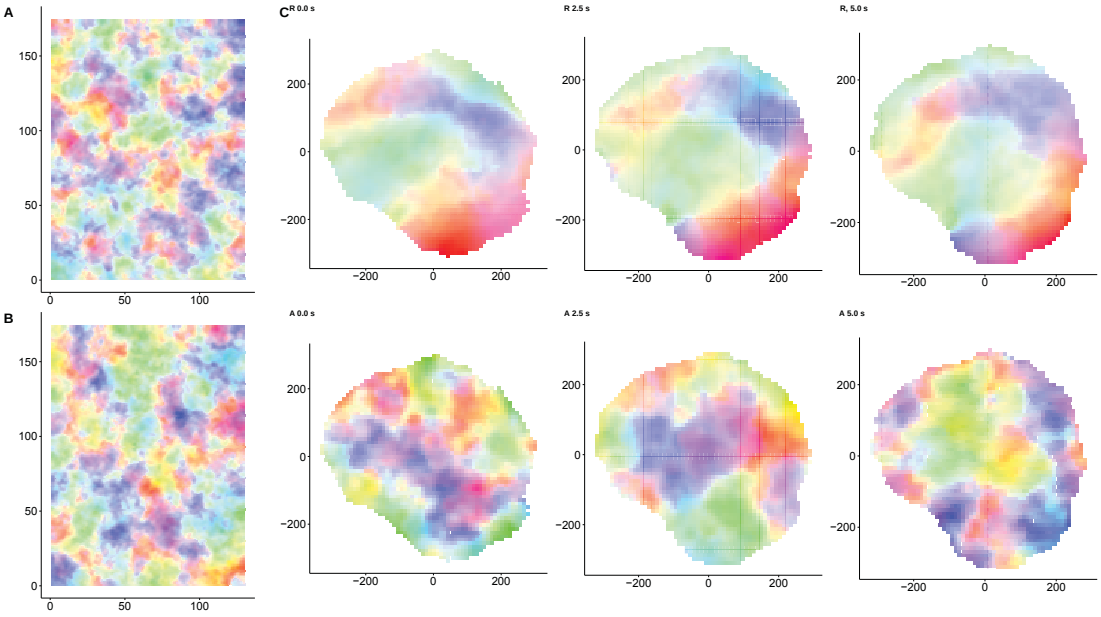

Figure A.1: Comparing animal velocity fluctuations to white noise. (A) A full velocity field generate from two subsequent scrambled images. (B) The velocity field generated for the subsequent scrambled image. (C) Time series comparison of velocity fluctuations measured from the animal's movement (top) with those generated by scrambled images (bottom) at 0, 2.5, and 5 seconds of recording.

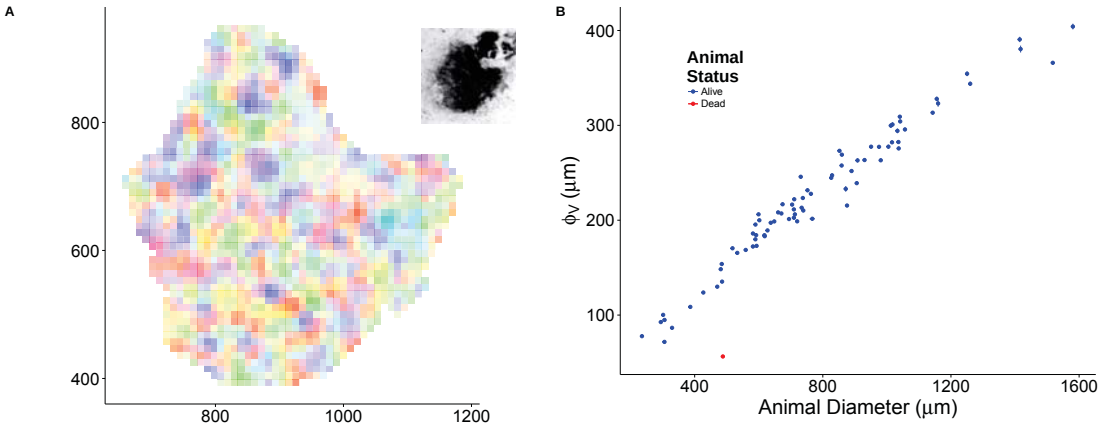

Figure A.2: Fluctuation correlations in dead animals are smaller than all live animal measurements. (A) A snapshot of the velocity fluctuation field for a dead animal, inset: image of the dead animal. Axes are in micrometers. (B) Comparison of the correlation length of velocity fluctuations from a dead animal in relation to the live measurements. The correlation length is smaller than that recorded for even our smallest live specimens.

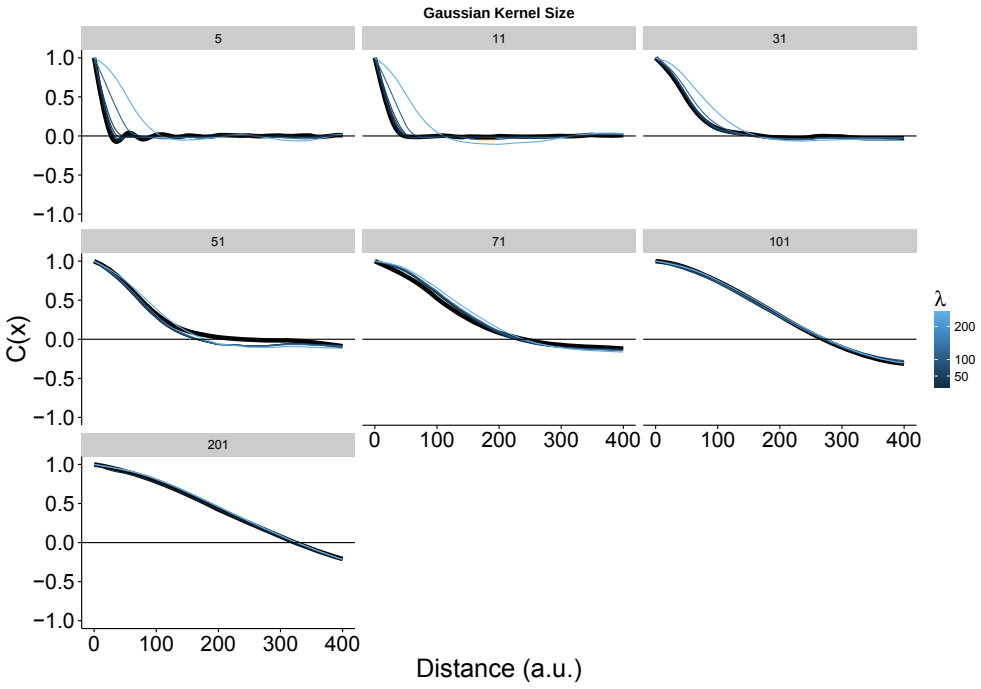

Figure A.3: Effect of changing the averaging window size of optical flow on the correlation profiles. Velocity correlation profiles measured with exact particle positions and velocities (solid black line) and estimates of this correlation function by using optical flow on videos of these moving particles. The Gaussian smoother kernel size has a direct effect on the actual correlation length and strength among particles. For each kernel size, optical flow was performed on videos, varying the averaging window size (λ).

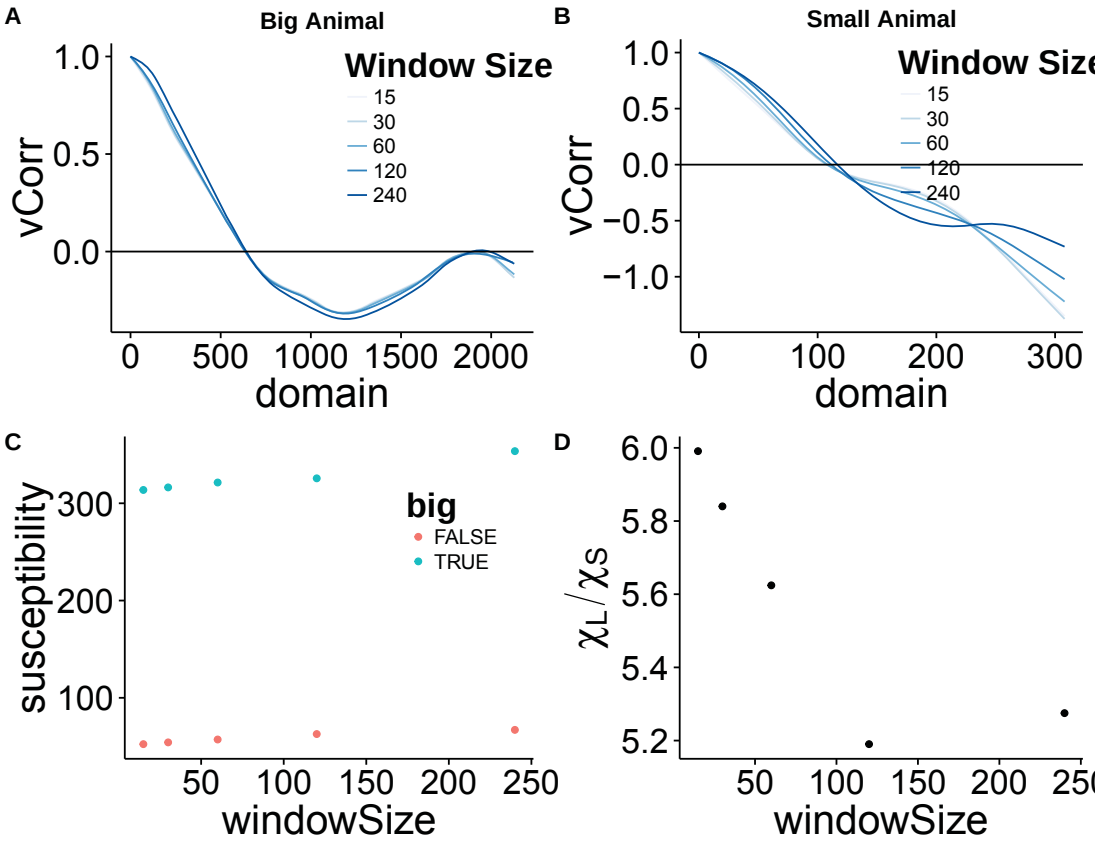

Figure A.4: Effect of window size on correlation profiles. The correlation profiles generated for two randomly-selected frames from our smallest (A) and largest (B) animal specimens, measured using the fluctuations of generated vector fields with different values of λ. (C) χ for the small and large animals at varying values of λ. (D) The ratio of susceptibility of the large animal in comparison with the smaller animal.

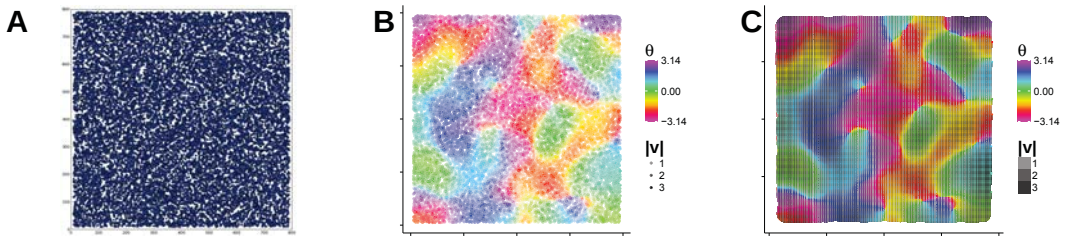

Figure A.5: Optical flow reconstruction of particle simulation. (A) Representative image of a deformable composed particles moving with correlated velocities. (B) The velocity fluctuations of all of the particles. (C) The velocity field measured on a video of moving particles ($\lambda = 45$, $k = 51$).

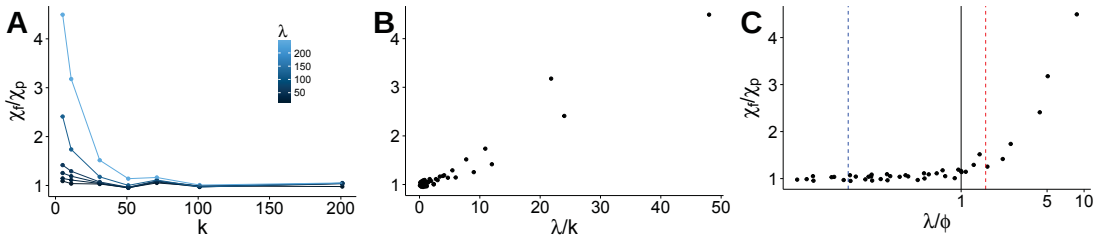

Figure A.6: Only overestimation of correlations is possible with optical flow, and occurs only when the smoothing window exceeds the actual correlation length in a system. (A) χ_f only diverges from chi_p by overestimation, and only for when correlations are much shorter than the flow averaging window size. (B) Overestimation dependence on the ratio between the flow estimation window size and the actual correlation kernel size. (C) Dependence of the in the cumulative correlation estimation on the ratio between the averaging window size and the observed correlation length (blue line: ratio of φ_v for the largest animal relative to the averaging window used in empirical flow fields; red line: similar ratio for our smallest observed animal).

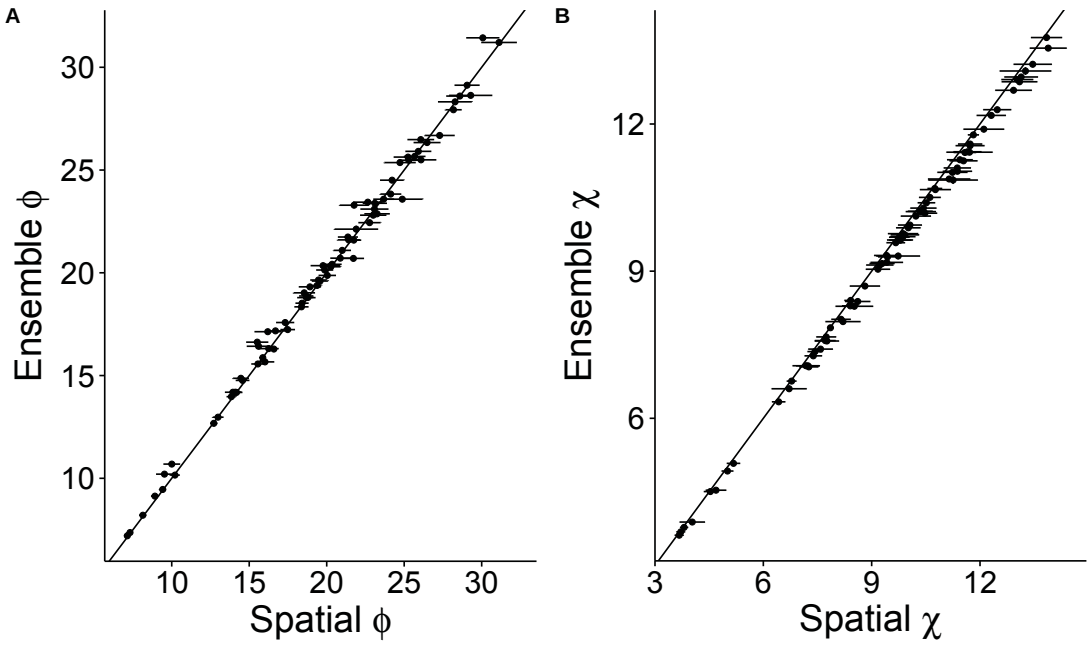

Figure A.7: Comparison of averaging methods. The correlation length (A) and susceptibility (B) are not significantly different regardless of whether one uses ensemble or spatial averaging (line: y = x).

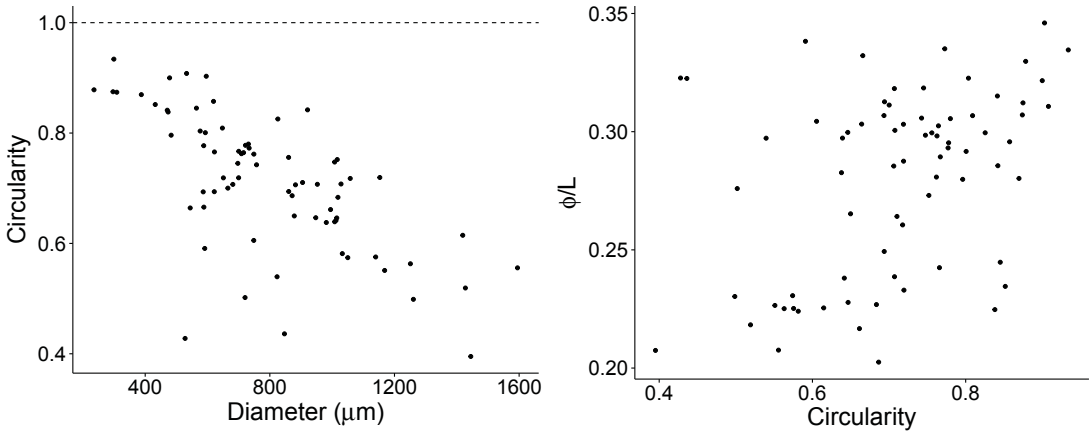

Figure A.8: Effect of shape on correlation structure. (A) Deviation from perfect circularity with increasing size (dashed line: perfect circle). (B) Circularity effect on proportional correlation length extent

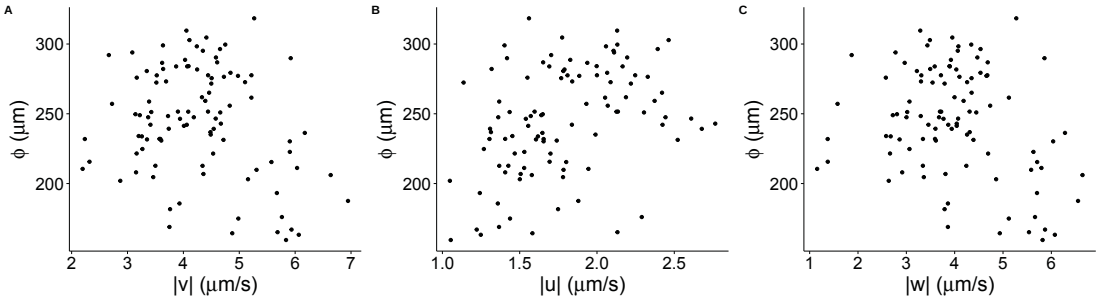

Figure A.9: Effect of collective mode magnitude on fluctuation size and intensity. (A) Rank-sorted snapshots of a single animal by $|\mathbf{w}|$. Highlighted regions are highest and lowest ten selected frames for comparison. (B) The distribution of correlation lengths between the highest and lowest ten frames.

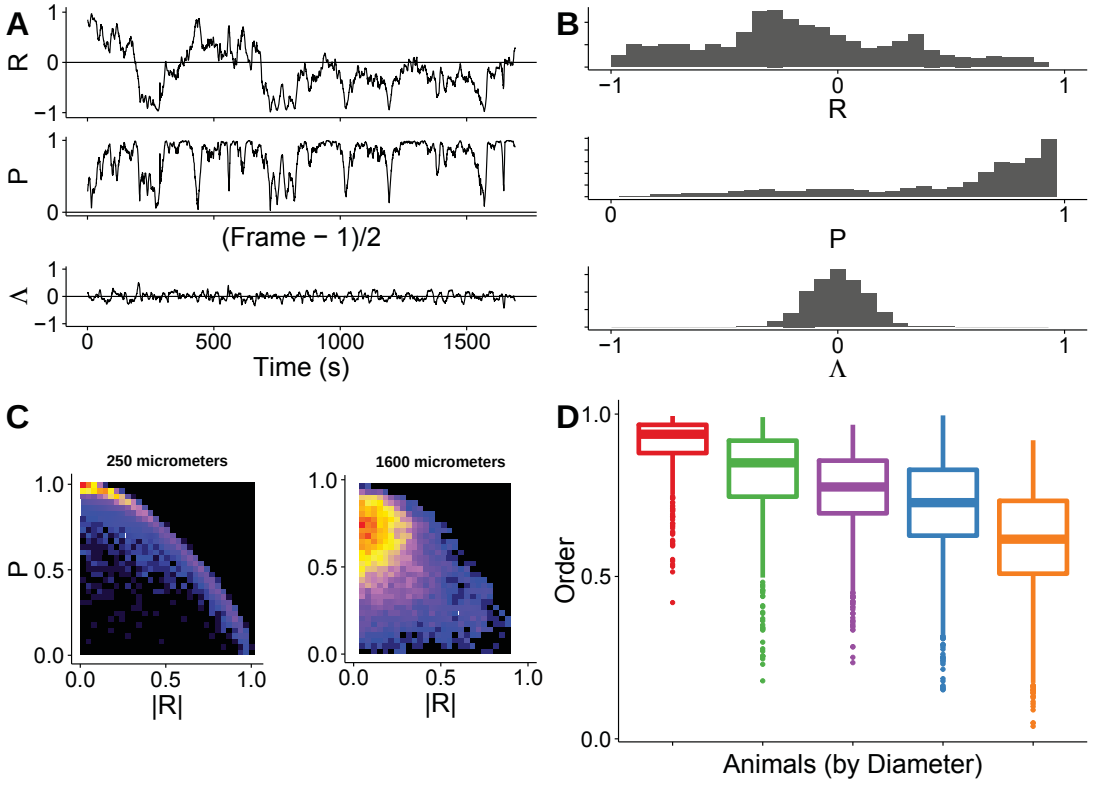

Figure A.10: Collective modes of locomotion in *T. adhaerens*. (A) A representative time series of the rotational (R), polarized (P), and dilatational (Λ) modes of collective order, showing large and high frequency variability in all parameters. (B) Histograms of the observed values for all three order parameters throughout the entire recording for one arbitrarily-selected animal. (C) Phase space histograms of the collective rotation and polarization order for the smallest and largest animals. (D) The collective order for five animals, ranked by their mean size.

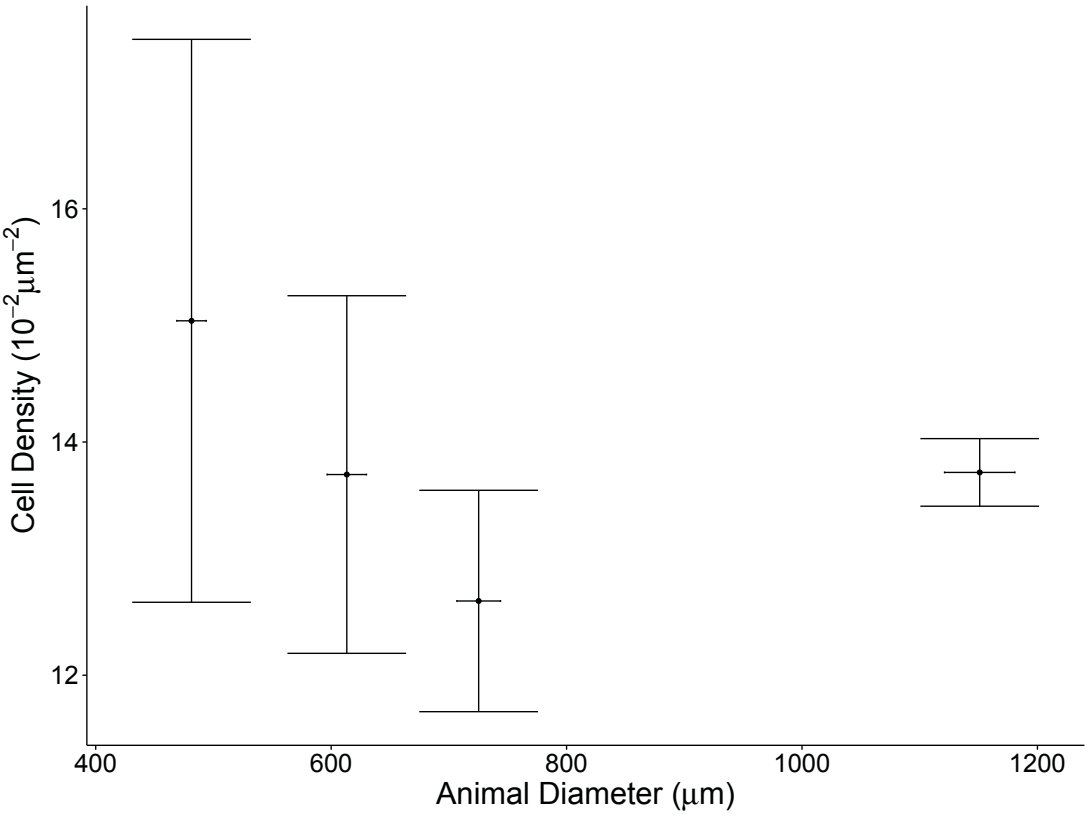

Figure A.11: Cell density is invariant with cell size. Cell counts were measured in 15 sub-regions of the animal for each animal, with regions ranging ins size from 2000 to 5000 μm^2. Error bars represent standard deviation.

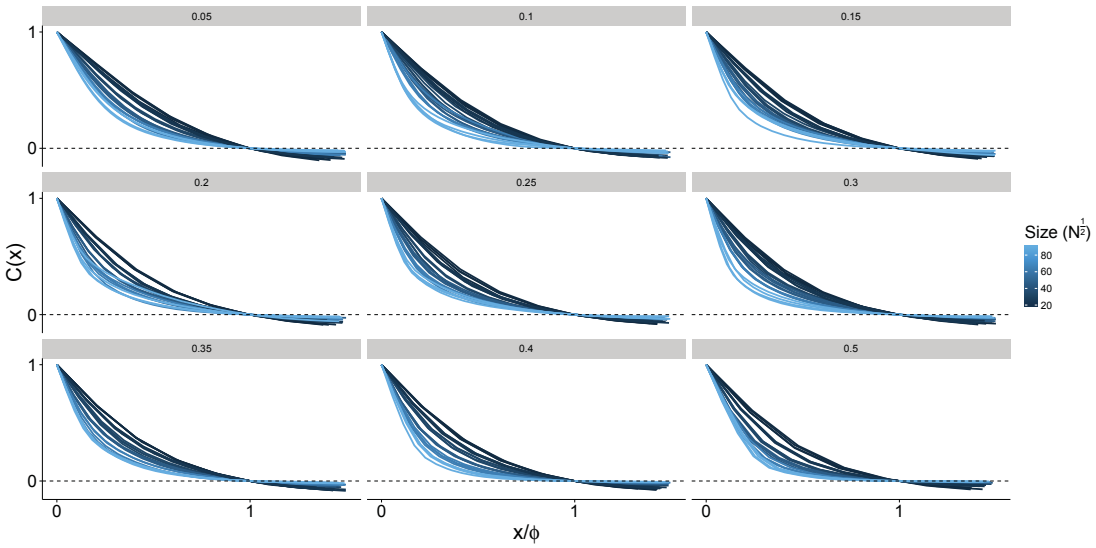

Figure A.12: Size-mediated effects on correlation strength are robust to noise. The correlation profiles for simulated systems of different sizes, with distances rescaled by their respective correlation lengths. We see that under a variety of conditions

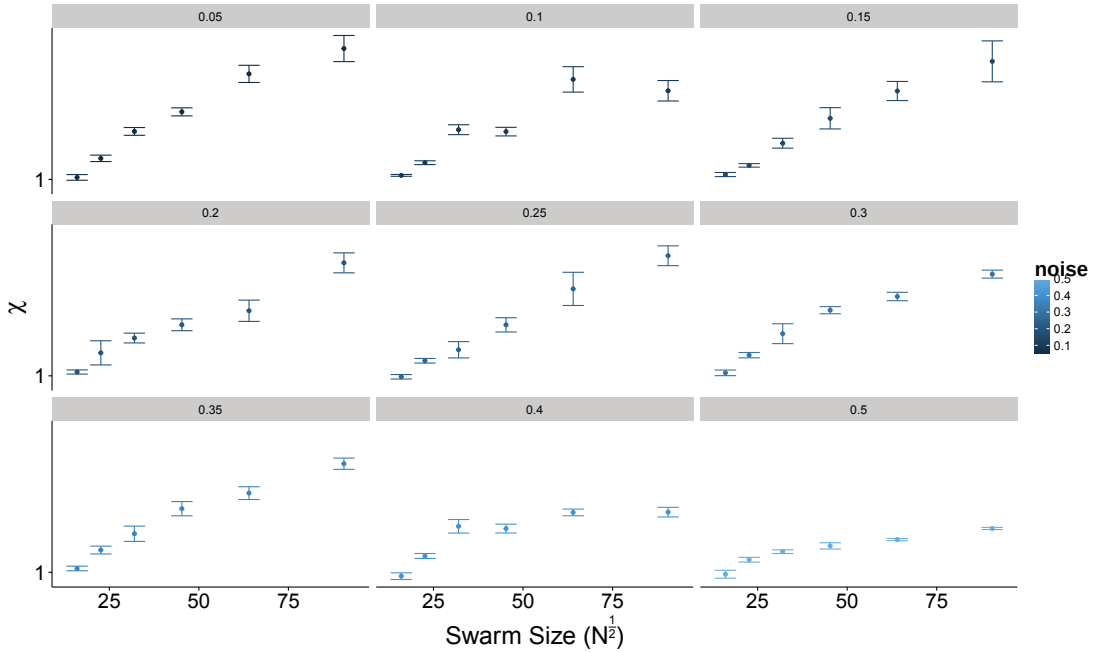

Figure A.13: Susceptibility increases sub-linearly with system size for all noise levels, though at low noise this trend approaches linearity.

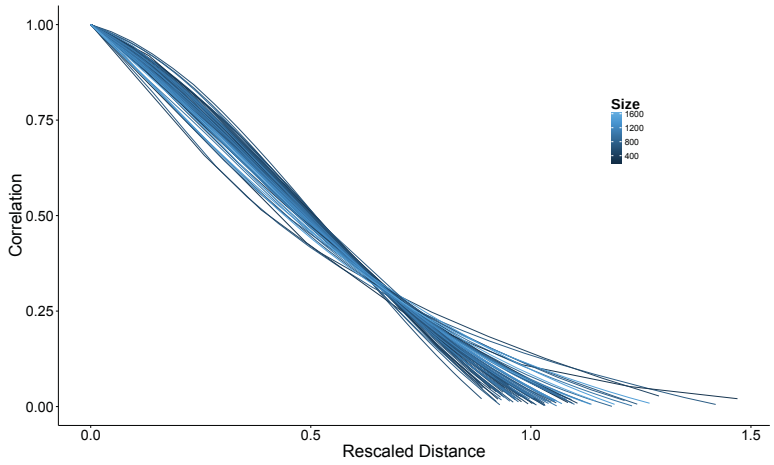

Figure A.14: χ-square minimization does not result in size invariance. The correlation profiles of all *T. adhaerens* individuals in our dataset, rescaled to align with the profile from the smallest individual after its domain was normalized by its correlation length (zero-intercept).

References

[1] Abouchar, L., Petkova, M. D., Steinhardt, C. R., and Gregor, T. (2014). Fly wing vein patterns have spatial reproducibility of a single cell. *Journal of The Royal Society Interface*, 11(97):20140443–20140443.

[2] Acebrón, J. A., Bonilla, L. L., Pérez Vicente, C. J., Ritort, F., and Spigler, R. (2005). The Kuramoto model: A simple paradigm for synchronization phenomena. *Reviews of Modern Physics*, 77(1):137–185.

[3] Adami, C. (1995). Self-organized criticality in living systems. *Physics Letters A*, 203(1):29–32.

[4] Adams, D. C., Rohlf, F. J., and Slice, D. E. (2004). Geometric morphometrics: Ten years of progress following the 'revolution'. *Italian Journal of Zoology*, 71(1):5–16.

[5] Albert, R. and Barab?si, A.-L. (2002). Statistical mechanics of complex networks. *Reviews of Modern Physics*, 74(1):47–97.

[6] Aleoshin, V. V., Konstantinova, A. V., Nikitin, M. A., and Okshtein, I. L. (2004). On the genetic uniformity of the genus Trichoplax (Placozoa). *Russian Journal of Genetics*, 40(12):1423–1425.

[7] Anderson, P. W. and others (1972). More is different. *Science*, 177(4047):393–396.

[8] Andrews, J. H. (1998). BACTERIA AS MODULAR ORGANISMS. *Annual Review of Microbiology*, 52(1):105–126.

[9] Attanasi, A., Cavagna, A., Del Castello, L., Giardina, I., Jelic, A., Melillo, S., Parisi, L., Pohl, O., Shen, E., and Viale, M. (2015). Emergence of collective changes in travel direction of starling flocks from individual birds' fluctuations. *Journal of The Royal Society Interface*, 12(108):20150319.

[10] Attanasi, A., Cavagna, A., Del Castello, L., Giardina, I., Melillo, S., Parisi, L., Pohl, O., Rossaro, B., Shen, E., Silvestri, E., and Viale, M. (2014a). Collective Behaviour without Collective Order in Wild Swarms of Midges. *PLoS Computational Biology*, 10(7):e1003697.

[11] Attanasi, A., Cavagna, A., Del Castello, L., Giardina, I., Melillo, S., Parisi, L., Pohl, O., Rossaro, B., Shen, E., Silvestri, E., and Viale, M. (2014b). Finite-Size Scaling as a Way to Probe Near-Criticality in Natural Swarms. *Physical Review Letters*, 113(23).

[12] Bak, P. (1996). The Discovery of Self-Organized Criticality. In *How Nature Works*, pages 33–48. Springer New York, New York, NY. DOI: 10.1007/978-1-4757-5426-1_2.

[13] Bak, P. (1999). *How nature works: the science of self-organized criticality*. Copernicus, New York, 1. softcover printing edition. OCLC: 246588332.

[14] Bak, P., Tang, C., and Wiesenfeld, K. (1988). Self-organized criticality. *Physical Review A*, 38(1):364–374.

[15] Bakshy, E., Hofman, J. M., Mason, W. A., and Watts, D. J. (2011). Everyone's an influencer: quantifying influence on twitter. page 65. ACM Press.

[16] Ball, E. E. and Miller, D. J. (2010). Putting placozoans on the (phylogeographic) map. *Molecular ecology*, 19(11):2181–2183.

[17] Ballerini, M., Cabibbo, N., Candelier, R., Cavagna, A., Cisbani, E., Giardina, I., Lecomte, V., Orlandi, A., Parisi, G., Procaccini, A., Viale, M., and Zdravkovic, V. (2008). Interaction ruling animal collective behavior depends on topological rather than metric distance: Evidence from a field study. *Proceedings of the National Academy of Sciences*, 105(4):1232–1237.

[18] Baylac, M. and Frie\s s, M. (2005). Fourier descriptors, Procrustes superimposition, and data dimensionality: an example of cranial shape analysis in modern human populations. In *Modern morphometrics in physical anthropology*, pages 145–165. Springer.

[19] Beggs, J. M. (2008). The criticality hypothesis: how local cortical networks might optimize information processing. *Philosophical Transactions of the Royal Society A: Mathematical, Physical and Engineering Sciences*, 366(1864):329–343.

[20] Behrendt, G. and Ruthmann, A. (1986). The cytoskeleton of the fiber cells of Trichoplax adhaerens (Placozoa). *Zoomorphology*, 106(2):123–130.

[21] Berman, G. J., Choi, D. M., Bialek, W., and Shaevitz, J. W. (2014). Mapping the stereotyped behaviour of freely moving fruit flies. *Journal of The Royal Society Interface*, 11(99):20140672–20140672.

[22] Bialek, W., Cavagna, A., Giardina, I., Mora, T., Pohl, O., Silvestri, E., Viale, M., and Walczak, A. M. (2014). Social interactions dominate speed control in poising natural flocks near criticality. *Proceedings of the National Academy of Sciences*, 111(20):7212–7217.

[23] Bialek, W., Cavagna, A., Giardina, I., Mora, T., Silvestri, E., Viale, M., and Walczak, A. M. (2012). Statistical mechanics for natural flocks of birds. *Proceedings of the National Academy of Sciences*, 109(13):4786–4791.

[24] Binder, K. (1981). Finite size scaling analysis of ising model block distribution functions. *Zeit. Physik B Condensed Matter*, 43(2):119–140.

[25] Binder, K. and Heerman, D. W. (1988). *Monte Carlo Simulations in Statistical Physics. An Introduction*. Number 80 in Springer series in solid-state sciences. Springer, Berlin, Germany, 1 edition.

[26] Boi, S., Couzin, I. D., Buono, N. D., Franks, N. R., and Britton, N. F. (1999). Coupled oscillators and activity waves in ant colonies. *Proceedings of the Royal Society B: Biological Sciences*, 266(1417):371–378.

[27] Bonhomme, V., Picq, S., Gaucherel, C., and Claude, J. (2014). Momocs : Outline Analysis Using *R*. *Journal of Statistical Software*, 56(13).

[28] Bonner, J. T. (2006). *Why size matters: from bacteria to blue whales*. Princeton University Press, Princeton. OCLC: 64335788.

[29] Bookstein, F. L. (1991). *Morphometric tools for landmark data: geometry and biology*. Cambridge University Press, Cambridge [England] ; New York.

[30] Bookstein, F. L. (1997). Landmark methods for forms without landmarks: morphometrics of group differences in outline shape. *Medical Image Analysis*, 1(3):225–243.

[31] Bookstein, F. L. (2005). After landmarks. In *Modern Morphometrics in Physical Anthropology*, pages 49–71. Springer.

[32] Boraas, M. E., Seale, D. B., and Boxhorn, J. E. (1998). Phagotrophy by a flagellate selects for colonial prey: a possible origin of multicellularity. *Evolutionary Ecology*, 12(2):153–164.

[33] Bouchard, F. and Huneman, P., editors (2013). *From groups to individuals: evolution and emerging individuality*. Vienna series in theoretical biology. The MIT Press, Cambridge, Massachusetts.

[34] Bouwman, A. M., Bosma, J. C., Vonk, P., Wesselingh, J. A., and Frijlink, H. W. (2004). Which shape factor(s) best describe granules? *Powder Technology*, 146(1-2):66–72.

[35] Bucher, D. and Anderson, P. A. V. (2015). Evolution of the first nervous systems - what can we surmise? *Journal of Experimental Biology*, 218(4):501–503.

[36] Buhl, J., Sumpter, D. J. T., Couzin, I. D., Hale, J. J., Despland, E., Miller, E. R., and Simpson, S. J. (2006). From Disorder to Order in Marching Locusts. *Science*, 312(5778):1402–1406.

[37] Buss, W., L. (1979). Habitat selection, directional growth and spatial refuges: why colonial animals have more hiding places. In Larwood, G. and Rosen, B. R., editors, *Biology and Systematics of Colonial Organisms*, volume II. Academic Press, Cambridge, UK.

[38] Buss, L. W. (1987). *The evolution of individuality*. Princeton University Press, Princeton, N.J.

[39] Camazine, S., editor (2001). *Self-organization in biological systems*. Princeton studies in complexity. Princeton University Press, Princeton, N.J.

[40] Cavagna, A., Cimarelli, A., Giardina, I., Parisi, G., Santagati, R., Stefanini, F., and Viale, M. (2010). Scale-free correlations in starling flocks. *Proceedings of the National Academy of Sciences*, 107(26):11865–11870.

[41] Chakraborty, A. and Bhattacharya, K. (2016). Spontaneous fluctuations in a zero-noise model of flocking. *EPL (Europhysics Letters)*, 116(4):48001.

[42] Charnov, E. L. (1993). *Life history invariants: some explorations of symmetry in evolutionary ecology*. Oxford series in ecology and evolution. Oxford University Press, Oxford [England] ; New York.

[43] Charnov, E. L., Turner, T. F., and Winemiller, K. O. (2001). Reproductive constraints and the evolution of life histories with indeterminate growth. *Proceedings of the National Academy of Sciences*, 98(16):9460–9464.

[44] Chaté, H. and Muñoz, M. (2014). Insect Swarms Go Critical. *Physics*, 7.

[45] Chen, X., Dong, X., Be'er, A., Swinney, H. L., and Zhang, H. P. (2012). Scale-Invariant Correlations in Dynamic Bacterial Clusters. *Physical Review Letters*, 108(14).

[46] Claude, J. (2008). *Morphometrics with R*. Use R! Springer, New York ; London.

[47] Couzin, I. (2007). Collective minds. *Nature*, 445(7129):715–715.

[48] Couzin, I. D. (2009). Collective cognition in animal groups. *Trends in Cognitive Sciences*, 13(1):36–43.

[49] Couzin, I. D., Krause, J., Franks, N. R., and Levin, S. A. (2005). Effective leadership and decision-making in animal groups on the move. *Nature*, 433(7025):513–516.

[50] Couzin, I. D., Krause, J., James, R., Ruxton, G. D., and Franks, N. R. (2002). Collective Memory and Spatial Sorting in Animal Groups. *Journal of Theoretical Biology*, 218(1):1–11.

[51] Crampton, J. S. (1995). Elliptic Fourier shape analysis of fossil bivalves: some practical considerations. *Lethaia*, 28(2):179–186.

[52] Dellaporta, S., Holland, P., Schierwater, B., Jakob, W., Sagasser, S., and Kuhn, K. (2004). The Trox-2 Hox/ParaHox gene of Trichoplax (Placozoa) marks an epithelial boundary. *Development Genes and Evolution*, 214(4):170–175.

[53] Dombrowski, C., Cisneros, L., Chatkaew, S., Goldstein, R. E., and Kessler, J. O. (2004). Self-Concentration and Large-Scale Coherence in Bacterial Dynamics. *Physical Review Letters*, 93(9).

[54] Dorigo, M., Bonabeau, E., and Theraulaz, G. (2000). Ant algorithms and stigmergy. *Future Generation Computer Systems*, 16(8):851–871.

[55] Drescher, K., Goldstein, R. E., and Tuval, I. (2010). Fidelity of adaptive phototaxis. *Proceedings of the National Academy of Sciences*, 107(25):11171–11176.

[56] Driscoll, M. K., McCann, C., Kopace, R., Homan, T., Fourkas, J. T., Parent, C., and Losert, W. (2012). Cell Shape Dynamics: From Waves to Migration. *PLoS Computational Biology*, 8(3):e1002392.

[57] Ebenman, B. and Persson, L., editors (1988). *Size-structured populations: ecology and evolution*. Springer-Verlag, Berlin ; New York.

[58] Eitel, M., Guidi, L., Hadrys, H., Balsamo, M., and Schierwater, B. (2011). New Insights into Placozoan Sexual Reproduction and Development. *PLoS ONE*, 6(5):e19639.

[59] Eitel, M., Osigus, H.-J., DeSalle, R., and Schierwater, B. (2013). Global Diversity of the Placozoa. *PLoS ONE*, 8(4):e57131.

[60] Eitel, M. and Schierwater, B. (2010). The phylogeography of the Placozoa suggests a taxon-rich phylum in tropical and subtropical waters: PLACOZOA BIODIVERSITY AND PHYLOGEOGRAPHY. *Molecular Ecology*, 19(11):2315–2327.

[61] Ender, A. and Schierwater, B. (2003). Placozoa Are Not Derived Cnidarians: Evidence from Molecular Morphology. *Molecular Biology and Evolution*, 20(1):130–134.

[62] Farnebäck, G. (2003). Two-Frame Motion Estimation Based on Polynomial Expansion. In Goos, G., Hartmanis, J., van Leeuwen, J., Bigun, J., and Gustavsson, T., editors, *Image Analysis*, volume 2749, pages 363–370. Springer Berlin Heidelberg, Berlin, Heidelberg. DOI: 10.1007/3-540-45103-X_50.

[63] Ferrante, E., Turgut, A. E., Dorigo, M., and Huepe, C. (2013). Collective motion dynamics of active solids and active crystals. *New Journal of Physics*, 15(9):095011.

[64] Ferson, S., Rohlf, F. J., and Koehn, R. K. (1985). Measuring Shape Variation of Two-dimensional Outlines. *Systematic Biology*, 34(1):59–68.

[65] Gelblum, A., Pinkoviezky, I., Fonio, E., Ghosh, A., Gov, N., and Feinerman, O. (2015). Ant groups optimally amplify the effect of transiently informed individuals. *Nature Communications*, 6:7729.

[66] Grebecka, L. and Grebecki, A. (1975). Morphometric Study of Moving Amoeba proteus. *Acta Protozoologica*, 14(3/4):337–361.

[67] Gregor, T., Fujimoto, K., Masaki, N., and Sawai, S. (2010). The Onset of Collective Behavior in Social Amoebae. *Science*, 328(5981):1021–1025.

[68] Grell, K. G. and Ruthmann, A. (1991). Placozoa. In Harrison, F. W., editor, *Microscopy Anatomy of Invertebrates*, volume 2, pages 13–27. Wiley-Liss, New York.

[69] Guidi, L., Eitel, M., Cesarini, E., Schierwater, B., and Balsamo, M. (2011). Ultrastructural analyses support different morphological lineages in the phylum placozoa Grell, 1971. *Journal of Morphology*, 272(3):371–378.

[70] Haines, A. J. and Crampton, J. S. (2000). Improvements to the method of Fourier shape analysis as applied in morphometric studies. *Palaeontology*, 43(4):765–783.

[71] Hall, V. R. and Hughes, T. P. (1996). Reproductive Strategies of Modular Organisms: Comparative Studies of Reef- Building Corals. *Ecology*, 77(3):950–963.

[72] Handegard, N., Boswell, K., Ioannou, C., Leblanc, S., Tjøstheim, D., and Couzin, I. (2012). The Dynamics of Coordinated Group Hunting and Collective Information Transfer among Schooling Prey. *Current Biology*, 22(13):1213–1217.

[73] Hartnett, A. T., Schertzer, E., Levin, S. A., and Couzin, I. D. (2016). Heterogeneous Preference and Local Nonlinearity in Consensus Decision Making. *Physical Review Letters*, 116(3).

[74] Hassett, W. P. (2006). *An a Analysis of Placozoan Nutrition and Biomineralization*. PhD thesis, University of Hawaii.

[75] Heino and Kaitala (1999). Evolution of resource allocation between growth and reproduction in animals with indeterminate growth. *Journal of Evolutionary Biology*, 12(3):423–429.

[76] Hemelrijk, C. K. and Hildenbrandt, H. (2011). Some Causes of the Variable Shape of Flocks of Birds. *PLoS ONE*, 6(8):e22479.

[77] Hertel, J., de Jong, D., Marz, M., Rose, D., Tafer, H., Tanzer, A., Schierwater, B., and Stadler, P. F. (2009). Non-coding RNA annotation of the genome of Trichoplax adhaerens. *Nucleic Acids Research*, 37(5):1602–1615.

[78] Hesse, J. and Gross, T. (2014). Self-organized criticality as a fundamental property of neural systems. *Frontiers in Systems Neuroscience*, 8.

[79] Highsmith, R. C. (1982). Reproduction by fragmentation in corals. *Marine ecology progress series. Oldendorf*, 7(2):207–226.

[80] Horn, B. K. and Schunck, B. G. (1981). Determining optical flow. *Artificial Intelligence*, 17(1-3):185–203.

[81] Huepe, C., Ferrante, E., Wenseleers, T., and Turgut, A. E. (2015). Scale-Free Correlations in Flocking Systems with Position-Based Interactions. *Journal of Statistical Physics*, 158(3):549–562.

[82] Hughes, D. J. and Huges, R. N. (1986). Metabolic Implications of Modularity: Studies on the Respiration and Growth of Electra pilosa. *Philosophical Transactions of the Royal Society B: Biological Sciences*, 313(1159):23–29.

[83] Hughes, R. and Jackson, J. (1985). An ecological overview of cloning in Metazoa. In Jackson, J. B. C., Buss, L. W., Cook, R. E., and Ashmun, J. W., editors, *Population biology and evolution of clonal organisms*. Yale University Press, New Haven.

[84] Hughes, R. N. (1989). *A functional biology of clonal animals*. Functional biology series. Chapman and Hall, London ; New York.

[85] Hughes, R. N. (2005). Lessons in modularity: the evolutionary ecology of colonial invertebrates. *Scientia Marina*, 69(S1):169–179.

[86] Hughes, T., Szmant, A. M., Steneck, R., Carpenter, R., and Miller, S. (1999). Algal blooms on coral reefs: what are the causes? *Limnology and Oceanography*, 44(6):1583–1586.

[87] Hughes, T. P. and Jackson, J. B. C. (1980). Do Corals Lie About Their Age? Some Demographic Consequences of Partial Mortality, Fission, and Fusion. *Science*, 209(4457):713–715.

[88] Huxley, J. S. and Teissier, G. (1936). Terminology of Relative Growth. *Nature*, 137(3471):780–781.

[89] Jackson, A. M. and Buss, L. W. (2009). Shiny spheres of placozoans (*Trichoplax*) function in anti-predator defense. *Invertebrate Biology*, 128(3):205–212.

[90] Jackson, J. B. C. (1979). Morphological strategies of sessile animals. In Larwood, G. P. and Rosen, B. R., editors, *Biology and Systematics of Colonial Organisms*, volume 11, pages 499–547. Academic Press, London, UK.

[91] Jackson, J. B. C., Buss, L. W., Cook, R. E., and Ashmun, J. W., editors (1985). *Population biology and evolution of clonal organisms*. Yale University Press, New Haven.

[92] Jackson, J. B. C. and Coates, A. G. (1986). Life Cycles and Evolution of Clonal (Modular) Animals. *Philosophical Transactions of the Royal Society B: Biological Sciences*, 313(1159):7–22.

[93] Karlson, R. H. (1991). Fission and the dynamics of genets and ramets in clonal cnidarian populations. In *Coelenterate Biology: Recent Research on Cnidaria and Ctenophora*, pages 235–240. Springer.

[94] Katz, Y., Tunstrom, K., Ioannou, C. C., Huepe, C., and Couzin, I. D. (2011). Inferring the structure and dynamics of interactions in schooling fish. *Proceedings of the National Academy of Sciences*, 108(46):18720–18725.

[95] Kauffman, S. A. (1993). *The origins of order: self-organization and selection in evolution*. Oxford University Press, New York.

[96] Kauffman, S. A. and Johnsen, S. (1991). Coevolution to the edge of chaos: Coupled fitness landscapes, poised states, and coevolutionary avalanches. *Journal of Theoretical Biology*, 149(4):467–505.

[97] Kaufmann, K. W. (1981). Fitting and using growth curves. *Oecologia*, 49(3):293–299.

[98] Kendall, D. G. (1989). A survey of the statistical theory of shape. *Statistical Science*, pages 87–99.

[99] Kessin, R. H., Gundersen, G. G., Zaydfudim, V., and Grimson, M. (1996). How cellular slime molds evade nematodes. *Proceedings of the National Academy of Sciences*, 93(10):4857–4861.

[100] Kim, K. and Lasker, H. R. (1998). Allometry of resource capture in colonial cnidarians and constraints on modular growth. *Functional Ecology*, 12(4):646–654.

[101] King, N. (2004). The unicellular ancestry of animal development. *Developmental cell*, 7(3):313–325.

[102] Kinouchi, O. and Copelli, M. (2006). Optimal dynamical range of excitable networks at criticality. *Nature Physics*, 2(5):348–351.

[103] Kirk, D. L. (2005). A twelve-step program for evolving multicellularity and a division of labor. *BioEssays*, 27(3):299–310.

[104] Kosterlitz, J. (1974). Topological Phase Transitions. *J. Phys. C: Solid State Phys.*, 7(1046).

[105] Kuhl, F. P. and Giardina, C. R. (1982). Elliptic Fourier features of a closed contour. *Computer Graphics and Image Processing*, 18(3):236–258.

[106] Kuramoto, Y. (2003). *Chemical oscillations, waves, and turbulence*. Dover Publications, Mineola, N.Y, dover ed edition.

[107] Langton, C. G. (1990). Computation at the edge of chaos: Phase transitions and emergent computation. *Physica D: Nonlinear Phenomena*, 42(1-3):12–37.

[108] Leblanc, S. (2017). FishFlow.

[109] Leonard, N. E., Shen, T., Nabet, B., Scardovi, L., Couzin, I. D., and Levin, S. A. (2012). Decision versus compromise for animal groups in motion. *Proceedings of the National Academy of Sciences*, 109(1):227–232.

[110] Liang, L., Cox, E. C., and Flyvbjerg, H. (2011). 'Dicty dynamics': Dictyostelium motility as persistent random motion. *Physical Biology*, 8(4).

[111] Liebeskind, B. J. (2011). Evolution of sodium channels and the new view of early nervous system evolution. *Commun Integr Biol*, 4(6):679–683.

[112] Lukeman, R., Li, Y.-X., and Edelstein-Keshet, L. (2010). Inferring individual rules from collective behavior. *Proceedings of the National Academy of Sciences*, 107(28):12576–12580.

[113] Malet-Engra, G., Yu, W., Oldani, A., Rey-Barroso, J., Gov, N., Scita, G., and Dupré, L. (2015). Collective Cell Motility Promotes Chemotactic Prowess and Resistance to Chemorepulsion. *Current Biology*, 25(2):242–250.

[114] Marfenin, N. N. (1997). Adaptation capabilities of marine modular organisms. *Hydrobiologia*, 355(1):153–158.

[115] Marković, D. and Gros, C. (2014). Power laws and self-organized criticality in theory and nature. *Physics Reports*, 536(2):41–74.

[116] Martinelli, C. and Spring, J. (2003). Distinct expression patterns of the two T-box homologues Brachyury and Tbx2/3 in the placozoan Trichoplax adhaerens. *Development Genes and Evolution*, 213(10):492–499.

[117] Martinelli, C. and Spring, J. (2004). Expression pattern of the homeobox gene Not in the basal metazoan Trichoplax adhaerens. *Gene Expression Patterns*, 4(4):443–447.

[118] Maynard Smith, J. and Szathmáry, E. (2010). *The major transitions in evolution*. Oxford Univ. Press, Oxford, reprinted edition.

[119] McCook, L., Jompa, J., and Diaz-Pulido, G. (2001). Competition between corals and algae on coral reefs: a review of evidence and mechanisms. *Coral Reefs*, 19(4):400–417.

[120] McGovern, T. M. (2003). Plastic reproductive strategies in a clonal marine invertebrate. *Proceedings of the Royal Society B: Biological Sciences*, 270(1532):2517–2522.

[121] Melfo, A. (2017). A note on Spontaneous Symmetry Breaking in flocks of birds. *arXiv preprint arXiv:1702.08067*.

[122] Meyer, S. L. (1992). *Data analysis for scientists and engineers*. Peer Management Consultants, Ltd., Evanston, IL. OCLC: 42795291.

[123] Michod, R. E. (2007). Evolution of individuality during the transition from unicellular to multicellular life. *Proceedings of the National Academy of Sciences*, 104(Suppl 1):8613–8618.

[124] Michod, R. E. and Roze, D. (2001). Cooperation and conflict in the evolution of multicellularity. *Heredity*, 86(1):1–7.

[125] Miller, D. J. and Ball, E. E. (2008). Animal Evolution:< i> Trichoplax</i>, Trees, and Taxonomic Turmoil. *Current Biology*, 18(21):R1003–R1005.

[126] Miller, D. J. and Technau, U. (2010). Understanding the evolution of multicellularity: insights from basal metazoans. *BioEssays*, 32(2):175–178.

[127] Mire, P. (1998). Evidence for stretch-regulation of fission in a sea anemone. *The Journal of Experimental Zoology*, 282(3):344–359.

[128] Mirollo, R. E. and Strogatz, S. H. (1990). Synchronization of Pulse-Coupled Biological Oscillators. *SIAM Journal on Applied Mathematics*, 50(6):1645–1662.

[129] Mitchell, M. (2009). *Complexity: a guided tour*. Oxford University Press, Oxford [England] ; New York. OCLC: ocn216938473.

[130] Mora, T. and Bialek, W. (2011). Are Biological Systems Poised at Criticality? *Journal of Statistical Physics*, 144(2):268–302.

[131] Mora, T., Walczak, A. M., Del Castello, L., Ginelli, F., Melillo, S., Parisi, L., Viale, M., Cavagna, A., and Giardina, I. (2016). Local equilibrium in bird flocks. *Nature Physics*.

[132] Murphy, C. T., McCarroll, S. A., Bargmann, C. I., Fraser, A., Kamath, R. S., Ahringer, J., Li, H., and Kenyon, C. (2003). Genes that act downstream of DAF-16 to influence the lifespan of Caenorhabditis elegans. *Nature*, 424(6946):277–283.

[133] Nadell, C. D., Bassler, B. L., and Levin, S. A. (2008). Observing bacteria through the lens of social evolution. *Journal of Biology*, 7(7):27.

[134] Nielsen, C. (2008). Six major steps in animal evolution: are we derived sponge larvae?: Six major steps in animal evolution. *Evolution & Development*, 10(2):241–257.

[135] Nivala, M., Ko, C., Nivala, M., Weiss, J., and Qu, Z. (2012). Criticality in Intracellular Calcium Signaling in Cardiac Myocytes. *Biophysical Journal*, 102(11):2433–2442.

[136] Nowak, M. A. (2006). Five Rules for the Evolution of Cooperation. *Science*, 314(5805):1560–1563.

[137] Osigus, H.-J., Eitel, M., and Schierwater, B. (2013). Chasing the urmetazoon: Striking a blow for quality data? *Molecular Phylogenetics and Evolution*, 66(2):551–557.

[138] Otsu, N. (1979). A threshold selection method from gray-level histograms. *IEEE Transactions on systems, man, and cybernetics*, 9(1):62–66.

[139] Pearse, V. (1989). Growth and Behavior of Trichoplax Adhaerens: First Record of the Phylum Placozoa in Hawaii. *Pacific Science*, 43(2):117–121.

[140] Pearse, V. B. and Voigt, O. (2007). Field biology of placozoans (Trichoplax): distribution, diversity, biotic interactions. *Integrative and Comparative Biology*, 47(5):677–692.

[141] Perrin, N. and Sibly, R. M. (1993). Dynamic models of energy allocation and investment. *Annual Review of Ecology and Systematics*, 24(1):379–410.

[142] Podczeck, F. (1997). A shape factor to assess the shape of particles using image analysis. *Powder Technology*, 93(1):47–53.

[143] Puillandre, N., Baylac, M., Boisselier, M.-C., Cruaud, C., and Samadi, S. (2009). An integrative approach to species delimitation in Benthomangelia (Mollusca: Conoidea): INTEGRATIVE TAXONOMY IN BENTHOMANGELIA. *Biological Journal of the Linnean Society*, 96(3):696–708.

[144] Ratcliff, W. C., Herron, M. D., Howell, K., Pentz, J. T., Rosenzweig, F., and Travisano, M. (2013). Experimental evolution of an alternating uni- and multicellular life cycle in Chlamydomonas reinhardtii. *Nature Communications*, 4.

[145] Rohlf, F. J. and Archie, J. W. (1984). A comparison of Fourier methods for the description of wing shape in mosquitoes (Diptera: Culicidae). *Systematic Biology*, 33(3):302–317.

[146] Rosenthal, S. B., Twomey, C. R., Hartnett, A. T., Wu, H. S., and Couzin, I. D. (2015). Revealing the hidden networks of interaction in mobile animal groups allows prediction of complex behavioral contagion. *Proceedings of the National Academy of Sciences*, 112(15):4690–4695.

[147] Rubilar, T., Villares, G., Epherra, L., Díaz-de Vivar, M., and Pastor-de Ward, C. (2011). Fission, regeneration, gonad production and lipids storage in the pyloric caeca of the sea star Allostichaster capensis. *Journal of Experimental Marine Biology and Ecology*, 409(1-2):247–252.

[148] Ruthmann, A., Behrendt, G., and Wahl, R. (1986). The ventral epithelium of Trichoplax adhaerens (Placozoa): Cytoskeletal structures, cell contacts and endocytosis. *Zoomorphology*, 106(2):115–122.

[149] Ryaland, J. S. and Warner, G. F. (1986). Growth and Form in Modular Animals: Ideas on the Size and Arrangement of Zooids. *Philosophical Transactions of the Royal Society B: Biological Sciences*, 313(1159):53–76.

[150] Ryan, J. F. and Chiodin, M. (2015). Where is my mind? How sponges and placozoans may have lost neural cell types. *Philosophical Transactions of the Royal Society B: Biological Sciences*, 370(1684):20150059–20150059.

[151] Sawai, S., Guan, X.-J., Kuspa, A., and Cox, E. C. (2007). High-throughput analysis of spatio-temporal dynamics in Dictyostelium. *Genome biology*, 8(7):R144.

[152] Scheffer, M., Carpenter, S. R., Lenton, T. M., Bascompte, J., Brock, W., Dakos, V., van de Koppel, J., van de Leemput, I. A., Levin, S. A., van Nes, E. H., Pascual, M., and Vandermeer, J. (2012). Anticipating Critical Transitions. *Science*, 338(6105):344–348.

[153] Schierwater, B. (2005). My favorite animal,Trichoplax adhaerens. *BioEssays*, 27(12):1294–1302.

[154] Schierwater, B. and Eitel, M. (2015). Placozoa. In Wanninger, A., editor, *Evolutionary Developmental Biology of Invertebrates 1*, pages 107–114. Springer Vienna, Vienna.

[155] Schleicherová, D., Dulias, K., Osigus, H.-J., Paknia, O., Hadrys, H., and Schierwater, B. (2017). The most primitive metazoan animals, the placozoans, show high sensitivity to increasing ocean temperatures and acidities. *Ecology and Evolution*, 7(3):895–904.

[156] Schmidt-Nielsen, K. (1984). *Scaling, why is animal size so important?* Cambridge University Press, Cambridge ; New York.

[157] Schuchert, P. (1993). Trichoplax adhaerens (Phylum Placozoa) has cells that react with antibodies against the neuropeptide RFamide. *Acta Zoologica*, 74(2):115–117.

[158] Schulze, F. E. (1891). Über Trichoplax adhaerens. *Physikalische Abhandlungen*, I.

[159] Schwab, D. J., Nemenman, I., and Mehta, P. (2014). Zipf's Law and Criticality in Multivariate Data without Fine-Tuning. *Physical Review Letters*, 113(6).

[160] Schwartz, V. (1984). Das radialpolare Differenzierungsmuster bei Trichoplax adhaerens F. E. Schulze (Placozoa). *Zeitschrift für Naturforschung C*, 39(7-8):818–832.

[161] Sebens, K. (1987). The Ecology of Indeterminate Growth in Animals. *Annual Review of Ecology and Systematics*, 18:371–407.

[162] Sebens, K. P. (1979). The energetics of asexual reproduction and colony formation in benthic marine invertebrates. *American Zoologist*, 19(3):683–699.

[163] Sebens, K. P. (1982). The Limits to Indeterminate Growth: An Optimal Size Model Applied To passive Suspension Feeders. *Ecology*, 63(1):209–222.

[164] Shew, W. L. and Plenz, D. (2013). The Functional Benefits of Criticality in the Cortex. *The Neuroscientist*, 19(1):88–100.

[165] Sibly, R. and Calow, P. (1982). Asexual reproduction in protozoa and invertebrates. *Journal of Theoretical Biology*, 96(3):401–424.

[166] Signorovitch, A. Y., Dellaporta, S. L., and Buss, L. W. (2005). Molecular signatures for sex in the Placozoa. *Proceedings of the National Academy of Sciences*, 102(43):15518–15522.

[167] Small, C. G. (2012). *Statistical theory of shape.* Springer, Place of publication not identified. OCLC: 968637478.

[168] Smith, C., Hamid, E., and Reese, T. (2014a). A neuropeptide initiates feeding pauses in Trichoplax adhaerens.

[169] Smith, C., Varoqueaux, F., Kittelmann, M., Azzam, R., Cooper, B., Winters, C., Eitel, M., Fasshauer, D., and Reese, T. (2014b). Novel Cell Types, Neurosecretory Cells, and Body Plan of the Early-Diverging Metazoan Trichoplax adhaerens. *Current Biology*, 24(14):1565–1572.

[170] Smith, C. L., Abdallah, S., Wong, Y. Y., Le, P., Harracksingh, A. N., Artinian, L., Tamvacakis, A. N., Rehder, V., Reese, T. S., and Senatore, A. (2017). Evolutionary insights into T-type Ca^{2+} channel structure, function, and ion selectivity from the *Trichoplax adhaerens* homologue. *The Journal of General Physiology*, 149(4):483–510.

[171] Smith, C. L., Pivovarova, N., and Reese, T. S. (2015). Coordinated Feeding Behavior in Trichoplax, an Animal without Synapses. *PLOS ONE*, 10(9):e0136098.

[172] Smith, C. L. and Reese, T. S. (2016). Adherens Junctions Modulate Diffusion between Epithelial Cells in *Trichoplax adhaerens*. *The Biological Bulletin*, 231(3):216–224.

[173] Sokolov, A., Aranson, I. S., Kessler, J. O., and Goldstein, R. E. (2007). Concentration Dependence of the Collective Dynamics of Swimming Bacteria. *Physical Review Letters*, 98(15).

[174] Solé, R. V., Manrubia, S. C., Benton, M., Kauffman, S., and Bak, P. (1999). Criticality and scaling in evolutionary ecology. *Trends in Ecology & Evolution*, 14(4):156–160.

[175] Srivastava, M., Begovic, E., Chapman, J., Putnam, N. H., Hellsten, U., Kawashima, T., Kuo, A., Mitros, T., Salamov, A., Carpenter, M. L., Signorovitch, A. Y., Moreno, M. A., Kamm, K., Grimwood, J., Schmutz, J., Shapiro, H., Grigoriev, I. V., Buss, L. W., Schierwater, B., Dellaporta, S. L., and Rokhsar, D. S. (2008). The Trichoplax genome and the nature of placozoans. *Nature*, 454(7207):955–960.

[176] Stephens, D. W. and Dunbar, S. R. (1993). Dimensional analysis in behavioral ecology. *Behavioral Ecology*, 4(2):172–183.

[177] Stephens, G. J., Bueno de Mesquita, M., Ryu, W. S., and Bialek, W. (2011). Emergence of long timescales and stereotyped behaviors in Caenorhabditis elegans. *Proceedings of the National Academy of Sciences*, 108(18):7286–7289.

[178] Stephens, G. J., Johnson-Kerner, B., Bialek, W., and Ryu, W. S. (2008). Dimensionality and Dynamics in the Behavior of C. elegans. *PLoS Computational Biology*, 4(4):e1000028.

[179] Stocker, L. J. (1991). Effects of size and shape of colony on rates of fission, fusion, growth and mortality in a subtidal invertebrate. *Journal of Experimental Marine Biology and Ecology*, 149(2):161–175.

[180] Strandburg-Peshkin, A., Farine, D. R., Couzin, I. D., and Crofoot, M. C. (2015). Shared decision-making drives collective movement in wild baboons. *Science*, 348(6241):1358–1361.

[181] Strandburg-Peshkin, A., Twomey, C. R., Bode, N. W., Kao, A. B., Katz, Y., Ioannou, C. C., Rosenthal, S. B., Torney, C. J., Wu, H. S., Levin, S. A., and Couzin, I. D. (2013). Visual sensory networks and effective information transfer in animal groups. *Current Biology*, 23(17):R709–R711.

[182] Strogatz, S. H. (2001). *Nonlinear dynamics and chaos: with applications to physics, biology, chemistry, and engineering*. Studies in Nonlinearity. Perseus Books, Cambridge, Mass, 2. print edition. OCLC: 248691524.

[183] Szabó, B., Szöllösi, G., Gönci, B., Jurányi, Z., Selmeczi, D., and Vicsek, T. (2006). Phase transition in the collective migration of tissue cells: Experiment and model. *Physical Review E*, 74(6).

[184] Szathmary, E. and Maynard Smith, J. (1995). The Major Evolutionary Transitions. *Nature*, 374(6519):227–32.

[185] Thiemann, M. and Ruthmann, A. (1989). Microfilaments and microtubules in isolated fiber cells of Trichoplax adhaerens (Placozoa). *Zoomorphology*, 109(2):89–96.

[186] Thiemann, M. and Ruthmann, A. (1991). Alternative modes of asexual reproduction inTrichoplax adhaerens (Placozoa). *Zoomorphology*, 110(3):165–174.

[187] Thiemann, O. H. (2001). Placozoa. In John Wiley & Sons, Ltd, editor, *Encyclopedia of Life Sciences*. John Wiley & Sons, Ltd, Chichester, UK.

[188] Thompson, D. (1944). *On Growth and Form*. Cambridge University Press, Cambridge.

[189] Tkačik, G., Mora, T., Marre, O., Amodei, D., Palmer, S. E., Berry, M. J., and Bialek, W. (2015). Thermodynamics and signatures of criticality in a network of neurons. *Proceedings of the National Academy of Sciences*, 112(37):11508–11513.

[190] Trepat, X. and Fredberg, J. J. (2011). Plithotaxis and emergent dynamics in collective cellular migration. *Trends in Cell Biology*, 21(11):638–646.

[191] Tunstrøm, K., Katz, Y., Ioannou, C. C., Huepe, C., Lutz, M. J., and Couzin, I. D. (2013). Collective States, Multistability and Transitional Behavior in Schooling Fish. *PLoS Computational Biology*, 9(2):e1002915.

[192] Tweedy, L., Meier, B., Stephan, J., Heinrich, D., and Endres, R. G. (2013). Distinct cell shapes determine accurate chemotaxis. *Scientific Reports*, 3.

[193] Ueda, T. and Kobatake, Y. (1983). Quantitative analysis of changes in cell shape of during locomotion and upon responses to salt stimuli. *Experimental Cell Research*, 147(2):466–471.

[194] Ueda, T., Koya, S., and Maruyama, Y. K. (1999). Dynamic patterns in the locomotion and feeding behaviors by the placozoan Trichoplax adhaerence. *Biosystems*, 54(1-2):65–70.

[195] Valletta, J. J., Torney, C., Kings, M., Thornton, A., and Madden, J. (2017). Applications of machine learning in animal behaviour studies. *Animal Behaviour*, 124:203–220.

[196] Valsecchi, G. B., Zappala, V., and others (1993). Catastrophes, phase shifts, and large-scale degradation of a Caribbean coral reef. *Annu. Rev. Earth Planet. Sci*, 21:333.

[197] Varennes, J. and Mugler, A. (2016). Sense and Sensitivity: Physical Limits to Multicellular Sensing, Migration, and Drug Response. *Molecular Pharmaceutics*, 13(7):2224–2232.

[198] Vicsek, T., editor (2001a). *Fluctuations and scaling in biology*. Oxford University Press, Oxford ; New York.

[199] Vicsek, T. (2001b). A question of scale. *Nature*, 411(6836):421–421.

[200] Vicsek, T., Czirók, A., Ben-Jacob, E., Cohen, I., and Shochet, O. (1995). Novel Type of Phase Transition in a System of Self-Driven Particles. *Physical Review Letters*, 75(6):1226–1229.

[201] Vicsek, T. and Zafeiris, A. (2012). Collective motion. *Physics Reports*, 517(3-4):71–140.

[202] Voigt, O., Collins, A. G., Pearse, V. B., Pearse, J. S., Ender, A., Hadrys, H., and Schierwater, B. (2004). Placozoa – no longer a phylum of one. *Current Biology*, 14(22):R944–R945.

[203] Watts, D. J. and Dodds, P. S. (2007). Influentials, Networks, and Public Opinion Formation. *Journal of Consumer Research*, 34(4):441–458.

[204] Watts, D. J. and Strogatz, S. H. (1998). Collective dynamics of 'small-world' networks. *Nature*, 393(6684):440–442.

[205] West, G. B. (1997). A General Model for the Origin of Allometric Scaling Laws in Biology. *Science*, 276(5309):122–126.

[206] West, S. A., Fisher, R. M., Gardner, A., and Kiers, E. T. (2015). Major evolutionary transitions in individuality. *Proceedings of the National Academy of Sciences*, 112(33):10112–10119.

[207] Wilson, K. (1979). Problems in physics with many scales of length. *Scientific American*, 241(2):158–179.

[208] Wiltschko, A., Johnson, M., Iurilli, G., Peterson, R., Katon, J., Pashkovski, S., Abraira, V., Adams, R., and Datta, S. (2015). Mapping Sub-Second Structure in Mouse Behavior. *Neuron*, 88(6):1121–1135.

[209] Winston, J. E. (1976). Experimental culture of the estuarine ectoproct *Conopeum Tenuissimum* from Chesapeake Bay. *The Biological Bulletin*, 150(2):318–335.

[210] Winston, J. E. (2010). Life in the Colonies: Learning the Alien Ways of Colonial Organisms. *Integrative and Comparative Biology*, 50(6):919–933.

[211] Wolf, M., Selig, C., Müller, T., Philippi, N., Dandekar, T., and Schultz, J. (2007). Placozoa: at least two. *Biologia*, 62(6).

[212] Yates, C. A., Erban, R., Escudero, C., Couzin, I. D., Buhl, J., Kevrekidis, I. G., Maini, P. K., and Sumpter, D. J. T. (2009). Inherent noise can facilitate coherence in collective swarm motion. *Proceedings of the National Academy of Sciences*, 106(14):5464–5469.